Measurement of Distance and Orientation of Two Atoms in Arbitrary Geometry

Master's Project in Physics
submitted by

Qurrat-ul-Ain Gulfam
born in Sargodha, Pakistan

2009

This master's project has been carried out at the
Max-Planck-Institute for Nuclear Physics
under the supervision of
PD Dr. Jörg Evers.

The following two projects have been carried out for this thesis. First one has been done under the supervision of PD Dr. J. Evers and the other was supervised by Dr. M. Ikram.

Zusammenfassungen

1. Die genaue Messung des relativen Abstands und der Orientierung zweier nahegelegener Quanten-Teilchen wird diskutiert. Wir sind insbesondere interessiert an einer realistischen Beschreibung, die möglichst wenig Vorwissen über das System benötigt. Anders als bei früheren Studien betrachten wir daher den Fall einer beliebigen relativen Orientierung der beiden Atome. Hierzu müssen die Atome mit kompletten Zeeman- Mannigfaltigkeiten modelliert werden, damit sowohl parallele also auch orthogonale Dipol-Dipol-Kopplungen zwischen allen relevanten Zuständen berücksichtigt werden. Wir zeigen, dass der Abstand der beiden Atome unabhängig von der Orientierung bestimmt werden kann, so lange die Teilchen einen geringen Abstand zueinander haben. Danach diskutieren wir die Messung der relativen Ausrichtung der Atome. Hierzu konzentrieren wir uns auf die beiden Fälle von Atomen in einem zweidimensionalen Wellenleiter und Atomen auf einer Oberfläche.

2. Wir schlagen eine Methode vor für die Quanten-Teleportation eines verallgemeinerten $(N+1)$2-dimensionalen verschr"ankten Zweiteilchenzustands. Der Zustand ist als Feldzustand in zwei Kavitäten von hoher Güte realisiert. Alle benötigten Schritte der Teleportation einschlielich der Präparation der verschränkten Zuständen in den Kavitäten, der Messung der verschränkten Zusände und der angewandten Transformationen sind durch Standardmethoden der Kavitäten- Quantenelektrodynamik realisiert.

Abstracts

1. Accurate measurement of relative distance and orientation of two nearby quantum particles is discussed. We are in particular interested in a realistic description requiring as little prior knowledge about the system as possible. Thus, unlike in previous studies, we consider the case of an arbitrary relative orientation of the two atoms. For this, we model the atom with complete Zeeman manifolds, and include parallel as well as orthogonal dipole-dipole couplings between all states of the two atoms. We find that it is possible to determine the distance of the two atoms independent of the orientation, as long as the particles are sufficiently close to each other. Next, we discuss how in addition the alignment of the atoms can be measured. For this, we focus on the two cases of atoms in a two-dimensional waveguide and of atoms on a surface.

2. We propose a scheme for the quantum teleportation of a generalized bipartite $(N+1)^2$ dimensional entangled field state in two high-Q cavities. All the processes of teleportation including preparation of entangled states in high-Q cavities, measurement of the basis states and transformations are carried out using standard cavity QED techniques.

Based on this reserch work, the following article has been accepted for publication.

- Qurrat-ul-Ain Gulfam and Jörg Evers:
  Measurement of distance and orientation of two atoms in arbitrary geometry
  J. Phys. B in print (arXiv:0909.5608 [quant-ph])

The following article has been published in a refereed journal.

- Qurrat-ul-Ain Gulfam, Rameez-ul-Islam and Manzoor Ikram:
  Quantum teleportation of a high-dimensional entangled state
  J. Phys. B. **41**, 165502 (2008).

Contents

Chapter 1

Introduction

The two projects carried out for the masters thesis are introduced in the following.

Measurement of Distance and Orientation of Two Atoms in Arbitrary Geometry

Progress in many areas of science and its application is fueled by the ongoing progress to measure and structure small objects. In many cases, light is used as a primary tool for reading or writing. However, the resolving power of a lens is ultimately limited by diffraction. Usually the limit to which the small distances can be accurately measured is half of the wavelength of incident light, Rayleigh diffraction limit, if lens-based imaging is used. So, a straightforward implementation is restricted to structures of order of the involved wavelength [1].

Fig. 1.1 illustrates the origin of this diffraction limit. Light from an object travels towards a near-by lens with a propagation vector **K** and is then detected by a detector. In order to be detected, the component of the wave vector **K** towards the detector must be positive. In this case, $k_z = \sqrt{\mathrm{K}^2 - k_x^2 - k_y^2} > 0$, where $\mathbf{K} = k_x\hat{i} + k_y\hat{j} + k_z\hat{k}$. This restricts the magnitude of the transverse wave vector components to be less than K, if they are non-zero. Now the Heisenberg's position-momentum uncertainty relation states $\Delta x \Delta p \approx \hbar$. This implies that $|\Delta x|_{min} \approx \lambda$ which means that the position-space measurements are limited to the order of λ.

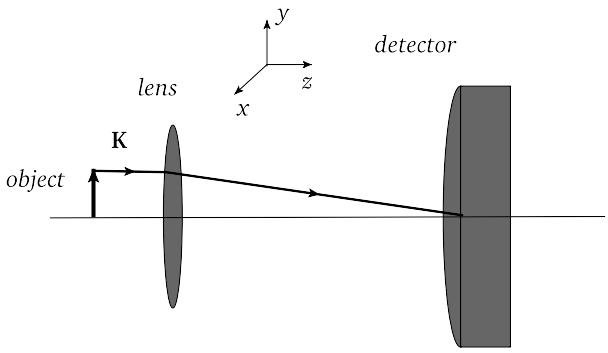

Figure 1.1: Light from an object with a wave vector **K** goes into the lens and is detected by a detector.

Different methods have been invented to surpass this limit. An important technique is to use near-field imaging [2], *i.e.*, to place the detector closed to the object in order to capture maximum light coming from the object. Near-field optics that do not involve any lenses is a tool which can be used to resolve distances up to nanometers. Techniques based on the selective addressing of nearby particles [3] also increase the spatial resolution. In

such methods each feature is identified and isolated on the basis of one or more distinguishing optical characteristics and then the relative spatial coordinates are measured [4]. Resolution enhancement can also be achieved due to non-classical effects [5], *e.g.*, highly entangled photon states can be used to write features in an N-photon absorbing resist which have a resolution of $\lambda/2N$. Thus a resolution by a factor of N below the classical Rayleigh diffraction limit can be achieved [6]. Multiphoton spectroscopy [7] which involves the simultaneous absorption of more than one photon can also be employed to obtain three dimensional resolution. Quantum lithography with classical fields [8] allows to do subwavelength imaging in an efficient manner. Position-dependent dark states or trapping states for which, under certain conditions, the absorption is cancelled are also used in interferometric optical lithography [9].

Measuring the interatomic distance between two closely spaced atoms has always been a fundamental problem in science. Therefore, many techniques have been developed to achieve the goal. One class among these high precision measurement techniques exploits the mutual interaction between the atoms. When the atoms are placed closed to each other, they interact with each other via vacuum radiation field. One atom initially in an excited state emits a virtual photon. This virtual photon is absorbed by the other nearby atom and consequently, it becomes excited. This phenomenon is called dipole dipole interaction [10, 11]. The dipole dipole interaction between two nearby atoms affects the optical properties of the system and it can be detected in the far field. The dipole-dipole interaction for two identical two-level atoms has been studied in great detail in the past [12–17].

The measurement of interatomic distance using dipole dipole interaction has been recently experimentally demonstrated in [18]. This is an important experiment because by combining the near field and far field spectroscopy techniques, two nearby fluorescent molecules could be resolved up to 12nm inside an inhomogeneous external electric field.

So far, all the techniques based on the dipole dipole interaction to measure the interatomic distance are limited to two two-level atoms in a specific geometry [15]. This is the case, when the atoms are placed in a line with respect to the driving laser. However, in most practical situations, the orientation of the atoms with respect to the laser is unknown. Therefore, we are motivated to develop techniques for distance measurement which work for arbitrary orientations of the two atoms. However, as one takes into account the situation of arbitrary orientations, the orthogonal dipole dipole couplings appear between the two atoms [13,19–22]. These couplings vanish when the atoms are aligned with respect to the laser. They have been discussed in the recent past by [13, 20, 21]. The electric field emitted by one of the particles has not only a component corresponding to the emitting transition dipole moment, but also a component along the interparticle distance vector. The projection of the latter field component on a transition dipole moment in the second atom can be non-zero even if it is orthogonal to the emitting dipole [13]. The couplings have a strong effect on the dynamics of the system. In a real atom with magnetic level structure, these couplings lead to the population of excited states even if they are not driven by the external laser field. So, it is required to include all the dipole dipole couplings and to consider the two atoms with complete Zeeman manifolds.

We consider two identical four-level atoms with ground state corresponding to a singlet S state and a triply near-degenerate set of excited states corresponding to P-triplet. The system is driven by a standing wave field. We assume arbitrary orientations for the system and thus consider all the dipole dipole couplings between the two atoms, Fig. 1.2. The goal is to measure the interatomic distance in any geometry and to estimate the relative orientation of the two atoms.

As an observable, we employ the incoherent parts of resonance fluorescence intensity and resonance fluorescence spectrum. This makes the detection possible in the far field. Also resonance fluorescence is not affected by the classical resolution limit because the information about the system is encoded in the spectrum of observed frequencies.

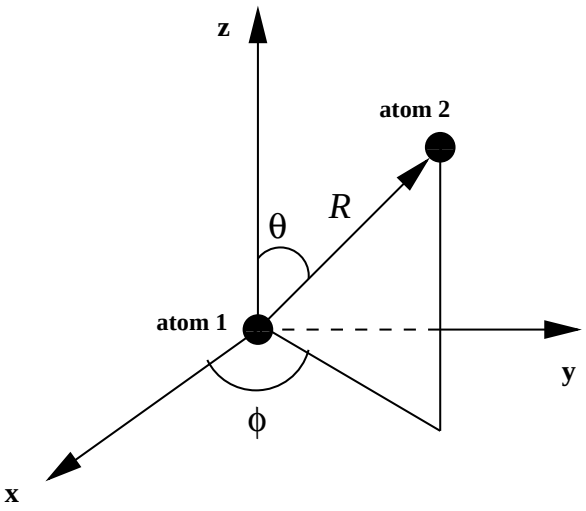

Figure 1.2: The position vectors of the two atoms are $\mathbf{r}_1$ and $\mathbf{r}_2$, respectively. The relative position $\boldsymbol{R} = \mathbf{r}_2 - \mathbf{r}_1$ of atom 2 with respect to atom 1 is arbitrarily chosen.

The resonance fluorescence spectrum of two identical atoms has peaks shifted from the laser frequency by the atomic position dependent Rabi frequencies of the laser when the interatomic separation is large. This is because the dipole dipole interaction is negligible when the atoms are well separated. The distance dependent dipole dipole interaction dominates in case of small interatomic distances and allows to determine the peak positions in the spectrum. Hence, resonance fluorescence gives a clue to the determination of the interatomic distance.

We study first the cases of known orientation and calculate the interatomic distance. We develop a deep understanding in terms of the intuitive dressed state pictures. The dressed states are the eigenstates of the Hamiltonian of the atoms and field, calculated in the interaction picture. Afterwards, we extend our analysis to include the situations of unknown orientation as well. As a result of our analysis, we have discovered that the interatomic distance can be measured over a wide range of small interatomic distances without any prior knowledge about the orientation of the system.

We can also measure the relative orientation of the two atoms with respect to the laser by employing resonance fluorescence spectrum and resonance fluorescence intensity. We have taken into account two interesting cases. In the first one, the atoms are placed inside a planar waveguide and the azimuthal angle is determined using the spectrum of resonance fluorescence. For the second case, the bi-atomic system is placed on a surface and the laser field propagates perpendicular to it. In this case, the intensity of fluorescent light emitted in a particular direction is used to determine the spherical polar angle. We also briefly discuss the methods to determine the orientation in arbitrary geometries.

In the following, we introduce the other project for this thesis which has been carried out partly in Pakistan and partly in Heidelberg under the supervision of Dr. M. Ikram. This

is included as **Chapter 6** in the thesis.

Quantum Teleportation of a High-Dimensional Entangled State

Entanglement is a purely quantum mechanical phenomenon having no classical analog. The basic concept states that in a quantum system of two or more particles, even if the particles are spatially separated, their quantum states are related to each other in such a manner that the state of one particle cannot be described without complete reference to the state of the other particle(s). Many applications like quantum teleportation [23] or quantum cryptography [24] are possible only due to the ability to engineer and manipulate the entangled states. Entanglement is the base of quantum computation. Unlike a classical bit which can only have the value of 0 or 1, a qubit (abbreviated from 'quantum bit' which is the basic unit of quantum information) can be a superposition of 0 and 1 simultaneously if the states are labelled by binary numbers. Thus more information can be transferred if qubits are employed. Increasing the number of terms in the superposition allows one to carry out parallel processing. A quantum register may have a superposition of many qubits. One quantum register cannot be copied to another. Therefore, the only way to communicate such states is quantum teleportation.

Quantum teleportation, introduced first by Bennett *et al.*, is a method to transfer the information securely from the sender to the receiver. It does not transfer the particle itself but its quantum state. It mainly consists of three steps. The first step consists of the preparation of a maximally entangled state. Both the sender and the receiver keep one particle of this entangled state. In the second step, the information at the sender's station is disassembled. One part of this is sent through a quantum channel run by non-local correlations between the two entangled quantum entities and a classical channel is used to send the other part. Ultimately, the receiver recovers the state by making use of the information obtained from both the classical and the quantum channel. Quantum teleportation does not allow the communication of information at a speed higher than the speed of light because a classical channel is involved in the process, as discussed above. However, it can help in the transmission of a quantum superposition states, which is useful for quantum computation.

A system of many qubit states is needed in applications where one needs to search an unordered database or to factorize a very large number. The teleportation of a single qubit state requires two-qubit maximally entangled state and the teleportation of a two-particle entangled state can be done by employing two quantum states each made up of two particles [25].

A scheme for the teleportation of a bipartite entangled state from a pair of high-Q cavities to another pair of high-Q cavities with quantum correlations shaping over $(N+1)^2$ is presented.

The preparation of the entangled states for a fixed number of photons is done by the interaction of excited two-level atoms with high-Q cavities [26]. The cavity field is assumed to be in a vacuum state initially. The interaction is assumed to be resonant. We employ Jaynes-Cummings Hamiltonian. The time period of the interaction is pre-calculated for the desired entangled state to be generated. By choosing proper interaction times, after the interaction of the first atom with the cavity field, a one-photon entangled state is

created. This entangled state serves as an initial condition for the second atom and so on. Finally, we use the condition that all the atoms must be detected in their ground states.

Measurement of the basis states includes the measurement of relative phases and the measurement of the photon numbers. This measurement information will be sent from the sender to the receiver through some classical channel. Standard cavity QED techniques, for example, Ramsey interferometry [27] and adiabatic passage [28] are used for carrying out the measurement of the photon numbers. For the measurement of the relative phases, we need to empty the cavities which can be done using adiabatic passage.

Finally, the transformation process at the receiver's end in order to recover the original state can also be divided into two steps, *i.e.*, the transformation of the photon numbers which is done by employing adiabatic passage and the transformation of the relative phases, for which Ramsey interferometry is required.

Our scheme needs interaction times of calculated duration which can be achieved by the Stark field adjustments of the electric field. We also need to have no spontaneous decay of the atoms so we propose to use rubidium atoms because they do not decay easily by spontaneous emission. There must be no losses in the cavities so cavities whose quality factor is high, are required.

The proposed scheme is experimentally realizable with the current experimental techniques.

Now we give a brief overview of the thesis.

Overview

This thesis is organized as follows. In **Chapter 2**, we exploit the density matrix approach since coherent as well as incoherent processes have to be taken into account, and derive the master equation for the density matrix of the system. We will consider time-independent density matrix because we wait for a long time so that the system reaches a steady state. **Chapter 3** includes a discussion of the observables in the steady state. **Chapter 4** targets to explain the physical understanding about the system; particularly about the various processes taking place in the system and the phenomenon of ac Stark effect for a single two level atom. **Chapter 5** describes the results of the project in detail. As already said, **Chapter 6** is a study of teleportation of a high-dimensional entangled state. Finally, in **Chapter 7**, we give the concluding remarks from both the above mentioned projects and give a brief outlook.

Chapter 2

Derivation of the Master Equation

2.1 Introduction

In this chapter, we describe the mathematical model that we use to analyze the interaction of the electromagnetic radiation field with the atomic system. We use the master equation approach which is a standard technique for the study of atom-field interactions. The system of atoms is usually coupled to a large reservoir such as vacuum field. The master equation explains the time evolution of the reduced density operator of the atomic system, and the quantized electromagnetic field having unlimited number of modes acts as a reservoir which undergoes slight perturbations due to the presence of atoms. The derivation of a master equation for different atomic systems has already been demonstrated in [10, 11, 29].

Generally, the quantum state of the radiation field is not required to be determined. This is because the correlation functions of the scattered electromagnetic field can be obtained from the correlation functions of the atomic operators. This will be illustrated in the next chapter where we explain our observables.

In Sec. 2.2, we set up the Hamiltonian for our bi-atomic system as well as the radiation field. We begin with the calculation of the Hamiltonian of the complete system, insert this Hamiltonian in the Liouville or Von Neumann equation and obtain an equation of motion for the combined density matrix. By tracing over all the field modes, we obtain the reduced density matrix.

We use certain approximations for the calculation of the master equation and we will explain each of them in Sec. 2.3. For example, the dipole approximation in which we assume that the wavelength of the incident electromagnetic field is larger than the size of the atom. These approximations considerably simplify the calculation of the equation of motion of the bi-atomic system.

The actual derivation is described in detail in Sec. 2.4. The explanation of various coupling constants that participate in the atom-vacuum coupling is presented in Sec. 2.5. In Sec. 2.6, the interaction with the laser is described.

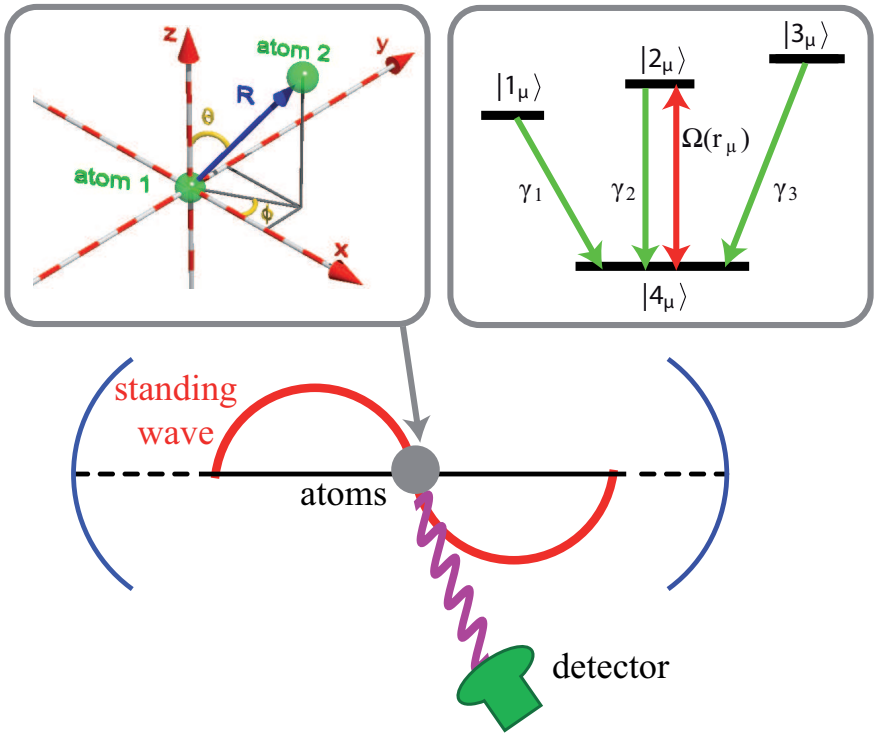

Figure 2.1: Scheme for the determination of relative distance and orientation of two nearby atoms. The atoms $\mu \in \{1, 2\}$ are driven on one transition by a standing wave laser field with Rabi frequency $\Omega(\mathbf{r}_\mu)$ and scatter light, which is registered in the far field with a detector. The interatomic distance vector $\boldsymbol{R}$ is arbitrary, as shown in the left inset. The right inset shows the level structure of each atom. Each atom has a single ground state (zero angular momentum) and three excited states (angular momentum 1).

2.2 System Hamiltonian

We consider a system of two identical four-level atoms. Each atom can be visualized as a ^{40}Ca atom. The ground state corresponds to a singlet S_0 state and the excited state multiplet P_1 has three Zeeman sublevels corresponding to the angular momentum eigenstates $m_j \in (-1, 0, 1)$. The alignment of the atoms is arbitrary. The atoms are being driven by a standing wave laser field which is polarized along the z-axis and propagates along x-axis, Fig. 2.1. The discussion of the laser field has been postponed to Sec. 2.6. The position of atom i is $\mathbf{r}_i, i \in \{1, 2\}$, Fig. 1.2. The interatomic distance vector in spherical coordinates is given by,

$$\boldsymbol{R} = R(\sin\theta\cos\phi, \sin\theta\sin\phi, \cos\theta)^T. \tag{2.1}$$

The raising and lowering operators on the $|\, 4_\mu\rangle \leftrightarrow |\, i_\mu\rangle$ transition of atom μ are $i \in \{1, 2, 3\}$

$$S_{i+}^{(\mu)} = |\, i_\mu\rangle\langle 4_\mu\,| \quad \text{and} \quad S_{i-}^{(\mu)} = |\, 4_\mu\rangle\langle i_\mu\,| \tag{2.2}$$

where $|\, 4_\mu\rangle$ is assumed to be the ground state of the atom μ.

We define $\omega_0 = ck_0$ as the mean transition frequency given by

$$\omega_0 = \frac{1}{3}\sum_{i=1}^{3}\omega_i. \tag{2.3}$$

The Hamiltonian that describes the system is composed of three parts.

$$\mathcal{H} = \mathcal{H}_a + \mathcal{H}_f + \mathcal{H}_{int} \tag{2.4}$$

where

$$\mathcal{H}_a = \hbar\sum_{\mu=1}^{2}\sum_{i=1}^{3}\omega_i S_{i+}^{(\mu)} S_{i-}^{(\mu)} \tag{2.5}$$

describes the free time evolution of the atoms. The energy of the state $|i\rangle$ is $\hbar\omega_i$. The energy of the ground state is assumed to be zero.

$$\mathcal{H}_f = \sum_{\boldsymbol{k}s}\hbar\omega_{\boldsymbol{k}} a_{\boldsymbol{k}s}^{\dagger} a_{\boldsymbol{k}s} \tag{2.6}$$

explains the Hamiltonian for the electromagnetic field. $a_{\boldsymbol{k}s}$ and $a_{\boldsymbol{k}s}^{\dagger}$ are the field annihilation and creation operators, respectively. $\omega_{\boldsymbol{k}}$ is the frequency of the mode whose wavevector is described by $\boldsymbol{k}$.

$$\mathcal{H}_{int} = \mathcal{H}_{vac} = -\sum_{\mu=1}^{2}\hat{\boldsymbol{d}}^{(\mu)}\cdot\hat{\mathbf{E}}(\mathbf{r}_\mu) \tag{2.7}$$

accounts for the interaction between the atoms and the radiation field in the electric dipole approximation. The subscript *vac* denote vacuum. The $\hat{\boldsymbol{d}}^{(\mu)}$ is independent of the atomic index μ since the two atoms are identical.

The Wigner-Eckart theorem [30] is used to determine the electric dipole moment operator of the atom μ which is given by

$$\hat{\boldsymbol{d}}^{(\mu)} = \sum_{i=1}^{3}[\boldsymbol{d}_i S_{i+}^{(\mu)} + H.c.], \tag{2.8}$$

where $H.c.$ denotes the hermition conjugate and $\mu \in \{1, 2\}$. The vector $\boldsymbol{d}_i$ represents the dipole moment of the i-th dipole transition. The dipole moments are given by the matrix elements of the electric dipole moment operator $\boldsymbol{d}_i = \langle i|\hat{\boldsymbol{d}}|4\rangle$ so that

$$\boldsymbol{d}_1 = \mathcal{D}\epsilon^{(+)}, \quad \boldsymbol{d}_2 = \mathcal{D}\mathbf{e}_z, \quad \boldsymbol{d}_3 = -\mathcal{D}\epsilon^{(-)}. \tag{2.9}$$

Here $\mathcal{D}$ denotes the reduced dipole matrix element and the circularly polarized vectors are defined as

$$\epsilon^{(\pm)} = \frac{1}{\sqrt{2}}(\mathbf{e}_x \pm \iota\mathbf{e}_y). \tag{2.10}$$

$\hat{\mathbf{E}}$ is defined as

$$\hat{\mathbf{E}}(\mathbf{r}) = \iota \sum_{\boldsymbol{ks}} \sqrt{\frac{\hbar\omega_k}{2\epsilon_0 V}} \epsilon_{\boldsymbol{ks}} e^{\iota \boldsymbol{k}\cdot\mathbf{r}} a_{\boldsymbol{ks}} + H.c., \tag{2.11}$$

where $a_{\boldsymbol{ks}}$ and $a^{\dagger}_{\boldsymbol{ks}}$ are the field annihilation and creation operators, respectively. $\boldsymbol{k}$ describes the wave vector, $\epsilon_{\boldsymbol{ks}}$ the polarization, ω_k the frequency and V the quantization volume of a field mode.

Before we start the detailed calculation of the master equation, it is important to outline all the assumptions that we will use in Sec. 2.4.

2.3 Assumptions

We introduce a number of approximations which simplify the equation of motion considerably.

(1) At some initial time $t = 0$, it is assumed that the combined system is in a product state where there are no correlations between the atoms and the field. The complete density operator can be written as a direct product

$$\varrho(0) = \varrho_f(0) \otimes \varrho_a(0). \tag{2.12}$$

where $\varrho_f(0) = |0_f\rangle\langle 0_f|$.

(2) We use the Born approximation which means that we assume that the coupling between the atoms and the radiation field is weak. This approximation implies that the atom-field interaction is so weak that an emitted photon is not reabsorbed by the atom.

(3) We assume the rotating wave approximation regime. The interaction between the atoms and the reservoir will have terms such as $S^{(\mu)}_{i+} S^{(\nu)}_{j+}, S^{(\mu)}_{i+} S^{(\nu)}_{j-}, S^{(\mu)}_{i-} S^{(\nu)}_{j+}, S^{(\mu)}_{i-} S^{(\nu)}_{j-}$. The raising-raising and lowering-lowering terms are so called counter-rotating terms. They vary very rapidly with time and so are excluded during the derivation.

(4) We assume that the future state of the system-reservoir density operator is determined by its current state, and is not a function of the history of the bath. This is called Markovian approximation.

(5) Our interaction Hamiltonian does not describe the relativistic effects. We consider all modes below a cut-off frequency ω_C of the vacuum field available for interaction with an atomic transition. Higher frequencies correspond to relativistic effects.

2.4 Master Equation

During the derivation of the master equation, we follow the analysis done in [11].The time derivative of the quantum state ϱ of the atoms and the radiation field is determined by

$$\dot{\varrho} = -\frac{\iota}{\hbar}[\mathcal{H}, \varrho]. \tag{2.13}$$

The above equation is called Liouville or Von Neumann equation of motion for the density matrix. The Schrödinger's equation, contains specific state vectors while the Liouville equation employs the density operator and so the latter is more general. One can get the statistical as well as the quantum mechanical information out of it.

We work in the interaction picture and employ the transformed density matrix which is given by

$$\tilde{\varrho}(t) = e^{\iota(\mathcal{H}_a+\mathcal{H}_f)t/\hbar}\varrho e^{-\iota(\mathcal{H}_a+\mathcal{H}_f)t/\hbar}. \tag{2.14}$$

This transformed density matrix evolves in time according to the atom-field interaction. The equation of motion obeyed by the density matrix is

$$\partial_t\tilde{\varrho}(t) = \frac{1}{\iota\hbar}[\tilde{\mathcal{H}}_{int}(t), \tilde{\varrho}(t)], \tag{2.15}$$

where

$$\tilde{\mathcal{H}}_{int}(t) = e^{\iota(\mathcal{H}_a+\mathcal{H}_f)t/\hbar}\mathcal{H}_{int}e^{-\iota(\mathcal{H}_a+\mathcal{H}_f)t/\hbar}, \tag{2.16}$$

is the Hamiltonian in the chosen interaction picture with respect to $\mathcal{H}_a + \mathcal{H}_f$. Now we trace over the field variables because we are interested only in the atomic density operator. In order to eliminate the reservoir variables, we work with the reduced density operator. One can obtain the reduced density operator for the atoms at a time t by taking the trace over reservoir coordinates, *i.e.*,

$$\tilde{\varrho}_a(t) = \mathrm{Tr}_f\tilde{\varrho}(t). \tag{2.17}$$

Such general reservoir approach is a standard technique in quantum optics and is outlined in different textbooks, *e.g.*, [11, 27]. The equation of motion then becomes

$$\partial_t\tilde{\varrho}_a(t) = \frac{1}{\iota\hbar}\mathrm{Tr}_f[\tilde{\mathcal{H}}_{int}(t), \tilde{\varrho}(t)]. \tag{2.18}$$

We use iteration method to solve this first order differential equation. At $t = 0$, it is formally integrated and the first order solution in $\tilde{\mathcal{H}}_{int}(t)$ is obtained.

$$\tilde{\varrho}_a(t) = \tilde{\varrho}_a(0) + \frac{1}{\iota\hbar}\int_0^t d\acute{t}\mathrm{Tr}_f[\tilde{\mathcal{H}}_{int}(\acute{t}), \tilde{\varrho}(\acute{t})]. \tag{2.19}$$

We back-substitute Eq. (2.19) into Eq. (2.18) and thus obtain the master equation for the reduced density operator.

$$\tilde{\varrho}_a(t) = \frac{1}{\iota\hbar}\mathrm{Tr}_f[\tilde{\mathcal{H}}_{int}(t), \tilde{\varrho}(0)] - \frac{1}{\hbar^2}\int_0^t d\acute{t}\mathrm{Tr}_f[\tilde{\mathcal{H}}_{int}(t), [\tilde{\mathcal{H}}_{int}(\acute{t}), \tilde{\varrho}(\acute{t})]]. \tag{2.20}$$

One can get an explicit exact solution for $\tilde{\varrho}_a(t)$ if this procedure is continued. The solution is an infinite series of integral terms, the so-called Born series.

We will however, solve the master equation in a different manner. We employ the Born approximation and evaluate the second term of the above equation that contains the

double commutator. The expression to be calculated is

$$\begin{aligned}\frac{1}{\hbar^2}\int_0^t d\acute{t}\mathrm{Tr}_f[\tilde{\mathcal{H}}_{int}(t),[\tilde{\mathcal{H}}_{int}(\acute{t}),\tilde{\varrho}(\acute{t})]] = \frac{1}{\hbar^2}\int_0^t d\acute{t}\mathrm{Tr}_f[\tilde{\mathcal{H}}_{vac}(t)\tilde{\mathcal{H}}_{vac}(\acute{t})\tilde{\varrho}(\acute{t})] \\ + \mathrm{Tr}_f[\tilde{\varrho}(\acute{t})\tilde{\mathcal{H}}_{vac}(\acute{t})\tilde{\mathcal{H}}_{vac}(t)] \\ - \mathrm{Tr}_f[\tilde{\mathcal{H}}_{vac}(t)\tilde{\varrho}(\acute{t})\tilde{\mathcal{H}}_{vac}(\acute{t})] \\ - \mathrm{Tr}_f[\tilde{\mathcal{H}}_{vac}(\acute{t})\tilde{\varrho}(\acute{t})\tilde{\mathcal{H}}_{vac}(t)]. \qquad (2.21)\end{aligned}$$

We concentrate on the first summand of the above equation. We plug in the explicit form of $\mathcal{H}_{vac}$ and use the correlation functions for temperature $T = 0$

$$\begin{aligned}&\mathrm{Tr}_f[\tilde{a}_{\boldsymbol{k}s}(t)\tilde{a}_{\acute{\boldsymbol{k}}\acute{s}}(\acute{t})\tilde{\varrho}_f(0)] = \mathrm{Tr}_f[\tilde{a}^\dagger_{\boldsymbol{k}s}(t)\tilde{a}^\dagger_{\acute{\boldsymbol{k}}\acute{s}}(\acute{t})\tilde{\varrho}_f(0)] = \mathrm{Tr}_f[\tilde{a}^\dagger_{\boldsymbol{k}s}(t)\tilde{a}_{\acute{\boldsymbol{k}}\acute{s}}(\acute{t})\tilde{\varrho}_f(0)] = 0, \\ &\mathrm{Tr}_f[\tilde{a}_{\boldsymbol{k}s}(t)\tilde{a}^\dagger_{\acute{\boldsymbol{k}}\acute{s}}(\acute{t})\tilde{\varrho}_f(0)] = \delta_{\boldsymbol{k}\acute{\boldsymbol{k}}}\delta_{s\acute{s}}e^{-\iota\omega_k(t-\acute{t})}. \qquad (2.22)\end{aligned}$$

where

$$\tilde{a}_{\boldsymbol{k}s}(t) = a_{\boldsymbol{k}s}(t)e^{-\iota\omega_k t} \qquad (2.23)$$

This results in the following expression:

$$\begin{aligned}&\frac{1}{\hbar^2}\int_0^t d\acute{t}\mathrm{Tr}_f[\tilde{\mathcal{H}}_{vac}(t)\tilde{\mathcal{H}}_{vac}(\acute{t})\tilde{\varrho}(\acute{t})] \\ &= \int_0^t d\acute{t}\sum_{\boldsymbol{k}s}(\hat{D}_{\boldsymbol{k}s}(t)\hat{D}^\dagger_{\boldsymbol{k}s}(\acute{t})e^{-\iota\omega_k(t-\acute{t})} + \hat{D}^\dagger_{\boldsymbol{k}s}(t)\hat{D}_{\boldsymbol{k}s}(\acute{t})e^{\iota\omega_k(t-\acute{t})})\tilde{\varrho}_a(t-\acute{t}). \qquad (2.24)\end{aligned}$$

Here,

$$\hat{D}_{\boldsymbol{k}s}(t) = \sum_{\mu=1}^{2}\mathbf{u}_{\boldsymbol{k}s}(\mathbf{r}_\mu).\sum_{i=1}^{3}[\boldsymbol{d}_i S^{(\mu)}_{i+}e^{\iota\omega_i t} + H.c.]. \qquad (2.25)$$

Proceeding in a similar fashion, one can obtain the remaining three terms of the Eq. (2.21).

Now we come to the rotating wave approximation. In the interaction picture, the terms proportional to $S^{(\mu)}_{i+}S^{(\nu)}_{j+}$ and $S^{(\mu)}_{i-}S^{(\nu)}_{j-}$ oscillate at the frequency $(\omega_i + \omega_j)$. On the other hand, the terms proportional to $S^{(\mu)}_{i+}S^{(\nu)}_{j-}$ and $S^{(\mu)}_{i-}S^{(\nu)}_{j+}$ oscillate at the frequency $(\omega_i - \omega_j)$. These terms conserve the energy. We ignore the so-called counter-propagating terms that rotate at the frequency $\pm(\omega_i + \omega_j)$ since we assumed that the differences$(\omega_i - \omega_j)$ between the resonance frequencies are much smaller than the frequencies ω_i themselves.

Being in the non-relativistic regime, we consider only wave vectors which obey $|k| \leq k_c$, where $ck_c = \omega_c$ is the cut-off frequency. This frequency is much larger than all relevant transition frequencies ω_i of the atoms, but smaller than $m_e c^2/\hbar$, where m_e is the mass of the electron. It follows that quasi-resonant absorption and emission processes are still correctly described, but virtual emissions and re-absorptions of "relativistic"high frequency photons are not taken into account. We replace the sum over discrete wave vectors by an integral over continuum modes:

$$\sum_{\boldsymbol{k}s} \to \frac{V}{(2\pi c)^3}\int_0^{\omega_C} d\omega_k\omega_k^2\int_{\Omega_k} d\Omega_k\sum_{s=1}^{2} \qquad (2.26)$$

where $\Omega_k = (\theta_k, \phi_k)$.

We have expressed the integral over the three-dimensional k-space in terms of spherical coordinates and changed the integration over k into an integral over frequencies $\omega_k = ck$. The master equation for the reduced density operator now simplifies to

$$\begin{aligned}\partial_t \tilde{\varrho}_a(t) = &\frac{1}{\iota\hbar}[\mathcal{H}_a(t), \tilde{\varrho}_a(t)] \\ &+ \sum_{\mu,\nu=1}^{2}\sum_{i,j=1}^{3}\{[S_{j-}^{(\nu)} X_{ij}^{\mu\nu}(t), S_{i+}^{(\mu)}] + [S_{j-}^{(\nu)}, (X_{ij}^{\mu\nu}(t))^\dagger S_{i+}^{(\mu)}] \\ &+ [S_{j+}^{(\nu)} Y_{ij}^{\mu\nu}(t), S_{i-}^{(\mu)}] + [S_{j+}^{(\nu)} (Y_{ij}^{\mu\nu}(t))^\dagger S_{i-}^{(\mu)}]\}. \end{aligned} \tag{2.27}$$

The time dependent operators used follow.

$$X_{ij}^{\mu\nu}(t) = \frac{1}{2\varepsilon_0\hbar(2\pi c)^3}\int_0^t d\tau \int_0^{\omega_C} d\omega_k \omega_k^3 \int d\Omega_k \sum_s e^{\iota \boldsymbol{k}\cdot\boldsymbol{R}}[\epsilon_{\boldsymbol{k}s}\cdot\boldsymbol{d}_i][\epsilon_{\boldsymbol{k}s}^*\cdot\boldsymbol{d}_j^*]e^{\iota(\omega_j-\omega_k)\tau}\tilde{\varrho}_a(t-\tau) \tag{2.28}$$

and

$$Y_{ij}^{\mu\nu}(t) = \frac{1}{2\varepsilon_0\hbar(2\pi c)^3}\int_0^t d\tau \int_0^{\omega_C} d\omega_k \omega_k^3 \int d\Omega_k \sum_s e^{\iota \boldsymbol{k}\cdot\boldsymbol{R}}[\epsilon_{\boldsymbol{k}s}\cdot\boldsymbol{d}_i^*][\epsilon_{\boldsymbol{k}s}^*\cdot\boldsymbol{d}_j]e^{-\iota(\omega_j+\omega_k)(\tau}\tilde{\varrho}(t-\tau). \tag{2.29}$$

In these equations, the vector $\boldsymbol{R} = \mathbf{r}_\mu - \mathbf{r}_\nu$ denotes the relative coordinates of atom μ with respect to atom ν. It is to be noted that the above integrals would be divergent if we had not introduced the cut-off frequency ω_C. We continue with the evaluation of the operators $X_{i,j}^{\mu\nu}$ and $Y_{i,j}^{\mu\nu}$. As the time difference τ increases, $e^{-\iota\omega_k\tau}$ oscillates faster and faster. Therefore, this term can be neglected when $\tau > \tau_c$. This τ_c is the correlation time of vacuum fluctuations of the free electromagnetic field. Assuming τ_c to be small means that the bandwidth of the electromagnetic vacuum field is assumed to be much larger than the atomic linewidth.

Since the atomic lifetimes γ_i^{-1} determine the timescale of evolution of the density matrix $\tilde{\varrho}_a(t-\tau)$, the above integrals can be further simplified as follows. During the vacuum correlation time τ_c, the density operator does not change considerably; Markovian approximation. We therefore, replace $\tilde{\varrho}_a(t-\tau)$ by $\tilde{\varrho}_a(t)$. We further extend the upper bound of the τ integral to infinity.

Using the relation

$$\lim_{t\to\infty}\int_0^t d\tau e^{-\iota\omega_k\tau} = [\pi\delta(\omega_k) - \iota\frac{\mathcal{P}}{\omega_k}], \tag{2.30}$$

the integral over time can be written as

$$\lim_{t\to\infty}\int_0^t d\tau \tilde{\varrho}_a(\acute{t}) e^{-\iota\omega_k\tau} = \tilde{\varrho}_a(t)[\pi\delta(\omega_k) - \iota\frac{\mathcal{P}}{\omega_k}], \tag{2.31}$$

where $\mathcal{P}$ denotes the Cauchy's Principal value of the integral.

Evaluating the integrals, the operators can be written as

$$X_{ij}^{\mu\nu}(t) = (\Gamma_{ij}^{\mu\nu} + \iota M_{ij}^{\mu\nu})\tilde{\varrho}(t) \tag{2.32}$$

and

$$Y_{ij}^{\mu\nu} = -\iota (P_{ij}^{\mu\nu})^* \tilde{\varrho}(t). \tag{2.33}$$

Here,

$$\begin{aligned}
\Gamma_{ij}^{\mu\nu} =& \frac{\pi}{2\varepsilon_0 \hbar (2\pi c)^3} \int_0^{\omega_C} d\omega_k \omega_k^3 [(\boldsymbol{d}_i)^T \overleftrightarrow{F}(\omega_k/c, \boldsymbol{R}) \boldsymbol{d}_j^*] \delta(\omega_k - \omega_0), \\
P_{ij}^{\mu\nu} =& \frac{\pi}{2\varepsilon_0 \hbar (2\pi c)^3} \mathcal{P} \int_0^{\omega_C} d\omega_k \omega_k^3 [(\boldsymbol{d}_i)^T \overleftrightarrow{F}(\omega_k/c, \boldsymbol{R}) \boldsymbol{d}_j^*] \frac{1}{\omega_0 + \omega_k}, \\
M_{ij}^{\mu\nu} =& \frac{\pi}{2\varepsilon_0 \hbar (2\pi c)^3} \mathcal{P} \int_0^{\omega_C} d\omega_k \omega_k^3 [(\boldsymbol{d}_i)^T \overleftrightarrow{F}(\omega_k/c, \boldsymbol{R}) \boldsymbol{d}_j^*] \frac{1}{\omega_0 - \omega_k}.
\end{aligned} \tag{2.34}$$

The components of the tensor $\overleftrightarrow{F}(\omega_k/c, \boldsymbol{R})$ for $p, q \in \{1, 2, 3\}$ read

$$\overleftrightarrow{F}_{pq}(k, \boldsymbol{R}) = \int d\Omega_k \sum_s e^{\iota \boldsymbol{k} \cdot \boldsymbol{R}} [\epsilon_{\boldsymbol{k}s}]_p [\epsilon_{\boldsymbol{k}s}^*]_q. \tag{2.35}$$

This tensor depends only on the absolute value of $\boldsymbol{k}$, because the spatial integration extends over the whole solid angle. Additionally, all the components of $\overleftrightarrow{F}$ are real. Thus, the constants obey the symmetry relations.

$$\Gamma_{ij}^{\mu\nu} = (\Gamma_{ji}^{\nu\mu})^*, \qquad P_{ij}^{\mu\nu} = (P_{ji}^{\nu\mu})^*, \qquad M_{ij}^{\mu\nu} = (M_{ji}^{\nu\mu})^*. \tag{2.36}$$

Also, we have

$$\Omega_{ij}^{\mu\nu} = P_{ij}^{\mu\nu} - M_{ij}^{\mu\nu}. \tag{2.37}$$

Now, the master equation becomes

$$\begin{aligned}
\partial_t \tilde{\varrho}_a(t) = & \frac{1}{\iota\hbar} [\mathcal{H}_a, \tilde{\varrho}_a(t)] + \iota \sum_{\substack{\mu,\nu=1 \\ \mu \neq \nu}}^{2} \sum_{i=1}^{3} \sum_{j=1}^{3} \Omega_{ij}^{\mu\nu} [S_{i+}^{(\mu)} S_{j-}^{(\nu)}, \tilde{\varrho}_a(t)] \\
& - \sum_{\mu,\nu=1}^{2} \sum_{i=1}^{3} \sum_{j=1}^{3} \Gamma_{ij}^{\mu\nu} (S_{i+}^{(\mu)} S_{j-}^{(\nu)} \tilde{\varrho}_a(t) + \tilde{\varrho}_a(t) S_{i+}^{(\mu)} S_{j-}^{(\nu)} - 2 S_{j-}^{(\nu)} \tilde{\varrho}_a(t) S_{i+}^{(\mu)})
\end{aligned} \tag{2.38}$$

In the final form, it can be written as

$$\begin{aligned}\partial_t\tilde{\varrho}_a(t) &= \frac{1}{\iota\hbar}[\mathcal{H}_a,\tilde{\varrho}_a(t)] + \iota\sum_{\substack{\mu,\nu=1\\ \mu\neq\nu}}^{2}\sum_{i=1}^{3}\sum_{j=1}^{3}\Omega_{ij}^{\mu\nu}[S_{i+}^{(\mu)}S_{j-}^{(\nu)},\tilde{\varrho}_a(t)]\\ &- \sum_{\mu,\nu=1}^{2}\sum_{i=1}^{3}\sum_{j=1}^{3}\gamma_{ij}(S_{i+}^{(\mu)}S_{j-}^{(\mu)}\tilde{\varrho}_a(t) + \tilde{\varrho}_a(t)S_{i+}^{(\mu)}S_{j-}^{(\mu)} - 2S_{j-}^{(\mu)}\tilde{\varrho}_a(t)S_{i+}^{(\mu)})\\ &- \sum_{\substack{\mu,\nu=1\\ \mu\neq\nu}}^{2}\sum_{i=1}^{3}\sum_{j=1}^{3}\Gamma_{ij}^{\mu\nu}(S_{i+}^{(\mu)}S_{j-}^{(\nu)}\tilde{\varrho}_a(t) + \tilde{\varrho}_a(t)S_{i+}^{(\mu)}S_{j-}^{(\nu)} - 2S_{j-}^{(\nu)}\tilde{\varrho}_a(t)S_{i+}^{(\mu)})\\ &= \frac{1}{\iota\hbar}[\mathcal{H}_a,\tilde{\varrho}_a(t)] - \frac{\iota}{\hbar}[\tilde{\mathcal{H}}_\Omega,\tilde{\varrho}_a(t)] + \mathcal{L}_\gamma\tilde{\varrho}_a(t),\end{aligned} \tag{2.39}$$

where

$$[\mathcal{H}_\Omega,\tilde{\varrho}_a(t)] = -\hbar\sum_{\substack{\mu,\nu=1\\ \mu\neq\nu}}^{2}\sum_{i=1}^{3}\sum_{j=1}^{3}\Omega_{ij}^{\mu\nu}[S_{i+}^{(\mu)}S_{j-}^{(\nu)},\tilde{\varrho}_a(t)], \tag{2.40}$$

and

$$\begin{aligned}\mathcal{L}_\gamma\tilde{\varrho}_a(t) = &- \sum_{\mu,\nu=1}^{2}\sum_{i=1}^{3}\sum_{j=1}^{3}\gamma_{ij}(S_{i+}^{(\mu)}S_{j-}^{(\mu)}\tilde{\varrho}_a(t) + \tilde{\varrho}_a(t)S_{i+}^{(\mu)}S_{j-}^{(\mu)} - 2S_{j-}^{(\mu)}\tilde{\varrho}_a(t)S_{i+}^{(\mu)})\\ &- \sum_{\mu,\nu=1}^{2}\sum_{i=1}^{3}\sum_{j=1}^{3}\Gamma_{ij}^{\mu\nu}(S_{i+}^{(\mu)}S_{j-}^{(\nu)}\tilde{\varrho}_a(t) + \tilde{\varrho}_a(t)S_{i+}^{(\mu)}S_{j-}^{(\nu)} - 2S_{j-}^{(\nu)}\tilde{\varrho}_a(t)S_{i+}^{(\mu)}).\end{aligned} \tag{2.41}$$

In the second line of Eq. (2.39), we used the parameters γ_{ij} which are given by

$$\gamma_{ij} = \Gamma_{ij}^{\mu\mu} = \sqrt{\gamma_i\gamma_j}\frac{\boldsymbol{d}_i.\boldsymbol{d}_j^*}{|\boldsymbol{d}_i||\boldsymbol{d}_j^*|}, \tag{2.42}$$

where

$$\gamma_i = \frac{\omega_0^3|\boldsymbol{d}_i|^2}{6\pi\epsilon_0\hbar c^3}. \tag{2.43}$$

For $i=j,\gamma_{ii}=\gamma_i$ is the half-decay rate of the i-th atomic dipole transition. For $i\neq j$, the parameters γ_{ij} describe the cross-damping between the transitions i and j of the same atom. According to Eq. (2.42), the cross decay rates γ_{ij} involve a scalar product of the associated dipole moments $\boldsymbol{d}_i$ and $\boldsymbol{d}_j$. So, they depend on the mutual orientation of the involved dipoles and contribute to the master equation only if the two dipole moments are non-orthogonal. They describe the decay-induced coherence between atomic dipole transitions.

If we now include the external laser field, an additional term

$$\frac{-\iota}{\hbar}[\mathcal{H}_L(t),\tilde{\varrho}_a(t)] \tag{2.44}$$

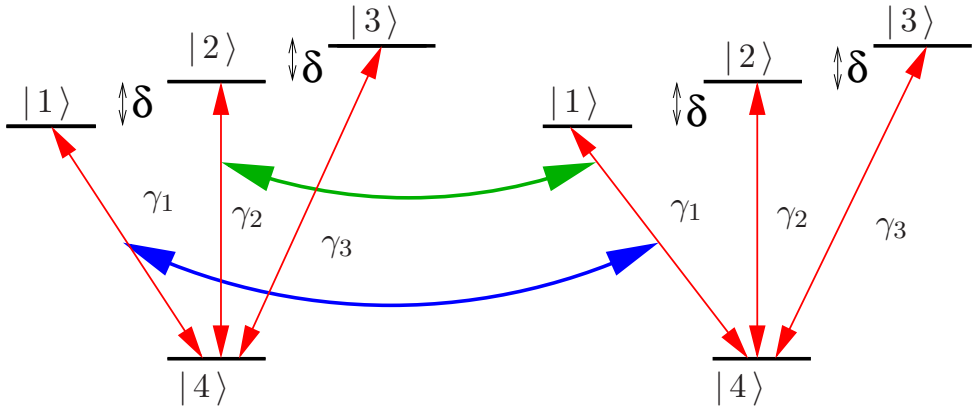

Figure 2.2: Figure showing examples for the parallel and orthogonal couplings: Parallel couplings Ω_{11}, Γ_{11}, Orthogonal couplings Ω_{21}, Γ_{21}

will be added to the right side of Eq. (2.39). $\mathcal{H}_L(t)$ represents the interaction between the atoms and the laser field. We assume that the Rabi frequencies and the detunings associated with the laser are much smaller than the mean transition frequency ω_0. So, we are justified to assume that the atom-vacuum interaction terms in Eq. (2.39) remain unaffected by the addition of the laser field.

In the following section, we will derive the explicit form of the tensor $\overleftrightarrow{F}(\omega_k/c, \boldsymbol{R})$ and the coupling constants and give some interpretation of these parameters. We intend to find some relations between the couplings. This will reduce the number of independent parameters in the master equation.

2.5 Dipole Dipole Coupling Constants

Now we find out the explicit forms of the coupling constants. First, we derive the components of the tensor $\overleftrightarrow{F}$. For the summation over polarization components, we find

$$\sum_s [\epsilon_{\boldsymbol{k}s}]_p [\epsilon^*_{\boldsymbol{k}s}]_q = \delta_{pq} - \frac{k_p k_q}{k^2}. \tag{2.45}$$

Inserting this into $\overleftrightarrow{F}(\omega_k/c, \boldsymbol{R})$, one arrives at

$$\overleftrightarrow{F_{pq}}(\omega_k/c, \boldsymbol{R}) = \int_0^{2\pi} d\phi_k \int_0^{\pi} d\theta_k e^{\imath \mathbf{k}\cdot\boldsymbol{R}} (\delta_{pq} - \frac{k_p k_q}{k^2}), \tag{2.46}$$

with the wave vector $\mathbf{k} = k(\sin\theta_k \cos\phi_k, \sin\theta_k \sin\phi_k, \cos\theta_k)$.
For $\boldsymbol{R} \neq 0$, we find

$$\begin{aligned}\overleftrightarrow{F_{pq}}(k,\boldsymbol{R}) =& 4\pi\{\delta_{pq}[(\frac{1}{kR} - \frac{1}{kR^3})\sin(kR) + \frac{1}{kR^2}\cos(kR)] \\ & - \frac{[\boldsymbol{R}]_p[\boldsymbol{R}]_q}{R^2}[(\frac{1}{kR} - 3\frac{1}{kR^3})\sin(kR) + \frac{3}{kR^3}\cos(kR)]\} \\ =& 4\pi \mathrm{Im}\{[\delta_{pq}(\frac{1}{kR} + \iota\frac{1}{kR^2} - \frac{1}{kR^3}) \\ & - \frac{[\boldsymbol{R}]_p[\boldsymbol{R}]_q}{R^2}(\frac{1}{kR} + \frac{3\iota}{kR^2} - \frac{3}{kR^3})]e^{\iota kR}\}. \end{aligned} \tag{2.47}$$

In the case of $\boldsymbol{R} = 0$, the tensor components are

$$\overleftrightarrow{F_{pq}}(k,0) = \frac{8}{3}\pi\delta_{pq}. \tag{2.48}$$

One can either directly integrate Eq. (2.46) or calculate the limit $\boldsymbol{R} \to 0$ in Eq. (2.47) in order to obtain the above result. Now we calculate the couplings for $\mu \neq \nu$ and give their physical interpretation.

The generalized decay rates are given by

$$\begin{aligned}\Gamma_{ij}^{\mu\nu} =& \frac{k^3}{16\epsilon_0\hbar\pi^2}[\boldsymbol{d}_i^T \overleftrightarrow{F}(k,\boldsymbol{R})\boldsymbol{d}_j^*] \\ =& \frac{3}{2}\frac{\sqrt{\gamma_i\gamma_j}}{|\boldsymbol{d}_i||\boldsymbol{d}_j|}\{\boldsymbol{d}_i \cdot \boldsymbol{d}_j^*[(\frac{1}{\eta} - \frac{1}{\eta^3})\sin\eta + \frac{1}{\eta^2}\cos\eta] \\ & - \frac{[\boldsymbol{d}_i \cdot \boldsymbol{R}][\boldsymbol{d}_j^* \cdot \boldsymbol{R}]}{R^2}[(\frac{1}{\eta} - \frac{3}{\eta^3})\sin\eta + \frac{3}{\eta^2}\cos\eta]\} \\ =& \frac{1}{\hbar}[\boldsymbol{d}_i^T \mathrm{Im}\overleftrightarrow{\mathcal{X}}(\boldsymbol{R})\boldsymbol{d}_{\mathrm{i}}^*], \end{aligned} \tag{2.49}$$

where $\eta = kR$ and $\mathrm{Im}\overleftrightarrow{\mathcal{X}}$ denotes the imaginary part of the tensor $\overleftrightarrow{\mathcal{X}}(\boldsymbol{R})$ whose components for $p, q \in \{1,2,3\}$ are given by

$$\begin{aligned}\overleftrightarrow{\mathcal{X}_{pq}}(\boldsymbol{R}) =& \frac{1}{4\pi\epsilon_0 R}[k^2\delta_{pq} + \frac{\partial^2}{\partial R_p \partial R_q}]e^{\iota\eta} \\ =& \frac{k^3}{4\pi\epsilon_0}[\delta_{pq}(\frac{1}{\eta} + \frac{\iota}{\eta^2} - \frac{1}{\eta^3}) - \frac{[\boldsymbol{R}]_p[\boldsymbol{R}]_q}{R^2}(\frac{1}{\eta} + \frac{3\iota}{\eta^2} - \frac{3}{\eta^3})]e^{\iota\eta}. \end{aligned} \tag{2.50}$$

In the above equation ∂R_p denotes the derivative with respect to spatial Cartesian component $R_p = [\boldsymbol{R}]_p$ of the vector $\boldsymbol{R}$.
Since the parameters $\Gamma_{ij}^{\mu\nu}$, $\mu \neq \nu$ are present only in collective systems, they can be interpreted as collective decay rates. The origin of these collective decay rates is the interaction between the dipoles that belong to different atoms. The spontaneous decay of one atom influences the spontaneous emission of the other atom. Such a coupling between the two atoms is induced by the vacuum.

We now turn to the other coupling constants $\Omega_{ij}^{\mu\nu} = P_{ij}^{\mu\nu} - M_{ij}^{\mu\nu}$ which occur in the second term in Eq. (2.39). They can be written as a sum of two integrals as follows:

$$\begin{aligned}\Omega_{ij}^{\mu\nu} =& \frac{1}{\hbar\epsilon_0(2\pi c)^3}\Big(\int_0^{\omega_C} d\omega_k \omega_k^2 [\boldsymbol{d}_i^T \overleftrightarrow{\mathcal{X}}(\boldsymbol{R})\boldsymbol{d}_j^*] \\ &+ \omega^2 \mathcal{P}\int_0^{\omega_C} d\omega_k [\boldsymbol{d}_i^T \overleftrightarrow{\mathcal{X}}(\boldsymbol{R})\boldsymbol{d}_j^*]\frac{\omega_k^2}{\omega_k^2-\omega^2}\Big).\end{aligned} \tag{2.51}$$

In the first part, there are no poles so $\mathcal{P}$ can be omitted. This integral gives

$$\frac{1}{\hbar}[\boldsymbol{d}_i^T\Big(\frac{1}{4\pi\epsilon_0 R^3}\Big(\frac{3[\boldsymbol{R}]_p[\boldsymbol{R}]_q}{R^2} - \delta_{pq}\Big)\Big)\boldsymbol{d}_j^*] \tag{2.52}$$

and represents the interaction of two static dipoles.

We now turn to the second integral and use the residue theorem $\tau > 0$ to find out the following relevant principal value integrals, which are required for the calculation of the second integral. Since the cutoff frequency ω_C is much larger than the mean transition frequency ω, the upper limit of the integration can be extended to infinity.

$$\begin{aligned}\mathcal{P}\int_0^{\infty} d\omega_k \frac{\omega_k}{\omega_k^2-\omega^2}\sin(\omega_k\tau) &= \frac{\pi}{2}\cos(\omega\tau),\\ \mathcal{P}\int_0^{\infty} d\omega_k \frac{\omega_k}{\omega_k(\omega_k^2-\omega^2)}\sin(\omega_k\tau) &= -\frac{\pi}{2}\omega^2(1-\cos(\omega\tau)),\\ \mathcal{P}\int_0^{\infty} d\omega_k \frac{\omega_k}{\omega_k^2-\omega^2}\cos(\omega_k\tau) &= -\frac{\pi}{2}\omega\sin(\omega\tau).\end{aligned} \tag{2.53}$$

Finally, after the evaluation of both the integrals and substitution into Eq. (2.51), we arrive at

$$\Omega_{ij}^{\mu\nu} = \frac{1}{\hbar}[\boldsymbol{d}_i^T \mathrm{Re}(\overleftrightarrow{\mathcal{X}})\boldsymbol{d}_j^*], \tag{2.54}$$

where $\mathrm{Re}(\overleftrightarrow{\mathcal{X}})$ denotes the real part of the tensor $\overleftrightarrow{\mathcal{X}}$. Explicitly, the above equation can be written as

$$\begin{aligned}\Omega_{ij}^{\mu\nu} = \frac{3}{2}\frac{\sqrt{\gamma_i\gamma_j}}{|\boldsymbol{d}_i||\boldsymbol{d}_j|}\{\boldsymbol{d}_i\cdot\boldsymbol{d}_j^*[(\frac{1}{\eta}-\frac{1}{\eta^3})\cos\eta - \frac{1}{\eta^2}\sin\eta] \\ - \frac{[\boldsymbol{d}_i\cdot\boldsymbol{R}][\boldsymbol{d}_j^*\cdot\boldsymbol{R}]}{R^2}[(\frac{1}{\eta}-\frac{3}{\eta^3})\cos\eta - \frac{3}{\eta^2}\sin\eta]\}.\end{aligned} \tag{2.55}$$

These parameters describe a coherent interaction between two dipoles of different atoms. This interaction arises solely from the vacuum-mediated coupling between different atoms.

The number of independent coupling constants in the final master equation can be reduced by using the symmetry relation $\overleftrightarrow{\mathcal{X}}(-\boldsymbol{R}) = \overleftrightarrow{\mathcal{X}}(\boldsymbol{R})$.

This implies that:

$$\Gamma_{ij}^{\mu\nu} = \Gamma_{ij}^{\nu\mu} = (\Gamma_{ij}^{\mu\nu})^* = (\Gamma_{ij}^{\nu\mu})^* \qquad \text{and} \qquad \Omega_{\mathrm{ij}}^{\mu\nu} = \Omega_{\mathrm{ij}}^{\nu\mu} = (\Omega_{\mathrm{ij}}^{\mu\nu})^* = (\Omega_{\mathrm{ij}}^{\nu\mu})^*. \tag{2.56}$$

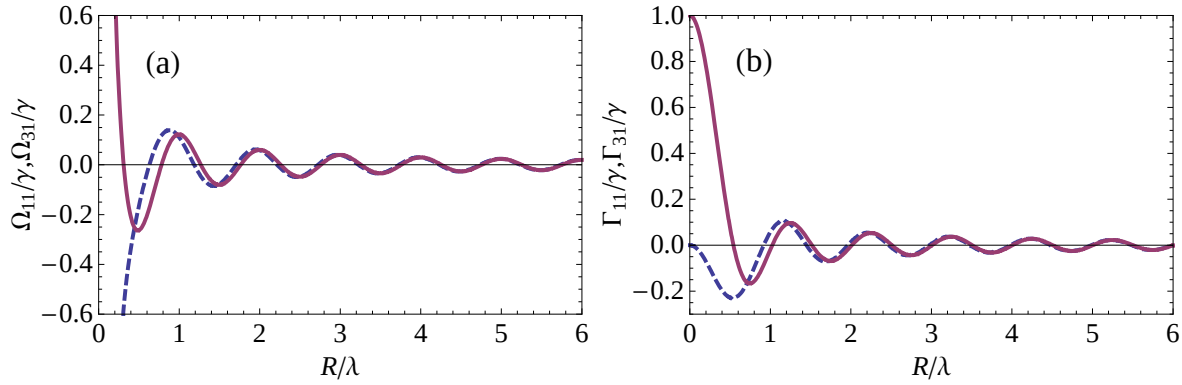

Figure 2.3: The parameters are $\theta = \pi/2$, $\phi = 0$. (a) Plot of dipole dipole coupling constants. Ω_{11} is shown by solid line and Ω_{31} by a dashed one. λ is the mean transition wavelength. Ω_{11} and Ω_{31} diverge in the limit $R \to 0$. (b) Plot of the collective decay rates. The solid line shows Γ_{11} and dashed one manifests Γ_{31}. Γ_{11} and Γ_{31} remain finite in the limit $R \to 0$.

From the above equations, it is evident that the parameters $\Gamma_{ii}^{\nu\mu}$ and $\Omega_{ii}^{\nu\mu}$ are real. Since the system under consideration consists of two atoms, whose relative position is described by a single separation vector $\boldsymbol{R}$, we can omit the superscripts μ and ν and denote the parameters $\Gamma_{ij}^{\nu\mu}$ and $\Omega_{ij}^{\nu\mu}$ by Γ_{ij} and Ω_{ij}, respectively.
$\mathcal{H}_\Omega$ in Eq. (2.40) can now be written as

$$\mathcal{H}_\Omega = -\hbar\sum_{i=1}^{3}\{\Omega_{ii}S_{i+}^{(2)}S_{i-}^{(1)} + H.c.\} - \hbar\{\Omega_{21}(S_{2+}^{(2)}S_{1-}^{(1)} + S_{2+}^{(1)}S_{1-}^{(2)}) + H.c.\} - \hbar\{\Omega_{31}(S_{3+}^{(2)}S_{1-}^{(1)} + S_{3+}^{(1)}S_{1-}^{(2)}) + H.c.\} - \hbar\{\Omega_{32}(S_{3+}^{(2)}S_{2-}^{(1)} + S_{3+}^{(1)}S_{2-}^{(2)}) + H.c.\}. \tag{2.57}$$

Similarly Eq. (2.41) becomes

$$\begin{aligned}\mathcal{L}_\gamma\tilde{\varrho}_a(t) = &-\sum_{\mu=1}^{2}\sum_{i=1}^{3}\gamma_i(S_{i+}^{(\mu)}S_{i-}^{(\mu)}\varrho + \varrho S_{i+}^{(\mu)}S_{i-}^{(\mu)} - 2S_{i-}^{(\mu)}\varrho S_{i+}^{(\mu)}) - \sum_{i=1}^{3}\{\Gamma_{ii}(S_{i+}^{(2)}S_{i-}^{(1)}\varrho + \varrho S_{i+}^{(2)}\tilde{S}_{i-}^{(1)} \\ &- 2S_{i-}^{(1)}\varrho S_{i+}^{(2)}) + H.c.\} - \sum_{\substack{\mu,\nu=1\\ \mu\neq\nu}}^{2}\{\Gamma_{21}(S_{2+}^{(\mu)}S_{1-}^{(\nu)}\varrho + \varrho S_{2+}^{(\mu)}S_{1-}^{(\nu)} - 2S_{1-}^{(\nu)}\varrho S_{2+}^{(\mu)}) + \Gamma_{31}(S_{3+}^{(\mu)} \\ &S_{1-}^{(\nu)}\varrho + \varrho S_{3+}^{(\mu)}S_{1-}^{(\nu)} - 2S_{1-}^{(\nu)}\varrho S_{3+}^{(\mu)}) + \Gamma_{32}(S_{3+}^{(\mu)}S_{2-}^{(\nu)}\varrho + \varrho S_{3+}^{(\mu)}S_{2-}^{(\nu)} - 2S_{2-}^{(\nu)}\varrho S_{3+}^{(\mu)}) + H.c.\}.\end{aligned} \tag{2.58}$$

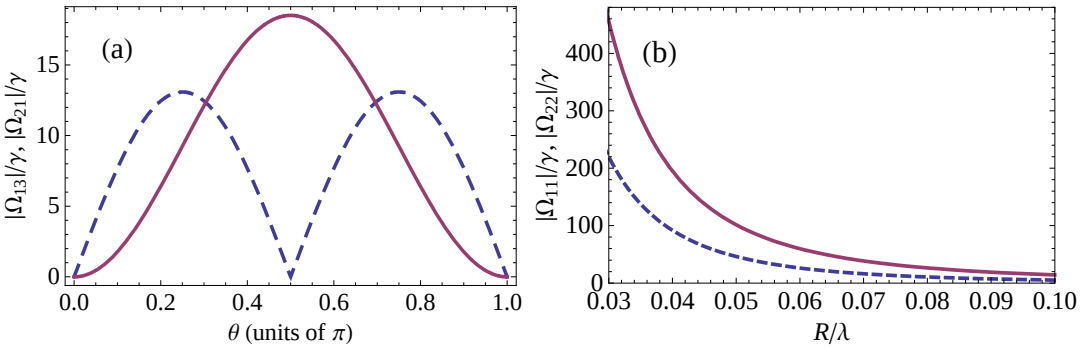

Figure 2.4: (a) Magnitude of few orthogonal dipole-dipole coupling constants. The parameters are $r = 0.08\lambda$ and $\phi = \pi/2$. The solid curve shows $|\Omega_{13}|$, while the dashed curve depicts $|\Omega_{21}| = |\Omega_{32}|$. (b) Magnitude of few parallel dipole-dipole coupling constants at $\theta = \pi$. The solid line shows $|\Omega_{22}|$, and the dashed line depicts $|\Omega_{11}| = |\Omega_{33}|$.

The different Ω_{ij} are as follows.

$$\Omega_{31} = \gamma\frac{3}{4\eta^3}[(\eta^2-3)\cos\eta - 3\eta\sin\eta]\sin^2\theta e^{-2\iota\phi}. \tag{2.59}$$

$$\Omega_{11} = 3\frac{\gamma}{8\eta^3}\{[3\eta^2-1+(\eta^2-3)\cos 2\theta]\cos\eta - \eta(1+3\cos 2\theta)\sin\eta\}. \tag{2.60}$$

$$\Omega_{21} = -\sqrt{2}\cot\theta\Omega_{31}e^{\iota\phi}. \tag{2.61}$$

$$\Omega_{22} = \Omega_{11} - (2\cot^2\theta - 1)\Omega_{31}e^{2\iota\phi}. \tag{2.62}$$

$$\Omega_{32} = -\Omega_{21}, \quad \Omega_{33} = \Omega_{11}. \tag{2.63}$$

The collective decay rates are as under.

$$\Gamma_{31} = \gamma\frac{3}{4\eta^3}[(\eta^2-3)\sin\eta + 3\eta\cos\eta]\sin^2\theta e^{-2\iota\phi}. \tag{2.64}$$

$$\Gamma_{11} = 3\frac{\gamma}{8\eta^3}\{[3\eta^2-1+(\eta^2-3)\cos 2\theta]\sin\eta + \eta(1+3\cos 2\theta)\cos\eta\}. \tag{2.65}$$

$$\Gamma_{21} = -\sqrt{2}\cot\theta\Gamma_{31}e^{\iota\phi}. \tag{2.66}$$

$$\Gamma_{22} = \Gamma_{11} - (2\cot^2\theta - 1)\Gamma_{31}e^{2\iota\phi}. \tag{2.67}$$

$$\Gamma_{32} = -\Gamma_{21}, \quad \Gamma_{33} = \Gamma_{11}. \tag{2.68}$$

From the above equations it is obvious that only $\Omega_{11}, \Omega_{31}, \Gamma_{11}$ and Γ_{31} are independent. All the others can be expressed in terms of these. Fig. (2.2) show some parallel and orthogonal dipole dipole coupling constants as they occur in the system. Fig. (2.3) and Fig. (2.4) show the dependence of some parallel and orthogonal dipole dipole coupling constants on θ or $\boldsymbol{R}$.

In the next section, we outline the calculation of the interaction Hamiltonian with respect to the laser field.

2.6 Atom-Laser Interaction

So far we have only considered the interaction of the bi-atomic system with the vacuum field. Now we include an external driving laser field. We assume that the Rabi frequencies and the detunings associated with the laser feild are much smaller than the mean transition frequency ω_0. In this case, it is justified to assume that the atom-vacuum interaction is not affected by the presence of the laser field [31]. The laser field is assumed to be polarized along z-axis. Its electric field is given by

$$\boldsymbol{E}_L = \mathcal{E}_z \mathbf{e}_z e^{\iota \boldsymbol{k}_L \cdot \mathbf{r}} e^{-\iota \omega_L t} + \text{c.c.}\,, \tag{2.69}$$

where $\mathcal{E}_z$ denotes the amplitude, ω_L the frequency, and $\boldsymbol{e}_z$ is the polarization of the field, and c.c. denotes the complex conjugate. The wave vector $\boldsymbol{k}_L$ with wave number $k_L = 2\pi/\lambda$ points along the positive x-axis. We would like to work in the interaction Hamiltonian in a suitable rotating frame.

We define

$$\mathcal{H}_x = \hbar \sum_{\mu=1}^{2} \sum_{i=1}^{3} (x_i S_{i+}^{(\mu)} S_{i-}^{(\mu)} + H.c.), \tag{2.70}$$

$$\mathcal{H}_{x,a} = \mathcal{H}_x + \mathcal{H}_a = \hbar \sum_{\mu=1}^{2} \sum_{i=1}^{3} ((x_i + \omega_i) S_{i+}^{(\mu)} S_{i-}^{(\mu)} + H.c.), \tag{2.71}$$

$$\mathcal{H}_{x,L} = \mathcal{H}_L - \mathcal{H}_x. \tag{2.72}$$

By these definitions, the sum $\mathcal{H}_{a,L}$ remains unaltered.

$$\mathcal{H}_{a,L} = \mathcal{H}_a + \mathcal{H}_L = \mathcal{H}_{x,a} + \mathcal{H}_{x,L} \tag{2.73}$$

In the following, we will make a choice for x_i in such a way that there remains no explicit time dependence in the interaction Hamiltonian. In a rotating frame defined by the unitary transformation

$$U = e^{-\iota \mathcal{H}_{x,a} t/\hbar}, \tag{2.74}$$

the atom-laser interaction is governed by

$$\tilde{\mathcal{H}}_{x,L} = U \mathcal{H}_{x,L} U^\dagger = \tilde{\mathcal{H}}_L - \tilde{\mathcal{H}}_x \qquad \text{where}$$

$$\tilde{\mathcal{H}}_L = -\hbar \sum_{\mu=1}^{2} (\Omega(\mathbf{r}_\mu) \tilde{S}_{2+}^{(\mu)} + H.c.) \qquad \text{and}$$

$$\tilde{\mathcal{H}}_x = \hbar \sum_{\mu=1}^{2} \sum_{i=1}^{3} \Delta_i \tilde{S}_{i+}^{(\mu)} \tilde{S}_{i-}^{(\mu)} \tag{2.75}$$

when we choose $x_1 = \Delta_1$, $x_2 = \Delta_2$, $x_3 = \Delta_3$ and $x_4 = 0$. $\Delta_i = \omega_L - \omega_i$ denote the laser detunings and $\Delta_i = \Delta_{i+1} + \delta$. δ is the frequency difference between consecutive excited energy levels. The position dependent Rabi frequencies are defined by

$$\Omega(\mathbf{r}_\mu) = \Omega \sin(\boldsymbol{k} \cdot \mathbf{r}_\mu), \tag{2.76}$$

since we assume the stationary driving field to be sinusoidal and

$$\Omega = \mathcal{D}\mathcal{E}_z/\hbar. \tag{2.77}$$

$\boldsymbol{k}$ and ω_L are the wave vectors and frequencies of the driving field. Due to its polarization, the laser field couples only to the $|2\rangle \leftrightarrow |4\rangle$ transitions in the two atoms, see Eq. (2.9).

Now there is no time dependence in the interaction Hamiltonian, the system reaches a steady state if we wait for a considerably long time.

We assume the energy difference δ to be zero. This means that we apply no external magnetic field. In this scenario, the laser detunings become equal and all the transition frequencies reach their mean value ω_0.

Chapter 3

Resonance Fluorescence Intensity and Resonance Fluorescence Spectrum

3.1 Introduction

In our endeavor to describe the bi-atomic system, we exploit the intensity and spectrum of the fluorescent light emitted by the atoms as the observables. This is because of the advantage that resonance fluorescence can be observed in the far field, and distance determination via fluorescence is not affected by the usual resolution limitations since the distance information is encoded in the frequency spectrum of the emitted light. In the following sections, *i.e.*, Sec. 3.2 and Sec. 3.3 we explain the intensity and spectrum, respectively in detail. Sec. 3.4 explains the calculation of incoherent spectral components using *Quantum Regression Theorem*. Finally, in Sec. 3.5 we show how we implemented the calculations to our system and for this purpose, we will explain the notation in which our basis states are defined. Since long time behavior of the system is considered, the density matrix evolves in a time-independent steady state. The calculation of steady state will also be explained at the end of this chapter.

3.2 Resonance Fluorescence Intensity

In this section, we present the calculation of our observables. We derive the resonance fluorescence intensity in terms of the atomic raising and lowering operators $\tilde{S}_{i+}^{(\mu)}$ and $\tilde{S}_{j-}^{(\nu)}$, respectively.

The total resonance fluorescence intensity is given by one-time normally ordered correlation function of the electric field operators.

$$\mathbf{I_{st}} = \langle \hat{\mathbf{E}}^{(-)}(\mathbf{r}, t) \cdot \hat{\mathbf{E}}^{(+)}(\mathbf{r}, t) \rangle_{\mathbf{st}}, \tag{3.1}$$

where **st** denotes the steady state. $\hat{\mathbf{E}}^{(-)}[\hat{\mathbf{E}}^{(+)}]$ is the negative [positive] frequency part of the field operators. In the far field zone, the negative frequency part can be calculated as

$$\hat{\mathbf{E}}^{(-)}(\mathbf{r},t) = \hat{\mathbf{E}}^{(-)}_{free}(\mathbf{r},t) - \frac{1}{4\pi\epsilon_0 c^2 r}\sum_{i=1}^{4}\omega_i^2\hat{\mathbf{r}}\times(\hat{\mathbf{r}}\times\boldsymbol{d}_i)\widetilde{S}_{i+}(\hat{t})e^{\iota\omega_L\hat{t}}, \tag{3.2}$$

where $\hat{t} = t - \dfrac{r}{c}$ is the retarded time, $\mathbf{r} = r\hat{\mathbf{r}}$ denotes the position of the photon detector and $\widetilde{S}_{i\pm}(t) = \exp(\mp\iota\omega_L t)\tilde{S}_{i\pm}(t)$. The first term indicates the negative frequency part of the free field and if the point of observation lies outside the driving field, its contribution to the resonance fluorescence is zero [32]. The second atom describes the retarded dipole field generated by the atom situated at the origin. The positive frequency part can be found out by the Hermitian conjugation of $\hat{\mathbf{E}}^{(-)}(\mathbf{r},t)$.

We define Ξ as the cross product factor:

$$\Xi(\boldsymbol{d}_i,\hat{\mathbf{r}}) = \hat{\mathbf{r}}\times(\hat{\mathbf{r}}\times\boldsymbol{d}_i). \tag{3.3}$$

The transition operators can be decomposed into mean values and fluctuations as follows,

$$\tilde{S}^{(\mu)}_{i\pm} = \langle\tilde{S}^{(\mu)}_{i\pm}\rangle_{\mathbf{st}}\mathbf{1} + \delta\tilde{S}^{(\mu)}_{i\pm}, \tag{3.4}$$

where $\mathbf{1} = \mathbf{1}_1\otimes\mathbf{1}_2$ and $\mathbf{1}_\mu$ is the identity operator in the subspace of the atom μ.

The mean values of Eq. (3.4) give the coherent intensity and the incoherent part of the intensity is determined by the fluctuations. Mathematical expressions for both can be calculated using Eq. (3.1)- (3.4) and are given below.

$$\mathbf{I}_{coh} = (-\frac{\omega_0^2}{4\pi\epsilon_0 r c^2})^2\sum_{\mu,\nu=1}^{2}\sum_{i,j=1}^{3}\Xi(\boldsymbol{d}_i,\hat{\mathbf{r}})\Xi^*(\boldsymbol{d}_j,\hat{\mathbf{r}})\langle\tilde{S}^{(\mu)}_{i+}(t)\rangle_{\mathbf{st}}\langle\tilde{S}^{(\nu)}_{j-}(t)\rangle_{\mathbf{st}}e^{\iota k_0\hat{\mathbf{r}}\cdot(\mathbf{r}_\mu-\mathbf{r}_\nu)}, \tag{3.5}$$

and

$$\mathbf{I}_{inc} = (-\frac{\omega_0^2}{4\pi\epsilon_0 r c^2})^2\sum_{\mu,\nu=1}^{2}\sum_{i,j=1}^{3}\Xi(\boldsymbol{d}_i,\hat{\mathbf{r}})\Xi^*(\boldsymbol{d}_j,\hat{\mathbf{r}})\langle\delta\tilde{S}^{(\mu)}_{i+}(t)\delta\tilde{S}^{(\nu)}_{j-}(t)\rangle_{\mathbf{st}}e^{\iota k_0\hat{\mathbf{r}}\cdot(\mathbf{r}_\mu-\mathbf{r}_\nu)}, \tag{3.6}$$

where the subscripts *coh* [*inc*] denote coherent [incoherent], respectively. The cross product factors $\Xi(\boldsymbol{d}_i,\hat{\mathbf{r}})$ determine whether the resonance fluorescence spectrum can be separated into different polarizations. A separation of the light emitted by the dipole $\boldsymbol{d}_i$ and $\boldsymbol{d}_j$ is possible, if and only if, the product of the cross product factors $\Xi(\boldsymbol{d}_i,\hat{\mathbf{r}})\Xi^*(\boldsymbol{d}_j,\hat{\mathbf{r}})$ vanishes. In the following, the point of observation is assumed to be along the z direction for the resonance fluorescence intensity, and along the y or $-x$ direction for the resonance fluorescence spectrum. Evaluating these cross products using Eq. (2.9), we find that our choice of observation direction enables us to separate linearly polarized light emitted on transitions $|2\rangle\leftrightarrow|4\rangle$ from the circularly polarized light emitted on transitions $|i\rangle\leftrightarrow|4\rangle$ ($i\in\{1,3\}$) by means of a polarization analyzer. The light emitted by $\boldsymbol{d}_2$ is polarized in z-direction whereas the light emitted by $\boldsymbol{d}_1$ and $\boldsymbol{d}_3$ is x-polarized. We designate linearly [circularly] polarized spectra as π [σ] ones, respectively.

3.2.1 Resonance Fluorescence Intensity: x Polarized Light

We are interested in the intensity of the light polarized in the x-direction, *i.e.*, the intensity of the fluorescent light emitted by the dipole moments $\boldsymbol{d}_1$ and $\boldsymbol{d}_3$. The total σ intensity is given by

$$\mathbf{I}^{\sigma} = \frac{\Phi_{\sigma}}{\pi} \sum_{\mu,\nu=1}^{2} \sum_{\substack{i,j=1 \\ i,j\neq 2}}^{3} \langle \tilde{S}_{i+}^{(\mu)}(t) \tilde{S}_{j-}^{(\nu)}(t) \rangle_{\mathbf{st}} e^{\iota k_0 \hat{\mathbf{r}}\cdot(\mathbf{r}_{\mu}-\mathbf{r}_{\nu})}. \tag{3.7}$$

In the above equation, $\Phi_{\sigma} = (-\frac{\omega_0^2}{4\pi\epsilon_0 r c^2})^2 \Xi(\boldsymbol{d}_i, \hat{\mathbf{r}}) \Xi^*(\boldsymbol{d}_j, \hat{\mathbf{r}})$, where $i, j \in \{1, 3\}$. Φ_{σ} is a geometrical factor which is constant in this situation since the detector is assumed to be at a fixed point. We have set this prefactor equal to unity in our numerical calculation.

We have placed a detector in the z-direction in order to observe the σ intensity because there is no σ intensity observed in the y-direction. We could also place the detector for the observation of the σ intensity in x-direction but we want to avoid such a setup. Since the incident laser light propagates in x-direction, there is a possibility that the detector fixed in x-direction may also observe it which is not desired.

Φ_{σ} contains the cross product factors which, for such a geometry are given by

$$\Xi(\boldsymbol{d}_i, \hat{\mathbf{r}}) \Xi^*(\boldsymbol{d}_j, \hat{\mathbf{r}}) = \begin{cases} \mathcal{D}^2 & \text{if } i = j, \\ 0 & \text{if } i \neq j. \end{cases} \tag{3.8}$$

In the following, we give the mathematical expressions for the calculation of the coherent and incoherent parts of the σ intensity.

$$\mathbf{I}_{coh}^{\sigma} = \frac{\Phi_{\sigma}}{\pi} \sum_{\mu,\nu=1}^{2} \sum_{\substack{i,j=1 \\ i,j\neq 2}}^{3} \langle \tilde{S}_{i+}^{(\mu)}(t) \rangle_{\mathbf{st}} \langle \tilde{S}_{j-}^{(\nu)}(t) \rangle_{\mathbf{st}} e^{\iota k_0 \hat{\mathbf{r}}\cdot(\mathbf{r}_{\mu}-\mathbf{r}_{\nu})}. \tag{3.9}$$

$$\mathbf{I}_{inc}^{\sigma} = \frac{\Phi_{\sigma}}{\pi} \sum_{\mu,\nu=1}^{2} \sum_{\substack{i,j=1 \\ i,j\neq 2}}^{3} \langle \delta\tilde{S}_{i+}^{(\mu)}(t) \delta\tilde{S}_{j-}^{(\nu)}(t) \rangle_{\mathbf{st}} e^{\iota k_0 \hat{\mathbf{r}}\cdot(\mathbf{r}_{\mu}-\mathbf{r}_{\nu})}. \tag{3.10}$$

3.2.2 Resonance Fluorescence Intensity: z Polarized Light

The π intensity and its coherent and incoherent components are as under.

$$\mathbf{I}^{\pi} = \frac{\Phi_{\pi}}{\pi} \sum_{\mu,\nu=1}^{2} \langle \tilde{S}_{2+}^{(\mu)}(t) \tilde{S}_{2-}^{(\nu)}(t) \rangle_{\mathbf{st}} e^{\iota k_0 \hat{\mathbf{r}}\cdot(\mathbf{r}_{\mu}-\mathbf{r}_{\nu})}. \tag{3.11}$$

$$\mathbf{I}_{coh}^{\pi} = \frac{\Phi_{\pi}}{\pi} \sum_{\mu,\nu=1}^{2} \langle \tilde{S}_{2+}^{(\mu)}(t) \rangle_{\mathbf{st}} \langle \tilde{S}_{2-}^{(\nu)}(t) \rangle_{\mathbf{st}} e^{\iota k_0 \hat{\mathbf{r}}\cdot(\mathbf{r}_{\mu}-\mathbf{r}_{\nu})}. \tag{3.12}$$

$$\mathbf{I}^{\pi}_{inc} = \frac{\Phi_\pi}{\pi} \sum_{\mu,\nu=1}^{2} \langle \delta\tilde{S}^{(\mu)}_{2+}(t)\delta\tilde{S}^{(\nu)}_{2-}(t)\rangle_{\mathbf{st}} e^{\iota k_0 \hat{\mathbf{r}}\cdot(\mathbf{r}_\mu - \mathbf{r}_\nu)}. \tag{3.13}$$

In the above equation, $\Phi_\pi = (-\frac{\omega_0^2}{4\pi\epsilon_0 r c^2})^2 \Xi(\boldsymbol{d}_2, \hat{\mathbf{r}})\Xi^*(\boldsymbol{d}_2, \hat{\mathbf{r}})$. Just like Φ_σ, Φ_π is also a constant prefactor.

Now we turn to our second observable, which is the spectrum of fluorescent light.

3.3 Resonance Fluorescence Spectrum

The total resonance fluorescence spectrum $S(\tilde{\omega})$ up to a geometrical factor is given by the real part of the Fourier transform of the two-time correlation function of the electric field operators [27],

$$S(\tilde{\omega}) = \mathrm{Re} \int_{-\infty}^{\infty} e^{-\iota\tilde{\omega}\tau} \langle \hat{\mathbf{E}}^{(-)}(\mathbf{r}, t+\tau) \cdot \hat{\mathbf{E}}^{(+)}(\mathbf{r}, t)\rangle_{\mathbf{st}} d\tau, \tag{3.14}$$

where $\tilde{\omega} = \omega - \omega_L$ is the observed frequency minus the laser frequency and $\hat{\mathbf{E}}^{(-)}[\hat{\mathbf{E}}^{(+)}]$ have already been defined in Eq. (3.2).

Using Eq. (3.4), the resonance fluorescence spectrum can also be decomposed into a coherent and an incoherent part. The coherent part is given by the mean values and can be written as

$$\begin{aligned} S(\tilde{\omega})_{coh} = (-\frac{\omega_0^2}{4\pi\epsilon_0 r c^2})^2 \int_0^{\infty} e^{-\iota\tilde{\omega}\tau} \sum_{\mu,\nu=1}^{2} \sum_{i,j=1}^{3} \Xi(\boldsymbol{d}_i, \hat{\mathbf{r}})\Xi^*(\boldsymbol{d}_j, \hat{\mathbf{r}}) \langle S^{(\mu)}_{i+}(t+\tau)\rangle_{\mathbf{st}} \langle S^{(\nu)}_{j-}(t)\rangle_{\mathbf{st}} \\ \times e^{\iota k_0 \hat{\mathbf{r}}\cdot(\mathbf{r}_\mu - \mathbf{r}_\nu)} d\tau. \end{aligned} \tag{3.15}$$

The incoherent spectrum contains the fluctuation parts of the atomic transition operators and is given by

$$\begin{aligned} S(\tilde{\omega})_{inc} = (-\frac{\omega_0^2}{4\pi\epsilon_0 r c^2})^2 \int_0^{\infty} e^{-\iota\tilde{\omega}\tau} \sum_{\mu,\nu=1}^{2} \sum_{i,j=1}^{3} \Xi(\boldsymbol{d}_i, \hat{\mathbf{r}})\Xi^*(\boldsymbol{d}_j, \hat{\mathbf{r}}) \langle \delta S^{(\mu)}_{i+}(t+\tau)\delta S^{(\nu)}_{j-}(t)\rangle_{\mathbf{st}} \\ \times e^{\iota k_0 \hat{\mathbf{r}}\cdot(\mathbf{r}_\mu - \mathbf{r}_\nu)} d\tau. \end{aligned} \tag{3.16}$$

As discussed in Sec. 3.2, the spectrum of fluorescent light can also be split into π and σ parts.

3.3.1 Spectrum of Resonance Fluorescence: z Polarized Light

We place the detector in the y-direction. The cross products $\Xi(\boldsymbol{d}_i, \hat{\mathbf{r}})\Xi^*(\boldsymbol{d}_j, \hat{\mathbf{r}})$ where $i \in \{1, 3\}$ and $j = 2$ are zero.

The total spectrum of resonance fluorescence emitted by the dipoles with z-polarized light is given by

$$S(\tilde{\omega})^{\pi}_{tot} = \frac{\Phi_{\pi}}{\pi}\int_0^{\infty} e^{-\iota\tilde{\omega}\tau}\sum_{\mu,\nu=1}^{2}\langle\tilde{S}^{(\mu)}_{2+}(t+\tau)\tilde{S}^{(\nu)}_{2-}(t)\rangle_{\mathbf{st}}e^{\iota k_0\hat{\mathbf{r}}\cdot(\mathbf{r}_{\mu}-\mathbf{r}_{\nu})}d\tau, \tag{3.17}$$

where $\Xi(\boldsymbol{d}_2,\hat{\mathbf{r}})\Xi^*(\boldsymbol{d}_2,\hat{\mathbf{r}}) = \mathcal{D}^2$.

Now we give the expressions for the coherent part of the π spectrum.

$$S(\tilde{\omega})^{\pi}_{coh} = \frac{1}{\pi}\int_0^{\infty} e^{-\iota\tilde{\omega}\tau}\sum_{\mu,\nu=1}^{2}\langle\tilde{S}^{(\mu)}_{2+}\rangle_{\mathbf{st}}\langle\tilde{S}^{(\nu)}_{2-}\rangle_{\mathbf{st}}e^{\iota k_0\hat{\mathbf{r}}\cdot(\mathbf{r}_{\mu}-\mathbf{r}_{\nu})}d\tau. \tag{3.18}$$

This can be expressed in terms of coherent resonance fluorescence π intensity (Eq. (3.12)) as

$$\begin{aligned} S(\tilde{\omega})^{\pi}_{coh} &= \frac{1}{\pi}\int_0^{\infty} e^{-\iota\tilde{\omega}\tau}\mathbf{I}^{\pi}_{coh}d\tau \\ &= \delta(\tilde{\omega})\mathbf{I}^{\pi}_{coh}. \end{aligned} \tag{3.19}$$

This means that the coherent part of the π spectrum is a δ function centered at the frequency $\tilde{\omega} = 0$ multiplied by coherently emitted π intensity.

Our interest chiefly lies in the calculating of the incoherent, inelastic spectral components as we found above that the coherent part is just a δ function times the coherent intensity. In the following, we will discuss the incoherent part of the spectrum and the actual calculation will be presented in Sec. 3.4.

The incoherent π spectrum is given by

$$S(\tilde{\omega})^{\pi}_{inc} = \frac{\Phi_{\pi}}{\pi}\int_0^{\infty} e^{-\iota\tilde{\omega}\tau}\sum_{\mu,\nu=1}^{2}\langle\delta\tilde{S}^{(\mu)}_{2+}(t+\tau)\delta\tilde{S}^{(\nu)}_{2-}(t)\rangle_{\mathbf{st}}e^{\iota k_0\hat{\mathbf{r}}\cdot(\mathbf{r}_{\mu}-\mathbf{r}_{\nu})}d\tau. \tag{3.20}$$

The required vectors in order to evaluate the above equation are $\tilde{S}^{(1)}_{2+}$, $\tilde{S}^{(1)}_{2-}$, $\tilde{S}^{(2)}_{2+}$ and $\tilde{S}^{(2)}_{2-}$. Four different combinations of the these operators are required in order to evaluate the incoherent π spectrum.

3.3.2 Spectrum of Resonance Fluorescence: x Polarized Light

The total spectrum of resonance fluorescence emitted by the dipoles with x-polarized light is given by

$$S(\tilde{\omega})^{\sigma}_{tot} = \frac{\Phi_{\sigma}}{\pi}\int_0^{\infty} e^{-\iota\tilde{\omega}\tau}\sum_{\mu,\nu=1}^{2}\sum_{\substack{i,j=1\\ i,j\neq 2}}^{3}\langle\tilde{S}^{(\mu)}_{i+}(t+\tau)\tilde{S}^{(\nu)}_{j-}(t)\rangle_{\mathbf{st}}e^{\iota k_0\hat{\mathbf{r}}\cdot(\mathbf{r}_{\mu}-\mathbf{r}_{\nu})}d\tau, \tag{3.21}$$

where

$$\Xi(\boldsymbol{d}_i,\hat{\mathbf{r}})\Xi^*(\boldsymbol{d}_j,\hat{\mathbf{r}}) = \begin{cases} +\mathcal{D}^2/2 & \text{if } i=j, \\ -\mathcal{D}^2/2 & \text{if } i\neq j. \end{cases} \tag{3.22}$$

Now we give the expressions for the coherent part of the σ spectrum.

$$S(\tilde{\omega})^{\sigma}_{coh} = \frac{\Phi_\sigma}{\pi}\int_0^\infty e^{-\iota\tilde{\omega}\tau}\sum_{\mu,\nu=1}^{2}\sum_{\substack{i,j=1\\ i,j\neq 2}}^{3}\langle\tilde{S}^{(\mu)}_{i+}\rangle_{\mathbf{st}}\langle\tilde{S}^{(\nu)}_{j-}\rangle_{\mathbf{st}}e^{\iota k_0\hat{\mathbf{r}}\cdot(\mathbf{r}_\mu-\mathbf{r}_\nu)}d\tau. \tag{3.23}$$

This can be expressed in terms of coherent resonance fluorescence σ intensity (see Eq. (3.9)) as

$$\begin{aligned} S(\tilde{\omega})^{\sigma}_{coh} &= \frac{1}{\pi}\int_0^\infty e^{-\iota\tilde{\omega}\tau}\mathbf{I}^{\sigma}_{coh}d\tau \\ &= \delta(\tilde{\omega})\mathbf{I}^{\sigma}_{coh}. \end{aligned} \tag{3.24}$$

Just like the π spectrum, the coherent part of the σ spectrum is a δ function at $\tilde{\omega}=0$ multiplied by coherently emitted σ intensity.

The incoherent σ spectrum is given by

$$S(\tilde{\omega})^{\sigma}_{inc} = \frac{\Phi_\sigma}{\pi}\int_0^\infty e^{-\iota\tilde{\omega}\tau}\sum_{\mu,\nu=1}^{2}\sum_{\substack{i,j=1\\ i,j\neq 2}}^{3}\langle\delta\tilde{S}^{(\mu)}_{i+}(t+\tau)\delta\tilde{S}^{(\nu)}_{j-}(t)\rangle_{\mathbf{st}}e^{\iota k_0\hat{\mathbf{r}}\cdot(\mathbf{r}_\mu-\mathbf{r}_\nu)}d\tau. \tag{3.25}$$

The eight transition operators required in order to evaluate the above equation are $\tilde{S}^{(1)}_{1+}, \tilde{S}^{(1)}_{1-}, \tilde{S}^{(1)}_{3+}, \tilde{S}^{(1)}_{3-}, \tilde{S}^{(2)}_{1+}, \tilde{S}^{(2)}_{1-}, \tilde{S}^{(2)}_{3+}$ and $\tilde{S}^{(2)}_{3-}$. There will be 16 terms in the incoherent σ spectrum as different combinations of the above operators.

Having given the mathematical expressions for different incoherent parts of the spectrum, we now show how they can actually be calculated using quantum regression theorem.

3.4 Calculation for the Incoherent Spectral Components

In the studies of spectral density, two-time correlation functions are involved. Using the *Markovian approximation*, the two time correlation function can be evaluated if one knows the single time expectation values.The correlation functions involving two-time averages which need to be evaluated are stated below.

$$\int_0^\infty e^{-\iota\tilde{\omega}\tau}\langle\delta\tilde{S}^{(\mu)}_{i+}(t+\tau)\delta\tilde{S}^{(\nu)}_{j-}(t)\rangle_{st}d\tau. \tag{3.26}$$

We employ the generalized Bloch equations and *quantum regression theorem* [33, 34], occasionally called *Onsager-Lax theorem* for this purpose. The theorem can be stated in terms of the time-evolution of single atom correlation functions, governed by

$$\langle B(t+\tau)\rangle = \sum_i \alpha_i(\tau)\langle B_i(t)\rangle, \tag{3.27}$$

where $B_i(t)$ is some complete set of operators, and the functions $\alpha_i(\tau)$ solve the averaged equations of motion for $\langle B_i(t)\rangle$. Now, the theorem states that we can write:

$$\langle A(t)B(t+\tau)C(t)\rangle = \sum_i \alpha_i(\tau)\langle A(t)B_i(t)C(t)\rangle. \tag{3.28}$$

The order of the operators is important since A, B_i, C are non-commuting operators.

We define a vector $\tilde{\mathbf{S}}$ which has 256 components and includes all the transformed transition operators of the basis states. According to the theorem, the time evolution of two-time averages $\langle\delta\tilde{\mathbf{S}}(t+\tau)\delta[\tilde{\mathbf{S}}(t)]_i\rangle$ where $i \in \{1, 2, ..., 255\}$ obey the same equations of motion as the one time averages $\langle\delta\tilde{\mathbf{S}}(t)\rangle$ do, which implies that

$$\partial_\tau\langle\delta\tilde{\mathbf{S}}(t+\tau)\delta[\tilde{\mathbf{S}}(t)]_i\rangle = \mathbf{M}\langle\delta\tilde{\mathbf{S}}(t+\tau)\delta[\tilde{\mathbf{S}}(t)]_i\rangle \qquad \text{for} \quad \tau \geq 0. \tag{3.29}$$

The Laplace transform of both sides of the above equation with respect to τ gives

$$\int_0^\infty e^{-z\tau}\partial_\tau\langle\delta\tilde{\mathbf{S}}(t+\tau)\delta[\tilde{\mathbf{S}}(t)]_i\rangle d\tau = \int_0^\infty e^{-z\tau}\mathbf{M}\langle\delta\tilde{\mathbf{S}}(t+\tau)\delta[\tilde{\mathbf{S}}(t)]_i\rangle d\tau. \tag{3.30}$$

The integral on the left hand side can be expressed as

$$\begin{aligned}&[e^{-z\tau}\langle\delta\tilde{\mathbf{S}}(t+\tau)\delta[\tilde{\mathbf{S}}(t)]_i\rangle]_0^\infty - \int_0^\infty \langle\delta\tilde{\mathbf{S}}(t+\tau)\delta[\tilde{\mathbf{S}}(t)]_i\rangle(-z)e^{-z\tau}d\tau \\ &= -\langle\delta\tilde{\mathbf{S}}(t)\delta[\tilde{\mathbf{S}}(t)]_i\rangle + z\mathcal{L}\{\langle\delta\tilde{\mathbf{S}}(t+\tau)\delta[\tilde{\mathbf{S}}(t)]_i\rangle\}(z).\end{aligned} \tag{3.31}$$

This implies that

$$\mathcal{L}\{\langle\delta\tilde{\mathbf{S}}(t+\tau)\delta[\tilde{\mathbf{S}}(t)]_i\rangle\}(z) = (z\mathcal{I} - \mathbf{M})^{-1}\langle\delta\tilde{\mathbf{S}}(t)\delta[\tilde{\mathbf{S}}(t)]_i\rangle \tag{3.32}$$

We replace z by $\iota\tilde{\omega}$ in order to evaluate the correlation functions stated in (3.26) and thus obtain

$$(\iota\tilde{\omega}\mathcal{I} - \mathbf{M})^{-1}\lim_{t\to\infty}\langle\delta\tilde{\mathbf{S}}(t)\delta[\tilde{\mathbf{S}}(t)]_i\rangle = \lim_{t\to\infty}\mathcal{L}\{\langle\delta\tilde{\mathbf{S}}(t+\tau)\delta[\tilde{\mathbf{S}}(t)]_i\rangle\}(\iota\tilde{\omega}). \tag{3.33}$$

More explicitly, we can write

$$\lim_{t\to\infty}\int_0^\infty e^{-\iota\tilde{\omega}\tau}\langle\delta\tilde{\mathbf{S}}(t+\tau)\delta[\tilde{\mathbf{S}}(t)]_i\rangle d\tau = (\iota\tilde{\omega}\mathcal{I} - \mathbf{M})^{-1}\lim_{t\to\infty}\langle\delta\tilde{\mathbf{S}}(t)\delta[\tilde{\mathbf{S}}(t)]_i\rangle. \tag{3.34}$$

In the limit $t \to \infty$, the system reaches the steady state.

3.5 Implementation to our system

We showed in the above sections that the observables can be expressed in terms of different transion operators of the two atoms. We now discuss the representation of these operators in term of the basis states. As a first step, we introduce the linearly independent spanning set of basis vectors that represents our two-atom product states. Next we show how

the operators are represented using these basis states. This is exactly the way how we implemented the calculation in our numerical code.

For the basis vectors, the notation that we exploit is a ket having two numbers where the first number corresponds to the state of first atom and the second one determines the state of the second atom. Mathematically,

$$|(\text{state of atom1})(\text{state of atom2})\rangle. \tag{3.35}$$

As an example, $|13\rangle$ means that the first atom is in the first excited state and the second atom is in the third excited state. We also use a *state index* which will be the only non-zero element in the column vector of length 16. All the basis vectors and their state indices are listed below.

$$\begin{aligned}
|i1\rangle &\quad \text{state} \quad \text{index} \in \{1,2,3,4\} \\
|i2\rangle &\quad \text{state} \quad \text{index} \in \{5,6,7,8\} \\
|i3\rangle &\quad \text{state} \quad \text{index} \in \{9,10,11,12\} \\
|i4\rangle &\quad \text{state} \quad \text{index} \in \{13,14,15,16\},
\end{aligned} \tag{3.36}$$

where $i \in \{1,2,3,4\}$. The vector representation of $|13\rangle$, state index = 9 is given by

$$\{0,0,0,0,0,0,0,0,1,0,0,0,0,0,0,0\}^T \tag{3.37}$$

The density matrix elements are given by the expectation values.

$$\begin{aligned}
\tilde{\varrho}[1,1] &= \langle 1|\tilde{\varrho}|1\rangle = \langle \tilde{\mathbf{S}}_1\rangle = \langle |1\rangle\langle 1|\rangle \\
\tilde{\varrho}[1,2] &= \langle 1|\tilde{\varrho}|2\rangle = \langle \tilde{\mathbf{S}}_2\rangle = \langle |2\rangle\langle 1|\rangle \\
\tilde{\varrho}[1,3] &= \langle 1|\tilde{\varrho}|3\rangle = \langle \tilde{\mathbf{S}}_3\rangle = \langle |3\rangle\langle 1|\rangle \\
&\vdots \\
\tilde{\varrho}[16,15] &= \langle 16|\tilde{\varrho}|15\rangle = \langle \tilde{\mathbf{S}}_{255}\rangle = \langle |15\rangle\langle 16|\rangle \\
\tilde{\varrho}[16,16] &= \langle 16|\tilde{\varrho}|16\rangle = \langle \tilde{\mathbf{S}}_{256}\rangle = \langle |16\rangle\langle 16|\rangle.
\end{aligned} \tag{3.38}$$

We proceed towards the representation of the atomic raising and lowering operators. We have a total of 12 operators corresponding to the 2 atoms and 6 (3 raising, 3 lowering) transitions in each of them. As an example, we demonstrate the calculation of the transition operator $S^{(1)}_{1+}$.

$$\begin{aligned}
S^{(1)}_{1+} &= |1\rangle_1\langle 4|_1 \otimes \mathbf{1}_2 \\
&= |11\rangle\langle 41| + |12\rangle\langle 42| + |13\rangle\langle 43| + |14\rangle\langle 44| \\
&= |1\rangle\langle 4| + |5\rangle\langle 8| + |9\rangle\langle 12| + |13\rangle\langle 16| \qquad \text{in terms of state indices} \\
&= \tilde{\mathbf{S}}_{49} + \tilde{\mathbf{S}}_{117} + \tilde{\mathbf{S}}_{185} + \tilde{\mathbf{S}}_{253}.
\end{aligned} \tag{3.39}$$

The subscripts following the kets on the left hand side of Eq. (3.39) denote the atom. In a similar manner, the expressions for all the operators can be evaluated. From the above

equations, it is evident that each atomic transition operator is a sum of four components of the vector $\tilde{\mathbf{S}}$. All other operators can be listed as follows.

$$\begin{aligned}
\tilde{S}^{(1)}_{2+} &= \tilde{\mathbf{S}}_{50} + \tilde{\mathbf{S}}_{118} + \tilde{\mathbf{S}}_{186} + \tilde{\mathbf{S}}_{254}, \qquad \tilde{S}^{(1)}_{2-} = \tilde{\mathbf{S}}_{20} + \tilde{\mathbf{S}}_{88} + \tilde{\mathbf{S}}_{156} + \tilde{\mathbf{S}}_{224}, \\
\tilde{S}^{(2)}_{2+} &= \tilde{\mathbf{S}}_{248} + \tilde{\mathbf{S}}_{197} + \tilde{\mathbf{S}}_{214} + \tilde{\mathbf{S}}_{231}, \qquad \tilde{S}^{(2)}_{2-} = \tilde{\mathbf{S}}_{128} + \tilde{\mathbf{S}}_{77} + \tilde{\mathbf{S}}_{94} + \tilde{\mathbf{S}}_{111},
\end{aligned} \tag{3.40}$$

will be used in the calculation of the inelastic π spectrum while

$$\begin{aligned}
\tilde{S}^{(1)}_{1+} &= \tilde{\mathbf{S}}_{49} + \tilde{\mathbf{S}}_{117} + \tilde{\mathbf{S}}_{185} + \tilde{\mathbf{S}}_{253}, \qquad \tilde{S}^{(1)}_{1-} = \tilde{\mathbf{S}}_{4} + \tilde{\mathbf{S}}_{72} + \tilde{\mathbf{S}}_{140} + \tilde{\mathbf{S}}_{208}, \\
\tilde{S}^{(1)}_{3+} &= \tilde{\mathbf{S}}_{255} + \tilde{\mathbf{S}}_{51} + \tilde{\mathbf{S}}_{119} + \tilde{\mathbf{S}}_{187}, \qquad \tilde{S}^{(1)}_{3-} = \tilde{\mathbf{S}}_{240} + \tilde{\mathbf{S}}_{36} + \tilde{\mathbf{S}}_{104} + \tilde{\mathbf{S}}_{172}, \\
\tilde{S}^{(2)}_{1+} &= \tilde{\mathbf{S}}_{244} + \tilde{\mathbf{S}}_{193} + \tilde{\mathbf{S}}_{210} + \tilde{\mathbf{S}}_{227}, \qquad \tilde{S}^{(2)}_{1-} = \tilde{\mathbf{S}}_{64} + \tilde{\mathbf{S}}_{13} + \tilde{\mathbf{S}}_{30} + \tilde{\mathbf{S}}_{47}, \\
\tilde{S}^{(2)}_{3+} &= \tilde{\mathbf{S}}_{252} + \tilde{\mathbf{S}}_{201} + \tilde{\mathbf{S}}_{218} + \tilde{\mathbf{S}}_{235}, \qquad \tilde{S}^{(2)}_{3-} = \tilde{\mathbf{S}}_{192} + \tilde{\mathbf{S}}_{141} + \tilde{\mathbf{S}}_{158} + \tilde{\mathbf{S}}_{175},
\end{aligned} \tag{3.41}$$

will be employed for inelastic σ spectrum.

The time evolution of the density matrix may be written as

$$\partial_t \tilde{\varrho}_a(t) = \mathbf{M}_{256} \tilde{\varrho}_a. \tag{3.42}$$

The matrix $\mathbf{M}_{256}$ is not invertible so there is no unique solution to the above equation. Therefore, we eliminate the last element of $\tilde{\varrho}_a$ *i.e.*, $\tilde{\varrho}[16,16](t)$ by exploiting the *population conservation*. We can use the trace condition $\mathrm{Tr}_a[\tilde{\varrho}_a] = 1$ and the Eq. (3.42) becomes,

$$\partial_t \tilde{\varrho}_a(t) = \mathbf{M} \tilde{\varrho}_a + \mathbf{K}. \tag{3.43}$$

In the above equation, $\mathbf{M}$ is a 255×255 matrix and $\mathbf{K}$ is a column vector with 255 elements. In the limit $t \to \infty$

$$\lim_{t\to\infty} \tilde{\varrho}_a(t) = \tilde{\varrho}_{\mathbf{st}} \tag{3.44}$$

is independent of time. The steady state solution reads

$$\tilde{\varrho}_{\mathbf{st}} = -\mathbf{M}^{-1}\mathbf{K} \tag{3.45}$$

for the situation in which $\mathbf{M}$ is not singular. If $\mathbf{M}$ is not singular the steady state is independent of the initial state of the system. Using Eq. (3.4), the vector $\tilde{\mathbf{S}}$ can be written as,

$$\langle \tilde{\mathbf{S}}(t) \rangle = \langle \tilde{\mathbf{S}} \rangle_{\mathbf{st}} + \langle \delta\tilde{\mathbf{S}}(t) \rangle. \tag{3.46}$$

The mean values in the stationary state can be written as

$$\langle \tilde{\mathbf{S}} \rangle_{\mathbf{st}} = \tilde{\varrho}_{\mathbf{st}} = -\mathbf{M}^{-1}\mathbf{K}. \tag{3.47}$$

Substituting this into Eq. (3.43), after simplification we obtain

$$\partial_t \langle \tilde{\mathbf{S}} \rangle_{\mathbf{st}} + \partial_t \langle \delta\tilde{\mathbf{S}}(t) \rangle = \mathbf{M} \langle \delta\tilde{\mathbf{S}}(t) \rangle + 0. \tag{3.48}$$

The time derivative of the $\langle \tilde{\mathbf{S}} \rangle_{\mathbf{st}}$ vanishes and hence we have,

$$\partial_t \langle \delta\tilde{\mathbf{S}}(t) \rangle = \mathbf{M} \langle \delta\tilde{\mathbf{S}}(t) \rangle. \tag{3.49}$$

Chapter 4

Relevant Processes

In order to develop the physical understanding of our system, it is important to know what processes take place when the atoms interact with the vacuum. Later we will discuss in detail the ac Stark splitting in the context of the interaction of a two-level atom with the laser field in Sec. 4.2.

4.1 Vacuum Induced Processes

The processes of the exchange of virtual photons via the common vacuum radiation field are of fundamental nature and take place between dipole transitions of two nearby atoms. They are responsible for the collective effects in a multi-atom system. Consider the case of two identical two-level atoms. One of the atoms initially in an excited state emits a virtual photon and comes to the ground state. This virtual photon is absorbed by a nearby atom which becomes excited after the absorption of the photon Fig. 4.1. The condition for this photon transfer process is that the distance between the two atoms is fairly small, *i.e.*, it should not exceed the respective transition wavelength. This is because the dipole dipole coupling parameters depend inversely as the cube of the interatomic distance vector [15].

If a photon emitted on one transition in one atom is absorbed by the same transition in the other atom, we refer to it as *parallel* dipole dipole coupling. An example has been shown in Fig. 4.1. Contrary to this, if a photon emitted by one transition in the first atom is coupled to a transition with a different polarization in the other atom, it is termed as *orthogonal* dipole dipole coupling. Of course, the orthogonal vacuum-induced couplings do not occur in two-level atoms as there is only one transition channel available. Fig. 4.2 shows an example of orthogonal dipole dipole coupling in two nearby identical multi-level atoms. In (a) left atom is in its excited state $|e_3\rangle$ while the right atom is in the ground state $|g\rangle$. In (b) the left atom emits a virtual photon as a result of spontaneous decay. In (c) the electron in the atom on the right absorbs the virtual photon emitted by the left atom and thus goes to the excited state $|e_1\rangle$ instead of $|e_3\rangle$. Thus the transition $|e_1\rangle \leftrightarrow |g\rangle$ in the left atom is coupled to the transition $|e_3\rangle \leftrightarrow |g\rangle$ in the right atom. The dipole dipole interaction varies as $1/r$, $1/r^2$ and $1/r^3$. As already briefly discussed in **chapter 1**, with

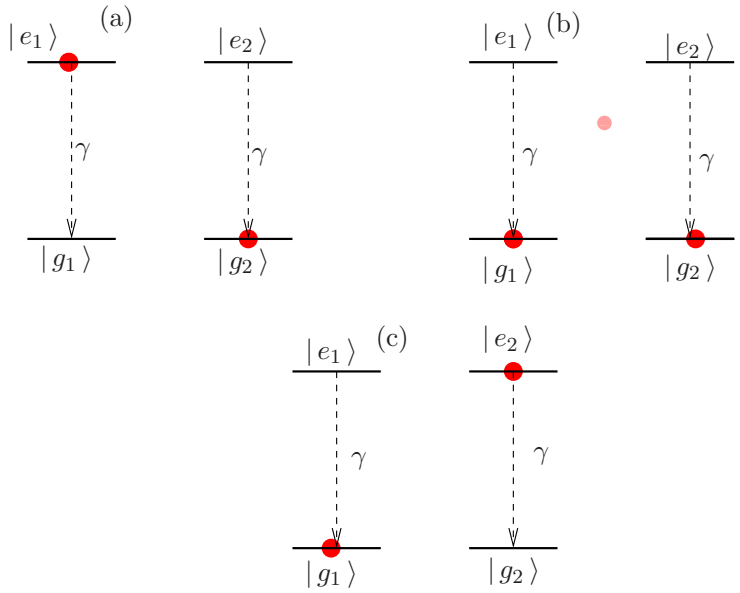

Figure 4.1: Dipole dipole coupling in two near by atoms. (a) Left atom is in its excited state while the right atom is in the ground state. (b) The left atom emits a virtual photon as a result of spontaneous decay. (c) The atom on the right absorbs the virtual photon emitted by the left atom and thus becomes excited.

the occurrence of the orthogonal dipole dipole couplings in multi-level atoms, few-level approximation can no more be applied to the Zeeman sub-levels of an atomic system.

Now it is worth giving a detailed account of the basic physics involved when a single two-level atom interacts with a laser field. This will help the reader understand the results of **Chapter 5** much better. We introduce the concept of *Stark splitting* of the entangled atom-field states when a single two-level atom is subject to an intense laser beam.We demonstrate that the occurrence of the different peaks in the resonance fluorescence spectrum originates from the different transitions taking place between the eigen states of the atom-field interaction Hamiltonian in the interaction picture.

4.2 AC Stark Splitting

We start with a simple system of a single two-level atom driven by a laser field of frequency ω_L, Fig. 4.3. We assume a very weak driving such that $\Omega << \gamma$, where Ω is the Rabi frequency associated with the laser and γ is the atomic decay rate. The spectrum of elastic scaterring will be a delta function centered at the laser frequency. The spectral width of the scattered light is very narrow following the conservation of energy, *i.e.*, the atom absorbs a photon at the laser frequency and then re-emits it at the same frequency.

We increase the Rabi frequency of the laser such that $\Omega > \gamma$. We go to the dressed state picture now. By dressed state we mean the quantum state of an atomic system interacting with a laser, roughly like an atom plus photons. The driving laser field *dresses* the atom

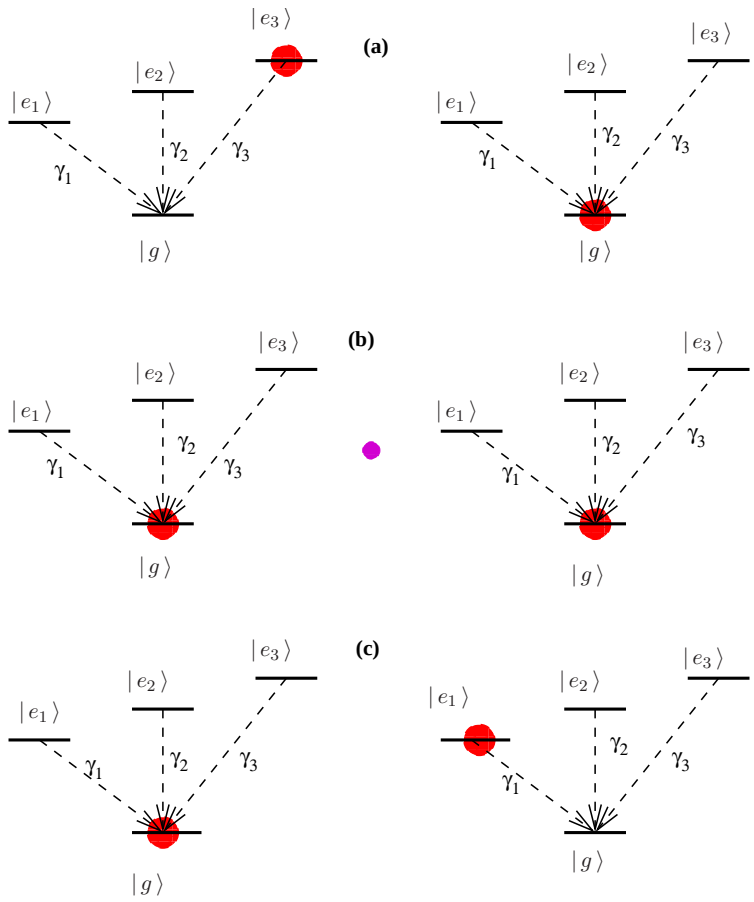

Figure 4.2: Orthogonal dipole dipole couplings in two near by multilevel atoms. (a) Left atom is in its excited state $|e_3\rangle$ while the right atom is in the ground state $|g\rangle$. (b) The left atom emits a virtual photon as a result of spontaneous decay. (c) The electron in the atom on the right absorbs the virtual photon emitted by the left atom and thus goes to the excited state $|e_1\rangle$ instead of $|e_3\rangle$.

with laser photons. Dressed states are always the eigenstates of the atom-field interaction Hamiltonian. The dynamics of the system can easily be understood if dressed states are employed.

We consider a general case when the frequency of the laser and the atomic transition frequency are different from each other. We use the Jaynes-Cummings Hamiltonian which is given by

$$\mathcal{H} = \hbar(\omega_e|e\rangle\langle e| + \omega_g|g\rangle\langle g|) + \hbar\omega_L a^\dagger a + \hbar g(a^\dagger|g\rangle\langle e| + a|e\rangle\langle g|), \tag{4.1}$$

where $|e\rangle$ and $|g\rangle$ designate the excited and ground state, respectively. g is a coupling constant related to the *generalized Rabi frequency*, Ω_n by $g = \Omega_n/\sqrt{n+1}$ and $\omega_0 = \omega_e - \omega_g$. The interaction picture Hamiltonian is given by

$$\mathcal{V} = -\hbar\Delta|e\rangle\langle e| + \hbar g a^\dagger|g\rangle\langle e| + \hbar g a|e\rangle\langle g|, \tag{4.2}$$

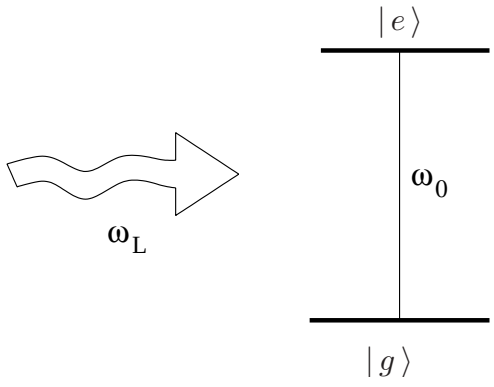

Figure 4.3: A two-level is being driven by a laser of frequency ω_L. ω_0 is the atomic transition frequency.

where $\Delta = \omega_L - \omega_0$. We consider the excitation of $n+1$ quanta. The basis states are chosen to be $|g, n+1\rangle$ and $|e, n\rangle$ *i.e.*, either the atom is in its ground state with $n+1$ quanta or it is in the excited state accompanied by n quanta. The matrix $\mathcal{V}$ is given by

$$\begin{bmatrix} -\hbar\Delta & \hbar g\sqrt{n+1} \\ \hbar g\sqrt{n+1} & 0 \end{bmatrix}.$$

The eigenvalues of the above matrix are

$$\frac{-\hbar\Delta}{2} \pm \frac{\hbar}{2}\sqrt{\Delta^2 + 4g^2(n+1)}. \tag{4.3}$$

For $\Delta > 0$, the dressed state picture of the atom is shown in Fig. 4.4. This phenomenon is known as *dynamic Stark splitting*.

In Fig. 4.4, $S_n = \hbar\sqrt{\Delta^2 + 4g^2 n}$, $S_{n+1} = \hbar\sqrt{\Delta^2 + 4g^2(n+1)}$ and so on. The different transitions are shown by colored arrows. Every transition corresponds to the frequency difference of the starting and the ending energy levels. For example, the blue, pink, golden and light blue transitions correspond to the frequency $\omega_L - (S_{n+2} + S_{n+1})/2$, $\omega_L + (S_{n+2} - S_{n+1})/2$, $\omega_L - (S_{n+2} - S_{n+1})/2$ and $\omega_L + (S_{n+2} + S_{n+1})/2$, respectively. These transitions determine the positions of the peaks in the resonance fluorescence spectrum.

In the classical limit, we assume a large number of photons and so we have $n-1 \simeq n \simeq n+1$ and so $S_{n-1} \simeq S_n \simeq S_{n+1} = s$. The transition frequencies of pink and golden transitions simplify to ω_L while the other two reduce to $\omega_L \pm s$. One would obtain a three peak spectrum of resonance fluorescence. The pink and golden transitions determine the middle peak and the other two locate the side peaks.

If we now consider the resonant case and assume that the laser frequency and the atomic transition frequency are the same, the effect of coupling is that the previously degenerate stationary states $|e, n\rangle$ and $|g, n+1\rangle$ are split into a doublet of dressed states separated by the Rabi frequency Ω associated with the laser. A similar splitting occurs in n-quanta states as well, Fig. 4.5. We have four possible transitions if the $n+1$ states decay to

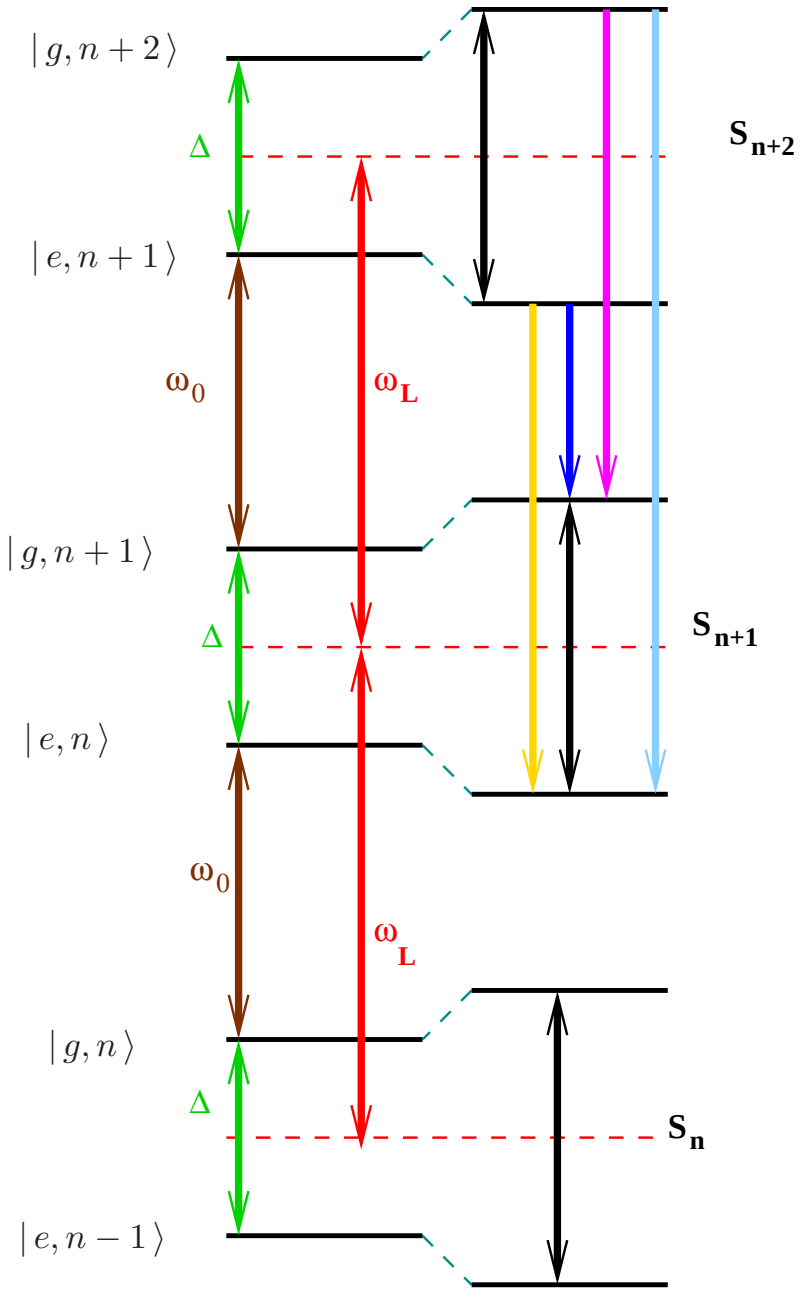

Figure 4.4: Splitting of the atomic levels of a two-level atom by the dynamic Stark effect. Double headed arrows indicate the frequency separation while single headed arrows indicate transitions.

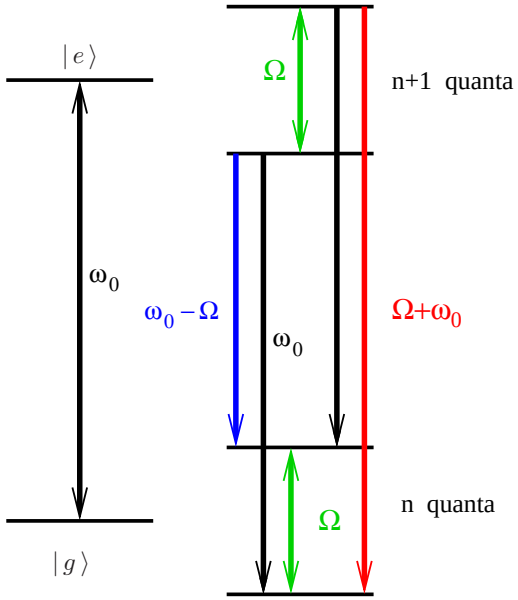

Figure 4.5: Splitting of the atomic levels of a two-level atom by the dynamic Stark effect. The laser frequency is assumed to be equal to the atomic transition frequency. Double headed arrows indicate the frequency separation while single headed arrows indicate transitions.

n states. Two of them correspond to the frequency $\omega_L \pm \Omega$. The other two have equal frequency ω_L [27,35]. We see a three peak spectrum of the resonance fluorescence, Fig. 4.6. The middle peak is at $\omega_0 = \omega_L$ and the symmetrically located side peaks are at $\omega_L \pm \Omega$.

The side peaks move away from the middle peak as the Rabi frequency is increased and they move closer if one decreases the Rabi frequency. So one would obtain a single peak specrum of fluorescent emission in the case $\Omega < \gamma$ as depicted in the Fig. 4.7.

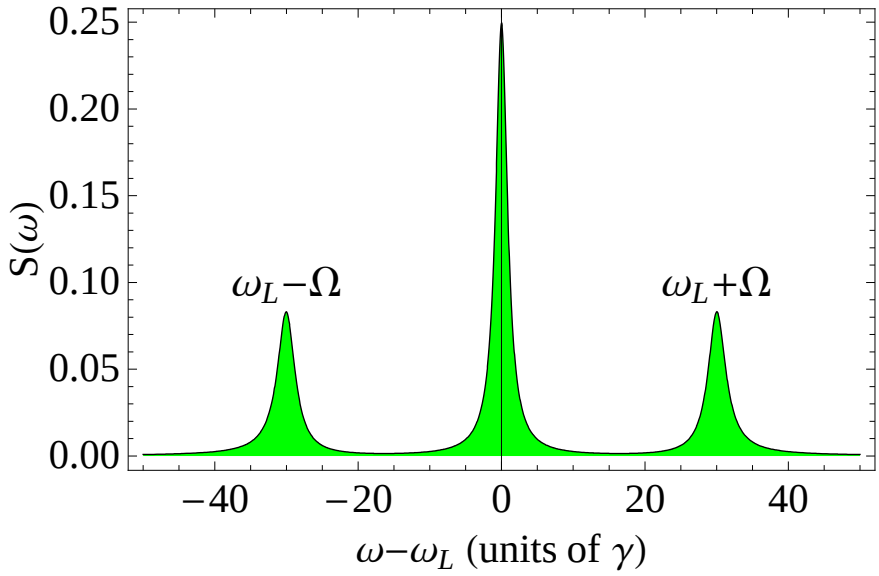

Figure 4.6: Incoherent resonance fluorescence spectrum of a two-level atom. $\Omega = 30\gamma$.

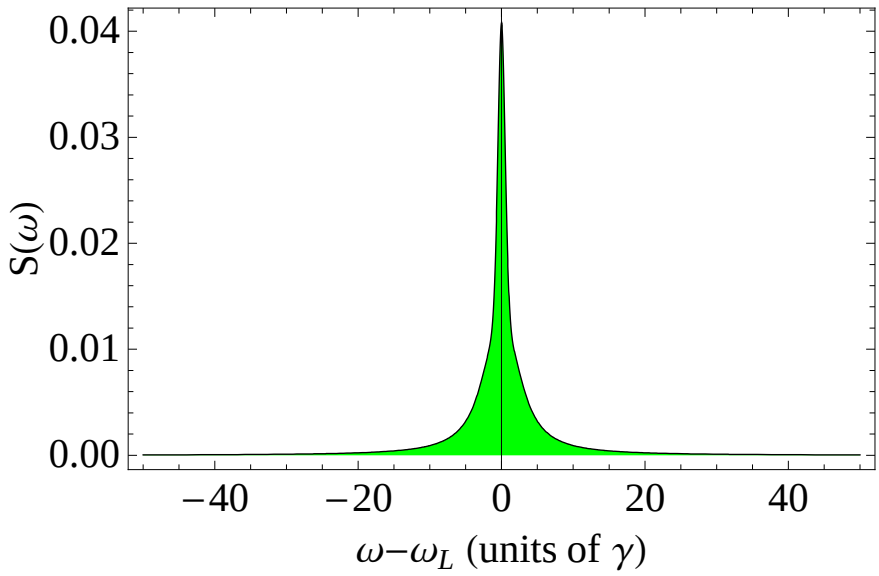

Figure 4.7: Inelastic spectrum of resonance fluorescence of a two-level atom. $\Omega = 0.95\gamma$.

Chapter 5

Results

5.1 Introduction

The resonance fluorescence spectrum Eq. (3.14) emitted by the two atoms in general is rather complicated, but it simplifies considerably in certain parameter cases, as it was found already in the case of two nearby two-level systems [15]. In the following, we will in particular refer to the case of either small or large interatomic spacing, on a length scale given by the involved transition wavelength. For small inter atomic distance, the coherent part of the dipole-dipole interaction dominates the system dynamics, with corrections due to the much weaker laser field Rabi frequencies. In the opposite case of larger separation, the Rabi frequencies dominate, with corrections from the dipole-dipole interaction. Spectra for situations in which the dipole-dipole interaction and the Rabi frequencies are comparable usually can not be interpreted in a straightforward way. In these cases, the driving field intensity can be increased or decreased in order to evolve in one of the two simpler cases. In the following, we will make use of this general observation, and present our results in two steps. First, we will describe methods to determine the interatomic separation in various cases of interest. Second, we will discuss the determination of the relative orientation of the two atoms.

For the numerical analysis, we assume that $\mathbf{r}_1 = (0.05\lambda, 0, 0)$. Our measurement techniques, however, also apply to other values of $\mathbf{r}_1$. A special case arises if one of the atoms is at a node of the standing wave field. Such situations can be circumvented by shifting the phase of the standing wave slightly.

We also assume the resonance condition, *i.e.*, $\omega_L = \omega_0$, $\Delta_i = 0$, see Eq. (2.75).

5.2 Measurement of the Interatomic Distance

We will discuss the techniques for the measurement of the interatomic distance. The strategy adopted is first to keep just R as a variable and fix θ and ϕ in such a way that the orthogonal dipole dipole couplings between the two atoms are zero. Afterwards, we

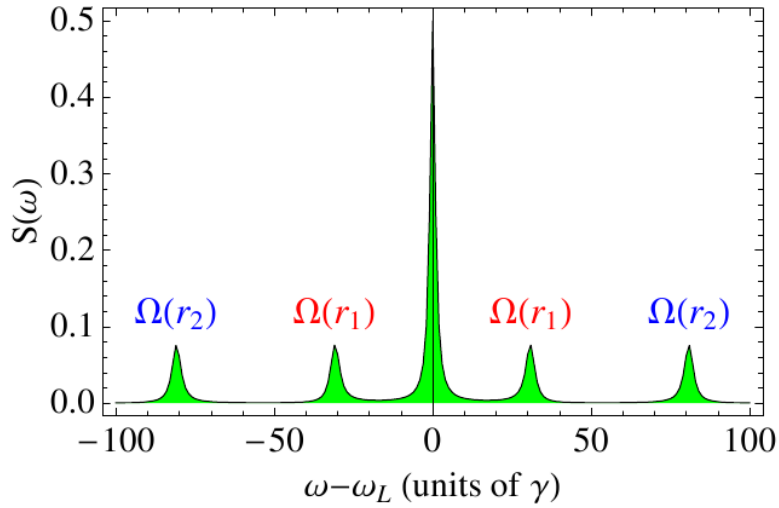

Figure 5.1: Inelastic spectrum of resonance fluorescence. The parameters are $R = 0.3\lambda$, $\phi = 0$, $\theta = \pi/2$ and $\Omega = 100\gamma$. The side peaks are located at the Rabi frequencies, $\Omega(\mathbf{r}_1) = 30.9017\gamma$ and $\Omega(\mathbf{r}_2) = 80.9017\gamma$

try to find the interatomic distance when none of the spherical variable R, θ, ϕ is known to us.

5.2.1 Fixed Orientation

As a first step, we will present results for the situation of a fixed, known orientation. In particular, for simplicity, we analyze the cases in which the orthogonal dipole-dipole couplings Ω_{2i} and Γ_{2i} ($i \in \{1, 3\}$) vanish. Thus, the population is trapped only in the levels $|2_\mu\rangle$ and $|4_\mu\rangle$, and the system essentially reduces to that of two two-level atoms [15]. As the main result of this section, we will interpret each case in detail in terms of the corresponding dressed state picture. This will enable us to explain later results for general geometries.

In principle, the results in this section also generalize to more complicated known orientations. While then the dressed-state analysis still gives rise to valid results, the analytical expressions are often considerably more complicated. In any case, if the orientation is known, a numerical fit of the measured spectrum leads to the desired distance information. In Sec. 5.2.2, we will extend our analysis to arbitrary orientations.

5.2.1.1 Large Separation Case

If the atoms are well-distant, *e.g.*, the separation between them is $\lambda/10 \leq R \leq \lambda/2$, the dipole-dipole interaction can be neglected, since it varies inversely as first, second and third power of the interatomic distance. In this regime, the driving field Rabi frequencies

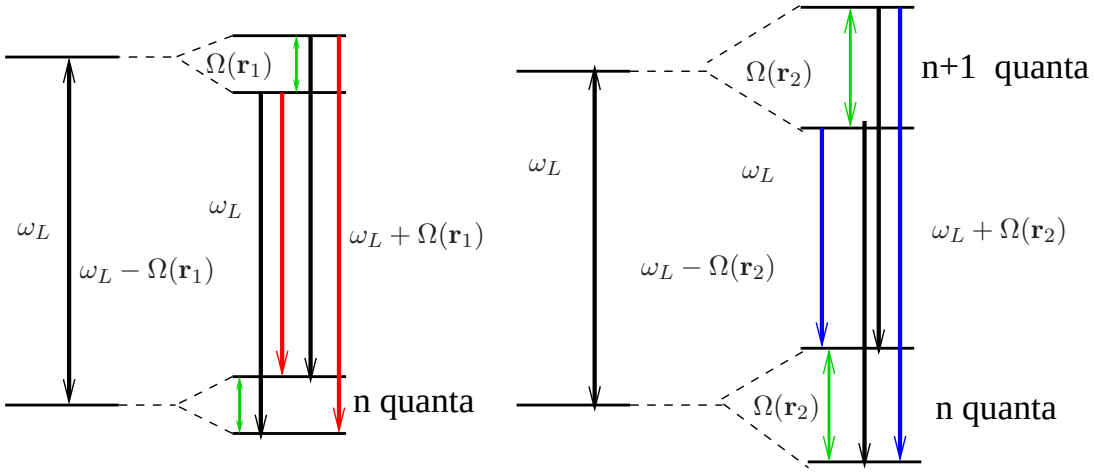

Figure 5.2: The *ac stark splitting* of two two-level atoms. Each of the level in an atom splits by the amount of effective position dependent Rabi frequency.

$\Omega(\mathbf{r}_1)$ and $\Omega(\mathbf{r}_2)$ are much stronger than the dipole-dipole coupling.

The spectrum of resonance fluorescence has five peaks, Fig. 5.1. The first side peaks in the spectrum symmetric around the middle peak occur at $\omega_L \pm \Omega(\mathbf{r}_1)$ and the end peaks are found to be at $\omega_L \pm \Omega(\mathbf{r}_2)$. In such a scenario, the atomic levels undergo a *Stark splitting* due to the position dependent Rabi frequencies as defined in Eq. (2.76). The atomic levels split as shown in the Fig. 5.2. This is a situation similar to a single two-level atom, Sec. 4.2 (see Fig. 4.5) except that due to large interatomic distance, the two Rabi frequencies are position dependent and are different from each other. The ground state and the excited state of both the atoms split by the amount of respective Rabi frequency *i.e.*, the atomic levels in the ith atom split by $\Omega(\mathbf{r}_i)$ where $i \in \{1, 2\}$. There are four possible transitions in an atom and so eight total transitions. Four out of these eight transitions correspond to the same frequency. They have been shown in black colour in the picture of the system with split atomic levels, Fig. 5.2. The four transitions with the frequency ω_L form the middle peak in the spectrum. The other transitions are at the frequencies $\omega_L \pm \Omega(\mathbf{r}_i)$ where $i \in (1, 2)$. These form four side peaks in the resonance fluorescence spectrum. The frequencies $\omega_0 + \Omega(\mathbf{r}_i)$ are situated on the right hand of the middle peak and $\omega_0 - \Omega(\mathbf{r}_i)$ appear at the left part of the spectrum. This means that the positions of the peaks relate directly to the positions of the two atoms relative to the nodes of the standing wave laser field inside the cavity. Thus by knowing the positions of the individual atoms from the positions of the peaks, one can find the mutual distance. Our results for Fig. 5.1 are in agreement with the results presented in [15].

In Fig. 5.1, we have chosen $R = 0.3\lambda$. The different parallel coupling constants are $\Omega_{11} = \Omega_{33} = 0.04\gamma$, $\Omega_{22} = -0.57\gamma$. The orthogonal coupling constants are $\Omega_{13} = \Omega_{31} = -0.62\gamma$ and $\Omega_{12} = \Omega_{21} = \Omega_{32} = \Omega_{23} = 0$ in this case. The corresponding Rabi frequencies are $\Omega(\mathbf{r}_1) = 30.90\gamma$ and $\Omega(\mathbf{r}_2) = 80.90\gamma$. From the comparison of the numerical values, one can see that the Rabi frequencies associated with the driving field dominate the coupling constants associated with the dipole dipole interaction between the two atoms.

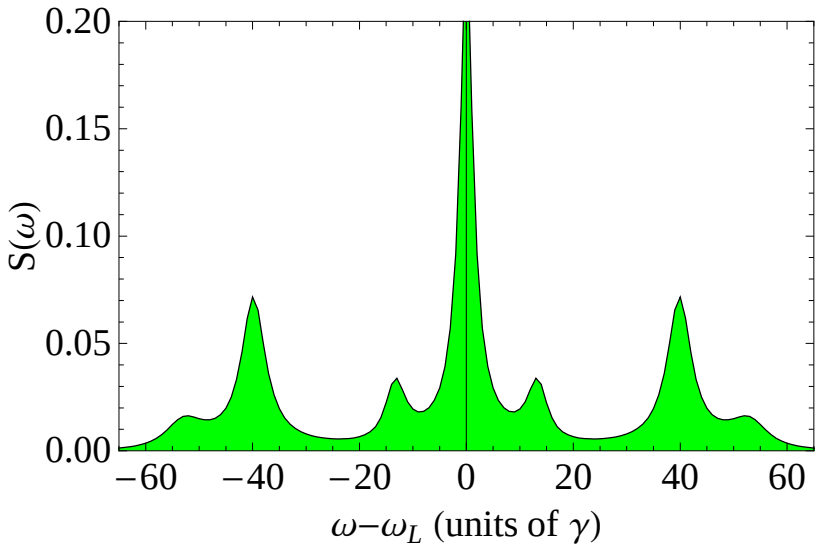

Figure 5.3: Incoherent spectrum of resonance fluorescence. The parameters are $R = 0.08\lambda$, $\phi = \pi/2$, $\theta = \pi$ and $\Omega = 75\gamma$. $\Omega(\mathbf{r}_1) = \Omega(\mathbf{r}_2) = 26.26\gamma$

5.2.1.2 Intermediate Separation Case

When the separation between the atoms is intermediate (approx. $\lambda/30 \leq R \leq \lambda/10$), the dipole-dipole interaction becomes prominent. The two atoms are no more independent.

The spectrum in Fig. 5.3 is difficult to interpret quantitatively. The main atomic level splitting due to one interaction is comparable to the further splitting due to the second interaction as both have comparable magnitudes. In this way, the split atomic levels overlap. It is difficult to associate a unique frequency to a transition because the driving field Rabi frequencies are comparable to the dipole dipole energy shifts. For a comparison, we state the numerical values. The parallel coupling constants are $\Omega_{11} = \Omega_{33} = -10.59\gamma$ and $\Omega_{22} = 26.42\gamma$ whereas the coupling constants due to the interaction between the orthogonal dipole moments in the two atoms vanish. The Rabi frequencies are $\Omega(\mathbf{r}_1) = \Omega(\mathbf{r}_2) = 26.26\gamma$. To avoid such a situation, we increase the driving field intensity so that the position-dependent driving field Rabi frequencies increase.

In Fig. 5.4, the laser Rabi frequency have been increased considerably, to the values 200γ. We see a spectrum in which there is a middle peak and two side band structures on its each side. The middle peak appears at the driving field frequency ω_L. The complete spectrum is symmetric around the middle peak. These side band doublets appear due to the dipole-dipole interaction between the two atoms. The position dependent Rabi frequencies lie at the centre of the side band structure. Again, this confirms the correctness of our analysis since this result is the same as the second result, Fig. 2c of [15].

Fig. 5.5 shows the dressed state picture. We simplify the eigen states and eigen values of the interaction picture Hamiltonian in the limit $\Omega(\mathbf{r}_i) >> \Omega_{22}$ and assume that $\Omega(\mathbf{r}_2) > \Omega(\mathbf{r}_1)$. As in Fig. 5.5(i), in the absence of any interaction between the atoms, the four

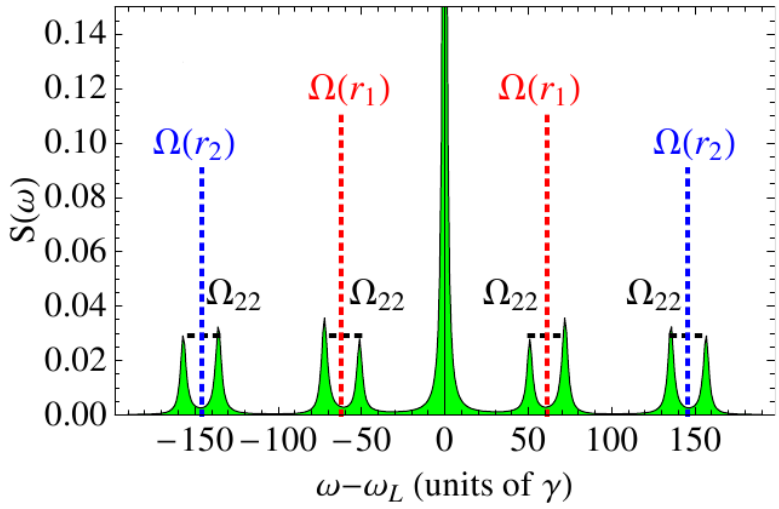

Figure 5.4: Incoherent spectrum of resonance fluorescence for intermediate distances. The parameters are $R = 0.08\lambda$, $\theta = \pi/2$, $\phi = 0$ and $\Omega = 200\gamma$, such that the laser Rabi frequencies are larger than the relevant dipole-dipole coupling constants. The centre of the side band structures are located at the respective position dependent Rabi frequencies, $\pm\Omega(\mathbf{r}_1) \approx \pm 61.8\gamma$ and $\pm\Omega(\mathbf{r}_2) \approx \pm 145.79\lambda$.

product states are degenerate. In Fig. 5.5(ii), there is no dipole dipole interaction. A strong laser field is applied which lifts the degeneracy and causes the product states to shift. The new states $|p\rangle, |l\rangle, |q\rangle$ and $|m\rangle$ are formed by combining the states $|+\rangle, |-\rangle, |s\rangle$ and $|a\rangle$. For example, the laser causes the levels of a single two-level atom to combine like $|e, n\rangle \pm |g, n+1\rangle$. For two two-level atoms, if we ignore the number of photons for simplicity and consider the un-normalized level $|p\rangle$ only, we find that

$$\begin{aligned} |p\rangle &= (|e\rangle_1 + |g\rangle_1) \times (|e\rangle_2 + |g\rangle_2) \\ &= (|e\rangle_1 + |g\rangle_1)|e\rangle_2 + (|e\rangle_1 + |g\rangle_1)|g\rangle_2 \\ &= |ee\rangle + |gg\rangle + |eg\rangle + |ge\rangle. \end{aligned} \tag{5.1}$$

In the last line of the above equation, we utilized the product states of two non-interacting two-level atoms which serve as the basis states. The level $|p\rangle$ level has been shifted by the amount $\hbar(\Omega(\mathbf{r}_1) + \Omega(\mathbf{r}_2))/2$. Similarly, the levels $|m\rangle, |l\rangle$ and $|q\rangle$ have been shifted by the amounts $-\hbar(\Omega(\mathbf{r}_1)+\Omega(\mathbf{r}_2))/2, \pm\hbar(\Omega(\mathbf{r}_2)-\Omega(\mathbf{r}_1))/2$, respectively. In Fig. 5.5(iii), the weak dipole dipole interaction comes into play and it further shifts the levels by the amounts $\pm\hbar\Omega_{22}/2$. When the dipole dipole interaction is much smaller than the driving field, the eigen vectors and the eigen energies are listed in Tab. 5.1. There are sixteen possible transitions between the eigen kets having $n+1$ and n photons. Transitions $|p, n+1\rangle \rightarrow |p, n\rangle$, $|l, n+1\rangle \rightarrow |l, n\rangle$ and $|q, n+1\rangle \rightarrow |q, n\rangle$ and $|m, n+1\rangle \rightarrow |m, n\rangle$ correspond to the same frequency, *i.e.*, ω_L, the laser frequency which is assumed to be equal to the atomic transition frequency. The eight transitions having frequencies $\omega_L \pm (\Omega(\mathbf{r}_i) \pm \Omega_{22})$, $i \in \{1, 2\}$ are important because they form the two prominent side band doublets (eight side peaks) which are crucial for the localization of the two atoms. The remaining four

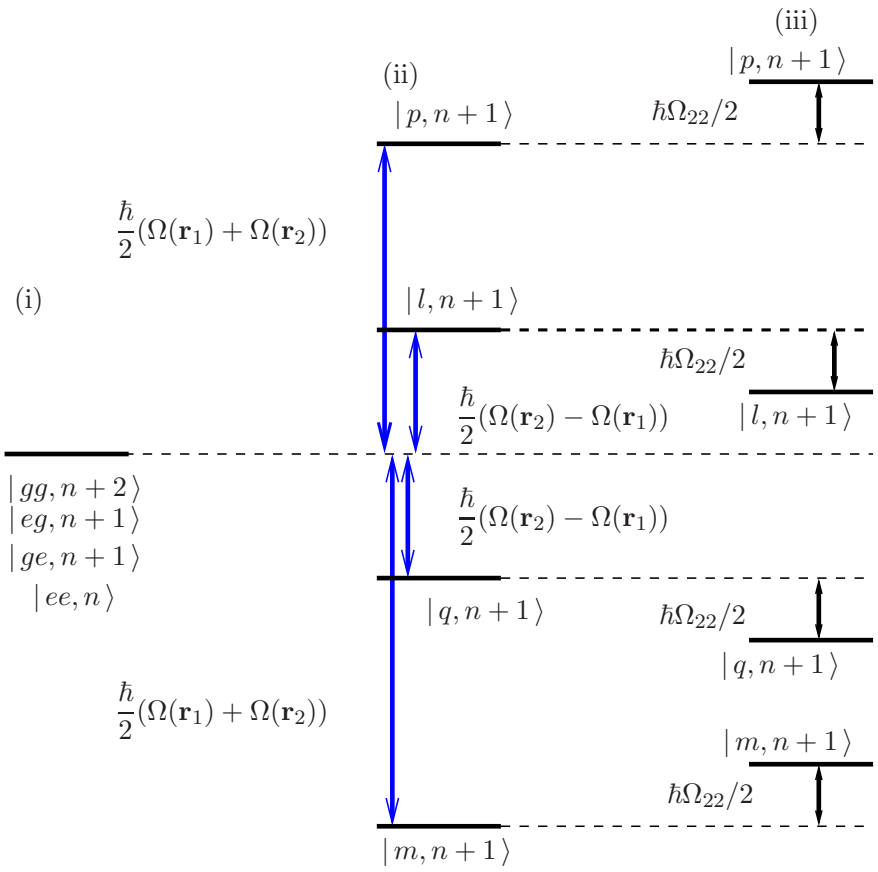

Figure 5.5: Dressed-state representation. (i) shows the system without couplings. (ii) includes the dominant laser field couplings. (iii) in addition includes corrections due to the dipole-dipole interaction.

transitions that involve both Rabi frequencies $\omega_L \pm (\Omega(\mathbf{r}_2) \pm \Omega(\mathbf{r}_1))$ are hardly visible.

In this case, distance measurement is possible in two ways. First, the center of the side-band peak doublets correspond to $\Omega(\mathbf{r}_\mu)$, such that again a direct position determination of the two atoms is possible via Eq. (2.76). Second, the doublets are split by the dipole-dipole coupling strength Ω_{22}. Thus, the distance can also be obtained by using Eq. (2.62). Best results are obtained by a combination of the two methods.

At $\theta \in \{0, \pi\}$, $\Omega(\mathbf{r}_1) = \Omega(\mathbf{r}_2)$ and so the side band doublets coincide as shown in Fig 5.6. The splitting between the two peaks in a side band structure is 26.2γ. In this case, $\Omega_{22} = 26.42\gamma$ is used to calculate the distance between the atoms. We solve Eq. (2.62) numerically to find the separation between the atoms. The distance obtained is 0.0802λ. We determine the percentage error using the formula

$$\frac{X_{calculated} - X_{actual}}{X_{actual}} * 100\%, \tag{5.2}$$

where $X_{calculated}$ is the value obtained through numerical calculation while X_{actual} refers

Eigen vectors	Composition	Eigen values
$\|p, n+1\rangle$	$(1/2)(1,1,1,1)$	$\hbar(\Omega(\mathbf{r}_1)+\Omega(\mathbf{r}_2)+\Omega_{12})/2$
$\|m, n+1\rangle$	$(1/2)(1,-1,-1,1)$	$-\hbar(\Omega(\mathbf{r}_1)\Omega(\mathbf{r}_2)-\Omega_{12})/2$
$\|q, n+1\rangle$	$(1/2)(-1,-1,1,1)$	$\hbar(\Omega(\mathbf{r}_1)-\Omega(\mathbf{r}_2)-\Omega_{12})/2$
$\|l, n+1\rangle$	$(1/2)(-1,1,-1,1)$	$-\hbar(\Omega(\mathbf{r}_1)-\Omega(\mathbf{r}_2)+\Omega_{12})/2$

Table 5.1: Eigenvectors and eigenvalues of the interaction Hamiltonian of two two-level atoms in the limit $\Omega(\mathbf{r}_i) \gg \Omega_{22}$

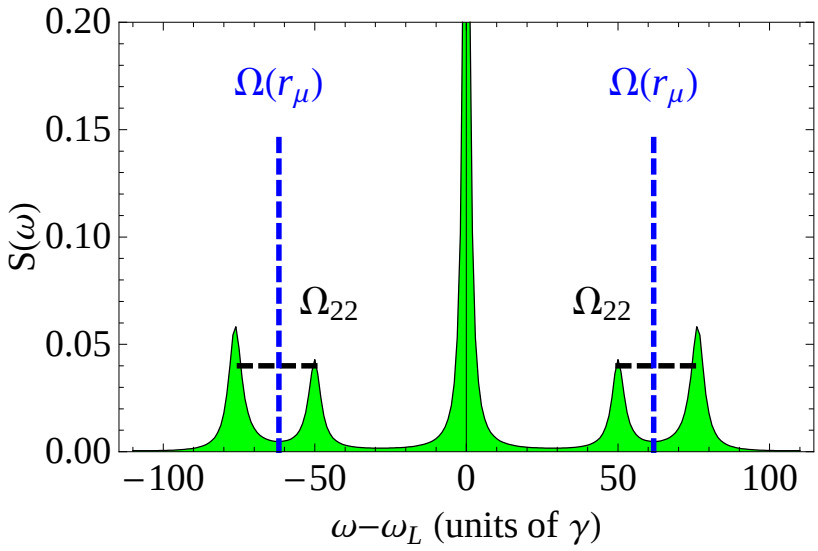

Figure 5.6: Incoherent spectrum of resonance fluorescence. The parameters are $R = 0.08\lambda$, $\phi = \pi/2$, $\theta = \pi$ and $\Omega = 200\gamma$. The centre of side band structure is at the Rabi frequencies, $\Omega(\mathbf{r}_1) = \Omega(\mathbf{r}_2) = 61.8\gamma$

to the actual value of the quantity X. The percentage error in the measurement of interatomic distance is 0.29.

This shows that for the interatomic distance determination, different intensities of the laser field are required for different positions of the atoms.

5.2.1.3 Small Separation Case

Now we discuss the situation when the interatomic distance is even smaller *i.e.*, $R \leq \lambda/30$. In this case, the dipole dipole interaction is very strong because the atoms are very closed to each other. We learn from the discussion done in the previous case that we should employ weak laser field in this case because we want to keep the strengths of the two interactions *i.e.*, the dipole dipole interaction and the laser field different from each other.

We obtain the spectrum shown in Fig. 5.7. The explanation of the peak positions follow.

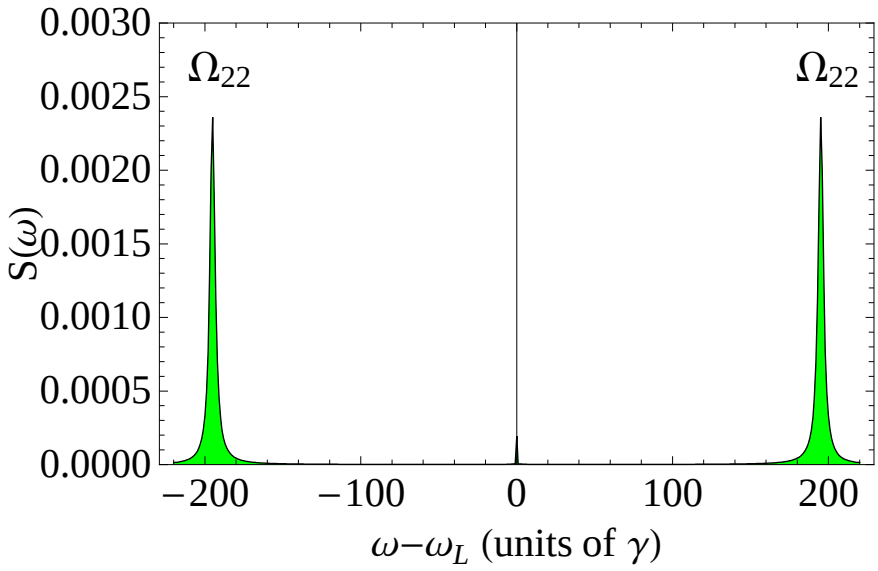

Figure 5.7: Incoherent resonance fluorescnce spectrum. The parameters are $R = 0.04\lambda$, $\phi = 0$, $\theta = \pi/2$ and $\Omega = 20\gamma$. The side peaks occur at $\omega_L \pm \Omega_{22}$.

In the presence of a strong dipole dipole interaction, the eigen states of the system are the collective states listed below.

$$\begin{aligned} |g\rangle &= |g_1\rangle|g_2\rangle, \\ |s\rangle &= \frac{1}{\sqrt{2}}(|e_1\rangle|g_2\rangle + |g_1\rangle|e_2\rangle), \\ |a\rangle &= \frac{1}{\sqrt{2}}(|e_1\rangle|g_2\rangle - |g_1\rangle|e_2\rangle), \\ |e\rangle &= |e_1\rangle|e_2\rangle. \end{aligned} \tag{5.3}$$

The corresponding non-degenerate eigen energies are

$$E_g = 0, \qquad E_s = \hbar(\omega_0 + \Omega_{22}), \qquad E_a = \hbar(\omega_0 - \Omega_{22}), \qquad E_e = 2\hbar\omega_0. \tag{5.4}$$

The states (5.3) form a complete set of states. The ground state $|g\rangle$ and the upper state $|e\rangle$ are not affected by the dipole dipole interaction. The states $|s\rangle$ and $|a\rangle$ have been shifted from their unperturbed energies by the amount $\pm\Omega_{22}$, the dipole dipole interaction energy. These are maximally entangled states of the two atom system. They are linear superpositions of the product states and cannot be separated into the product states of the individual atoms.

The collective states of two-identical atoms are shown in the Fig. 5.8. It is seen that in the collective state representation, a two-atom system behaves like a single four-level system, the ground state is $|g\rangle$, the upper state is $|e\rangle$ and the states $|s\rangle$ and $|a\rangle$ behave like intermediate states. The energies of the states $|s\rangle$ and $|a\rangle$ depend on the dipole dipole interaction and undergo a large shift when the atoms are closed to each other.

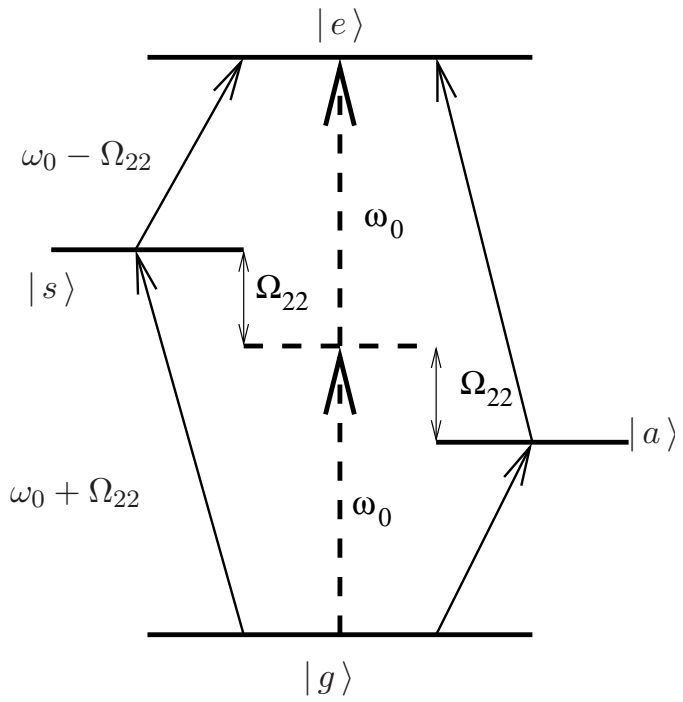

Figure 5.8: Collective states of two identical atoms. The energies of the symmetric and the antisymmetric states are shifted by the dipole dipole interaction Ω_{22}. Each single-headed arrow indicates a one photon transition.

There are two transition channels $|e\rangle \rightarrow |s\rangle \rightarrow |g\rangle$ and $|e\rangle \rightarrow |a\rangle \rightarrow |g\rangle$, each with two cascaded nondegenerate transitions. For two identical atoms, the transitions in these channels are damped with significantly different rates. The symmetric transitions decay with an enhanced (*superradiant*) rate $\gamma + \Gamma_{22}$ and the asymmetric transitions decay with a reduced (*subradiant*) rate $\gamma - \Gamma_{22}$. When the interatomic separation is much smaller than the transition wavelength, the two decay rates become equal, *i.e.*, $\gamma = \Gamma_{22}$. In this situation, the asymmetric channel completely decouples from the system and the system decays only through the transitions involving the symmetric state. So, the system reduces to a three level cascade system. There are three possible transitions at the frequencies $\omega_L \pm \Omega_{22}$ and ω_L as shown in Fig. 5.8.

So, in the presence of a weak laser driving, when the atoms are very close to each other, they interact only through the dipole-dipole interaction, the spectrum of resonance fluorescence has three peaks. The peaks are located at the frequencies ω_L and $\omega_L \pm \Omega_{22}$.

In Fig. 5.7, the numerical values for the driving field Rabi frequencies are $\Omega(\mathbf{r}_1) = \Omega(\mathbf{r}_2) = 6.18\gamma$ whereas the dipole dipole coupling constants are $\Omega_{11} = \Omega_{33} = -91.64\gamma$ and $\Omega_{22} = 194.84\gamma$. As the side peaks are found to be at $\omega_L \pm \Omega_{22}$, Eq. (2.62) is solved numerically to find the distance. The measured value of the interatomic distance comes out to be 0.039λ. The percentage error using Eq. (5.2) is -0.02. This result coincides again with the results presented in [15].

If the Rabi frequency associated with the laser is high, the peaks in Fig. 5.7 split. We

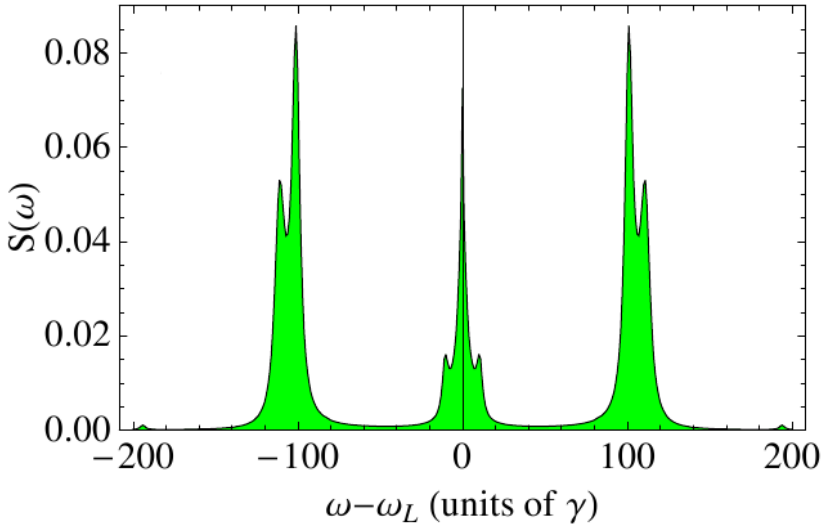

Figure 5.9: Incoherent spectrum of resonance fluorescence. The parameters are $R = 0.04\lambda, \theta = \pi/2$, $\phi = 0$, $\Omega = 75\gamma$, such that the dynamics is dominated by the dipole-dipole interaction, but notably perturbed by the driving field.

Dressed State	Composition	Energy
$\|a, n+1\rangle$	$(0,-1,1,0)/\sqrt{2}$	$-\hbar(\Omega_{22} + (\Omega(\mathbf{r}_1) - \Omega(\mathbf{r}_2))^2/(4\Omega_{22}))$
$\|+, n+1\rangle$	$(-1,0,0,1)/\sqrt{2}$	$\hbar(\Omega(\mathbf{r}_1) - \Omega(\mathbf{r}_2))^2/(4\Omega_{22})$
$\|-, n+1\rangle$	$(1,0,0,1)/\sqrt{2}$	$-\hbar(\Omega(\mathbf{r}_1) + \Omega(\mathbf{r}_2))^2/(4\Omega_{22})$
$\|0, n+1\rangle$	$(0,1,1,0)/\sqrt{2}$	$\hbar(\Omega_{22} + (\Omega(\mathbf{r}_1) + \Omega(\mathbf{r}_2))^2/(4\Omega_{22}))$

Table 5.2: Eigen vectors and eigen values of two identical two-level atoms in the limit $\Omega(\mathbf{r}_\mu) \ll \Omega_{22}$

obtain a spectrum as shown in Fig. 5.9. The explanation in terms of dressed states follow in Fig. 5.10, assuming $\Omega(\mathbf{r}_\mu) \ll \Omega_{22}$. Starting from the non-interacting system in (i), in part (ii), the dominating dipole-dipole interaction is included. It combines the states $|eg, n+1\rangle$ and $|ge, n+1\rangle$ to form $|s, n+1\rangle$ and $|a, n+1\rangle$ as symmetric and anti symmetric combinations, respectively, and shifts their energies by the amount of the dipole-dipole interaction energy. In part (iii), the laser field is included into the dynamics. After another basis transformation to also dress the system with the laser field, this results in the further shifting of the eigenstates by approximately $[\Omega(\mathbf{r}_1) \pm \Omega(\mathbf{r}_2)]^2/(4\Omega_{22})$, as shown in (iv). The corresponding eigenenergies and eigenstates are listed in Tab. 5.2.

Sixteen transitions between the eigenkets having $n+1$ and n quanta take place. Transitions $|0, n+1\rangle \to |0, n\rangle$, $|+, n+1\rangle \to |+, n\rangle$, $|-, n+1\rangle \to |-, n\rangle$ and $|a, n+1\rangle \to |a, n\rangle$ occur at transition frequency ω_L. Transitions $|0, n+1\rangle \to |+, n\rangle$ and $|+, n+1\rangle \to |0, n\rangle$ have respective frequencies $\omega_L \pm \Omega_{22} \pm \Omega(\mathbf{r}_1)\Omega(\mathbf{r}_2)/\Omega_{22}$. The transitions $|0, n+1\rangle \to |-, n\rangle$ and $|-, n+1\rangle \to |0, n\rangle$ involve frequency differences equal to $\omega_L \pm \Omega_{22} \pm (\Omega(\mathbf{r}_1) + \Omega(\mathbf{r}_2))^2/(2\Omega_{22})$,

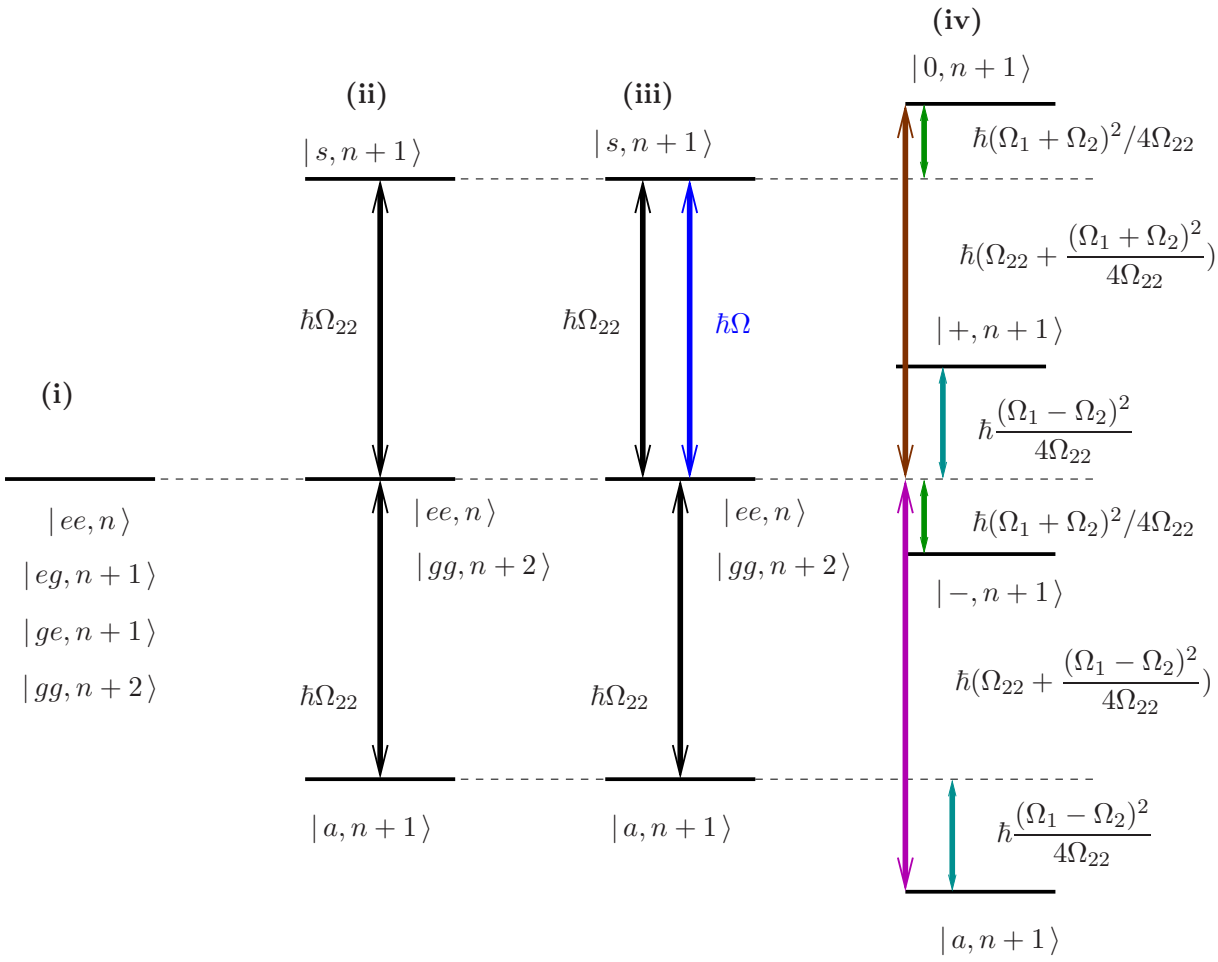

Figure 5.10: Dressed state representation of Fig. 5.9. (i) uncoupled states. (ii) includes the dipole-dipole splitting. (iii) indicates the additional coupling to the laser field, and (iv) shows the full dressed states induced by the dipole-dipole coupling perturbed by the laser field Rabi frequencies, Ω_i means $\Omega(\mathbf{r}_i)$.

respectively. The separation in frequency for the transitions $|0,n+1\rangle \rightarrow |a,n\rangle$ and $|a,n+1\rangle \rightarrow |0,n\rangle$ approximates to $\omega_L \pm 2\Omega_{22} \pm (\Omega^2(\mathbf{r}_1)+\Omega^2(\mathbf{r}_2))/(2\Omega_{22})$, respectively. Finally the transitions $|+,n+1\rangle \rightarrow |-,n\rangle$ and $|-,n+1\rangle \rightarrow |+,n\rangle$ correspond to the frequency difference $\omega_L \pm (\Omega^2(\mathbf{r}_1)+\Omega^2(\mathbf{r}_2))/(2\Omega_{22})$, respectively. These transition frequencies are the positions of the peaks in the resonance fluorescence spectrum of Fig. 5.9(a). The corresponding frequencies for the transitions $|+,n+1\rangle \rightarrow |a,n\rangle$ and $|a,n+1\rangle \rightarrow |+,n\rangle$ are $\omega_L \pm \Omega_{22} \pm (\Omega(\mathbf{r}_1)-\Omega(\mathbf{r}_2))^2/(2\Omega_{22})$ and for the transitions $|-,n+1\rangle \rightarrow |a,n\rangle$ and $|a,n+1\rangle \rightarrow |-,n\rangle$ are $\omega_L \pm \Omega_{22} \mp \Omega(\mathbf{r}_1)\Omega(\mathbf{r}_2)/\Omega_{22}$, respectively. The last four transitions do not show up in the spectrum.

Next we discuss the case when the two position-dependent Rabi frequencies are equal to each other. This is the situation when $\theta \in \{0,\pi\}$. We employ $\Omega(\mathbf{r}_1) = \Omega(\mathbf{r}_2) = 55.62\gamma$ such that we are still in the regime where the laser field acts as a small perturbation to the dipole dipole interacting system. The incoherent spectrum of resonance fluorescence is

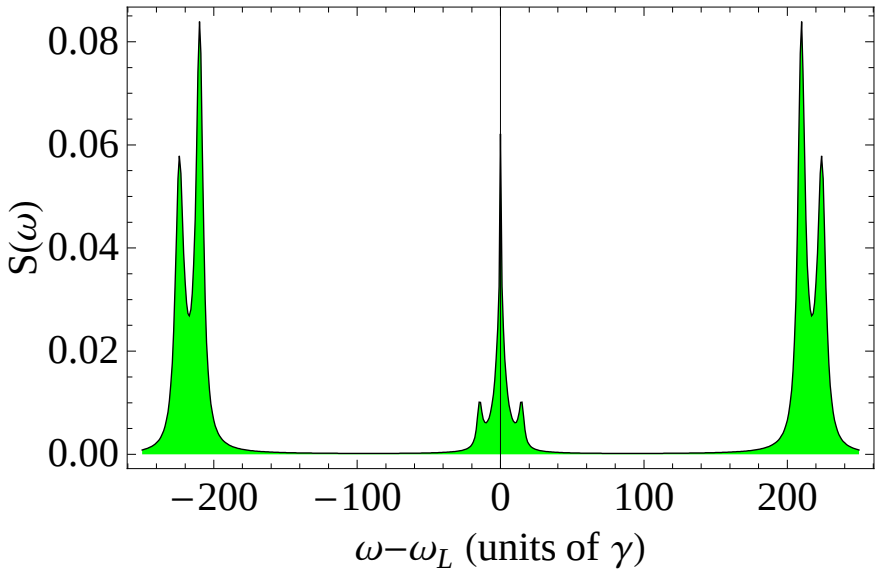

Figure 5.11: Incoherent resonance fluorescence spectrum. The parameters are same as in Fig. (5.7) except $\Omega = 180\gamma$.

Dressed State	Composition	Energy
$\|a, n+1\rangle$	$(1/\sqrt{2})(0,-1,1,0)$	$-\hbar\Omega_{22}$
$\|+, n+1\rangle$	$(1/\sqrt{2})(-1,0,0,1)$	0
$\|-, n+1\rangle$	$(1/\sqrt{2})(1,0,0,1)$	$-\hbar\Omega^2(\mathbf{r}_\mu)/\Omega_{22}$
$\|0, n+1\rangle$	$(1/\sqrt{2})(0,1,1,0)$	$\hbar(\Omega_{22}+\Omega^2(\mathbf{r}_\mu)/\Omega_{22})$

Table 5.3: Eigenvectors and eigenvalues of two identical two-level atoms in the limit $\Omega(\mathbf{r}_\mu) \ll \Omega_{22}$ for $\Omega(\mathbf{r}_1) = \Omega(\mathbf{r}_2)$

shown in Fig. 5.11 and Fig. 5.12 explains the underlying physics in terms of dressed states. The explanation of Fig. 5.12 is same as that of Fig. 5.10 except that the laser field will not affect the transition channel that involves the asymmetric state when $\Omega(\mathbf{r}_1) = \Omega(\mathbf{r}_2)$ because

$$\langle a|\mathcal{H}_L|g\rangle = 0 \quad \text{and} \quad \langle e|\mathcal{H}_L|a\rangle = 0, \tag{5.5}$$

and $\mathcal{H}_L$ is given by Eq. (2.75). The laser induces transitions only in the symmetric channel shown in Fig. 5.8. The eigen energies and the eigen vectors of the interaction Hamiltonian simplify as in Tab. 5.3.

There are nine possible transitions between the eigen kets having $n+1$ and n quanta. Transitions $|0, n+1\rangle \rightarrow |0, n\rangle$, $|+, n+1\rangle \rightarrow |+, n\rangle$ and $|-, n+1\rangle \rightarrow |-, n\rangle$ correspond to the same frequency, *i.e.*, ω_L, which is assumed to be the atomic transition frequency as well. Transitions $|0, n+1\rangle \rightarrow |+, n\rangle$ and $|+, n+1\rangle \rightarrow |0, n\rangle$ have respective frequencies $\omega_L \pm (\Omega_{22} + \Omega^2(\mathbf{r}_\mu)/\Omega_{22})$. The transitions $|0, n+1\rangle \rightarrow |-, n\rangle$ and $|-, n+1\rangle \rightarrow |0, n\rangle$ involve frequency differences equal to $\omega_L \pm (\Omega_{22} + 2\Omega^2(\mathbf{r}_\mu)/\Omega_{22})$ and finally the corresponding

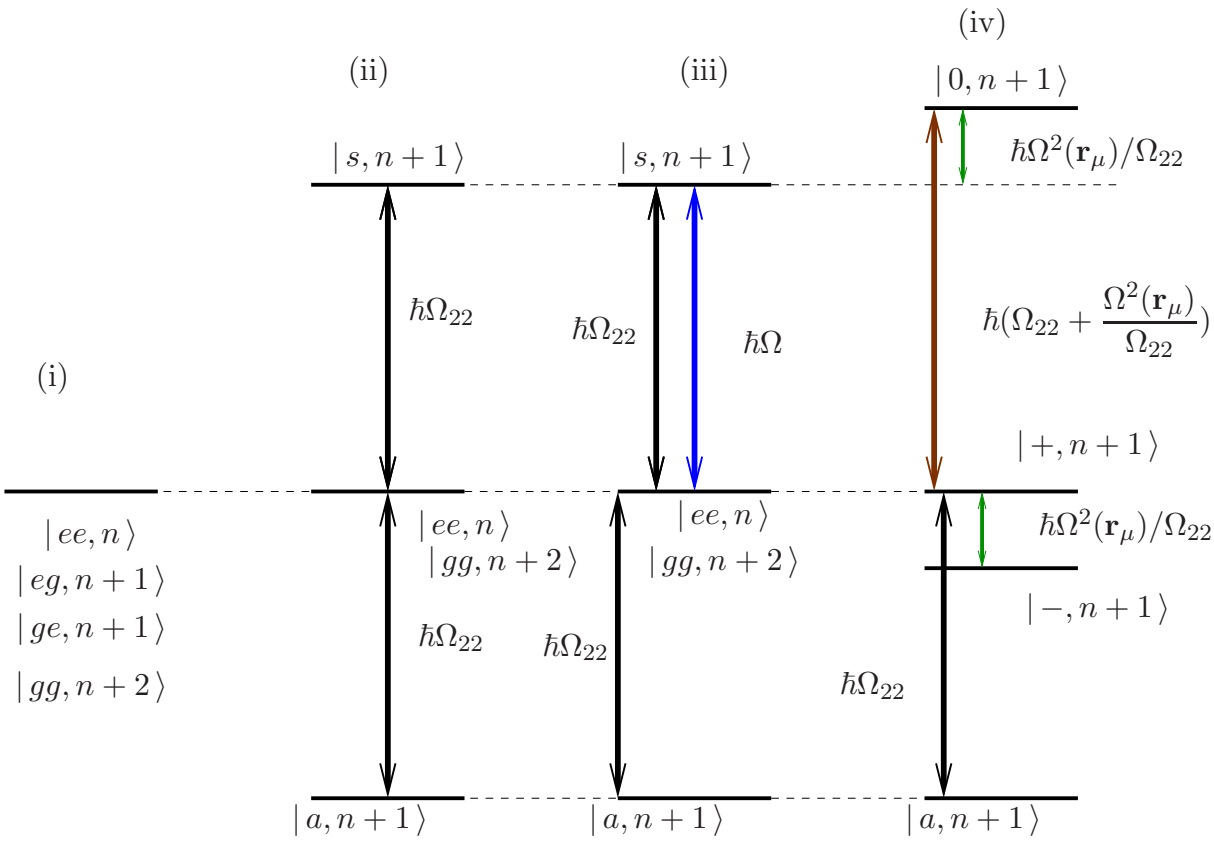

Figure 5.12: Fig. 5.10 simplified for $\Omega(\mathbf{r}_1) = \Omega(\mathbf{r}_2)$. (i) product states with no interaction. (ii) dipole dipole interacting atoms. (iii) laser field is introduced to the dipole dipole interacting system. (iv) Shifting of the dressed states caused by the dipole dipole interaction and perturbed by the laser field.

frequencies for the transitions $|+,n+1\rangle \rightarrow |-,n\rangle$ and $|-,n+1\rangle \rightarrow |+,n\rangle$ are $\omega_L \pm \Omega^2(\mathbf{r}_\mu)/\Omega_{22}$, respectively. The transition frequencies are the positions of the peaks in the resonance fluorescence spectrum, Fig. 5.11.

In Fig. 5.11, the peak in the middle is situated at the frequency $\omega_0 = \omega_L$. The very next peaks on both sides of this peak are determined by the frequencies $\omega_L \pm \Omega^2(\mathbf{r}_\mu)/\Omega_{22}$. The second next peaks symmetrically located on both sides correspond to the frequencies $\omega_L \pm (\Omega_{22} + \Omega^2(\mathbf{r}_\mu)/\Omega_{22})$ and $\omega_0 \pm (\Omega_{22} + 2\Omega^2/\Omega_{22})$ determine the end peaks on both sides. Hence, all the peaks can be determined by the transitions that take place between the eigenstates of the interaction Hamiltonian.

5.2.2 Arbitrary Orientation

The methods presented so far allow for a determination of the interatomic distance if the orientation of the two atoms is known and fixed. Often, however, the orientation is unknown. Therefore, in this section, we turn to our main results, and present a method

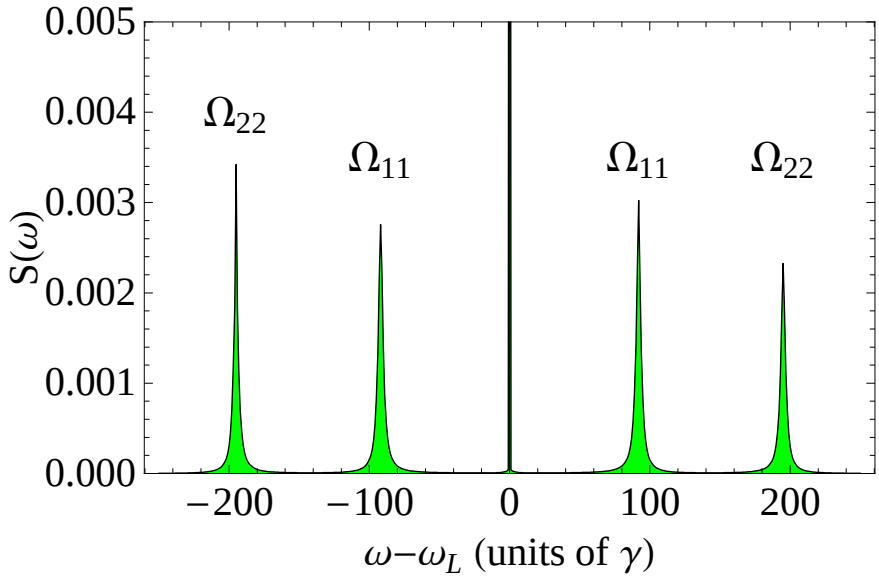

Figure 5.13: Incoherent spectrum of resonance fluorescence for small distance and weak driving fields. The parameters are $R = 0.04\lambda$, $\phi = \pi/15$, $\theta = \pi/5$ and $\Omega = 20\gamma$.

to obtain the interatomic distance for arbitrary orientations. This method can be applied if the interatomic distance is sufficiently small, such that the dipole-dipole interaction dominates the system dynamics. Fortunately, this usually is exactly the parameter range in which a distance determination is desired. In order to explain the method, we first imagine the two atoms without any driving fields. Then, it turns out that the eigenenergies of the dressed states are independent of the orientation of the two atoms [20]. An interpretation of this fact is that without external field, there is no preferred direction in space, such that the energies cannot depend on the orientation. Since the spontaneously emitted light is emitted at frequencies corresponding to the dressed state energies, it follows that the positions of the peaks in the fluorescence spectrum of the atoms are unaffected by the orientation of the atoms. This property is approximately preserved if the atoms are driven by a weak driving field, which has a Rabi frequency much smaller than the dipole-dipole couplings. We therefore find that at small distance and weak driving, the resonance fluorescence spectrum has peak positions independent of the alignment of the two atoms. Only the relative widths and heights of the spectral features change with the orientation. It is important to note that these properties of the two-atom system are only described correctly if all dipole-dipole couplings are included in the modelling [20]. This is the reason why we included complete Zeeman manifolds in our analysis.

It remains to deduce the interatomic distance from the peak positions in the resonance fluorescence spectrum. For this, we again analyze the eigenvalues of the full interaction Hamiltonian of two four-level atoms, which determine the peak positions. Since the peak positions and thus these eigenvalues are independent of the orientation, it suffices to evaluate analytic expressions for the peak positions in a simple configuration. Investigating the eigenvalues for $\theta = 0$, and assuming $\Omega(\boldsymbol{r}_\mu) \ll \Omega_{ii}$, we find that the eigenenergies are

given by 0, $\pm\Omega_{11}(\theta = 0)$, and $\pm\Omega_{22}(\theta = 0)$. An example is shown in Fig. 5.13. The four side peaks are located at $\omega_L \pm \Omega_{11}$ and $\omega_L \pm \Omega_{22}$, and the interatomic distance can be gained from both coupling constants via Eq. (2.60) and (2.62). As can be seen from Fig. 2.4(b), for $\theta \in \{0, \pi\}$, the coupling constant $|\Omega_{22}|$ is larger than $|\Omega_{11}|$ for small interatomic distances R. Thus, the inner [outer] peaks in Fig. 5.13 correspond to $|\Omega_{11}|$ [$|\Omega_{22}|$]. Due to the dependence of the amplitude of the spectral peaks on the orientation, the peaks at $\omega_L \pm \Omega_{11}$ visible in Fig. 5.13 may be suppressed. For example, in Fig. 5.7, we found only a single pair of sidebands corresponding to $\pm\Omega_{22}$. This can be understood by observing that these peaks at $\omega_L \pm \Omega_{22}$ correspond to states $|2\rangle$ populated by the driving laser field, while states $|1\rangle$ and $|3\rangle$ are only populated in certain geometries.

We end this section by noting that in the case of large interatomic separation, the dipole-dipole interaction vanishes, such that the interatomic coupling also becomes independent of the orientation. The driving field Rabi frequencies experienced by the two atoms, however, may not be the same, as they depend on the scalar product $\mathbf{k_L} \cdot \mathbf{r}_\mu$. Thus, by applying a driving field with larger Rabi frequency, it is possible to measure the position of the atoms projected on the propagation axis of the driving field. For arbitrary orientations, however, a single measurement of this type does not allow to deduce the interatomic distance since the position transverse to the wave vector remains unknown.

We thus conclude that by applying weak driving fields, the interatomic distance can be measured from a pair of nearby atoms independent of their mutual orientation, as long as the dipole-dipole interaction is strong enough to dominate the system dynamics.

5.3 Determination of the Orientation

So far, we have discussed techniques for the measurement of the interatomic distance, and have demonstrated how the distance can be measured independent of the orientation of the interparticle distance vector. In this section, we augment our analysis by discussing the determination of the relative orientation of the two atoms. We discuss two different cases, corresponding to two different methods to determine the orientation. First, we discuss the case of unknown ϕ, assuming $\theta = \pi/2$. This case corresponds to an effective two-dimensional geometry of the system which can be realized, *e.g.*, by embedding the atoms in a planar matter waveguide [36–38]. In this case, the orientation is deduced from the ϕ-dependent peak positions in the fluorescence spectrum induced by the driving laser field. Second, we study the case of unknown θ and $\phi = \pi/2$. This corresponds to atoms on a surface, driven by a laser field propagating perpendicular to the surface. In this case, we will determine θ via the resonance fluorescence intensity emitted in a particular direction.

5.3.1 Unknown ϕ: Planar Waveguide

In this section, we assume that the two atoms are confined in the x-y plane ($\theta = \pi/2$) as shown in Fig. 5.14, as it is the case, for example, in a planar waveguide. A standing wave

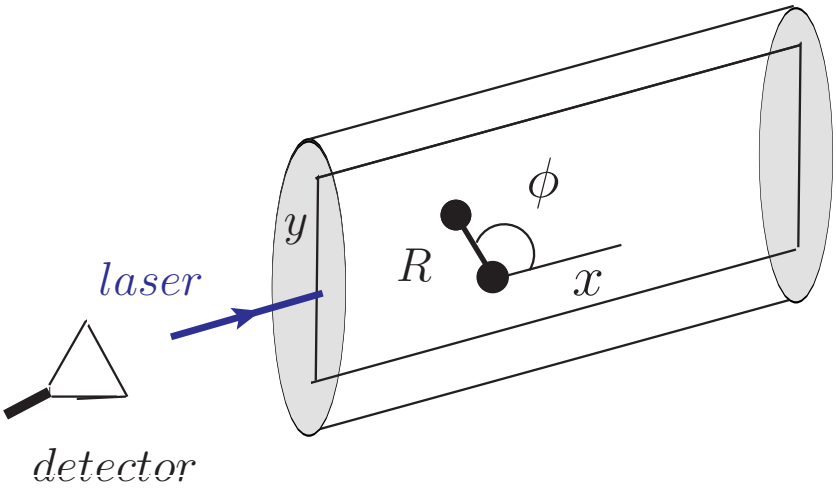

Figure 5.14: Setup with the two nearby atoms confined inside a two-dimensional waveguide. The atoms are located in the x-y plane.

inside a planar waveguide could be realized, *e.g.*, in a photonic crystal waveguide [39]. The waveguide is formed by a line defect in the crystal structure, and the end of the waveguide inside the crystal forms a retro-reflector that leads to the standing wave. A different implementation could be photonic crystal fibers. The atoms could be embedded into a filled central core, or flow through a hollow core, and at the same time interact with light fields propagating through the fiber [40]. Since such a setup may also constrain the observation direction, we assume detection in a direction anti-parallel to the incident driving field, i.e., along the $-x$ direction. This way, the spectrum can be measured without background from the incident laser field. In this geometry, the coupling constants Ω_{21} and Ω_{32} are zero for all values of ϕ. Since only the second transition $|2\rangle \leftrightarrow |4\rangle$ is driven, the populations of the levels $|1\rangle$ and $|3\rangle$ are zero for the whole range of ϕ. The parallel coupling constants $\Omega_{11} = \Omega_{33}$ and Ω_{22} are independent of ϕ. Nevertheless, the spectra depend strongly on ϕ because of the ϕ-dependence of the Rabi frequency $\Omega(\mathbf{r}_2)$. The obtained spectra are identical if ϕ is replaced by $2\pi - \phi$.

From the results of Sec. 5.2.2 it is clear that the peak positions in the resonance fluorescence spectrum cannot be used to determine the orientation as long as the dipole-dipole interaction dominates the dynamics. Therefore, we apply stronger driving fields, such that the external driving dominates the dynamics.

In this case, for most values of ϕ, a typical spectrum obtained is shown in Fig. 5.15. Using the results of Sec. 5.2.1, we conclude that the two doublets on each side corresponding to Mollow sidebands at the two Rabi frequencies experienced by the atoms, split by the dipole-dipole interaction. The doublets can thus be used to approximately read off the two position-dependent Rabi frequencies. Assuming that the distance is known from a measurement with a weaker driving field as described in Sec. 5.2.2, the components of the position vectors of the individual atoms as well as the relative alignment of the atoms along the laser can be found out by using the position dependent Rabi frequencies $\Omega(\mathbf{r}_\mu)$

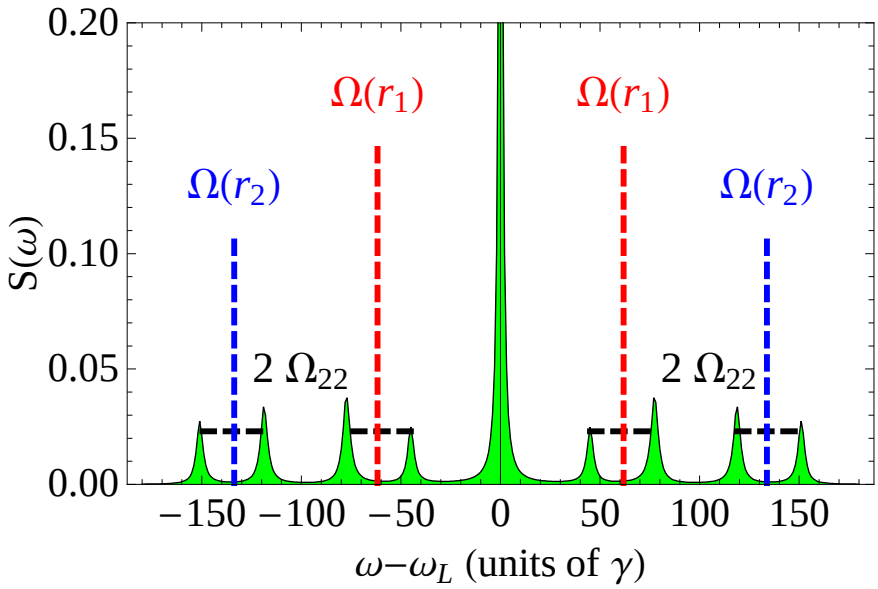

Figure 5.15: Incoherent spectrum of resonance fluorescence. The parameters are $R = 0.07\lambda$, $\phi = 0.1\pi$, $\Omega = 200\gamma$.

as follows:

$$\phi = \cos^{-1}\left\{\frac{1}{k_L R}\left[\sin^{-1}\left(\frac{\Omega(\mathbf{r}_2)}{\Omega}\right) - \sin^{-1}\left(\frac{\Omega(\mathbf{r}_1)}{\Omega}\right)\right]\right\}. \tag{5.6}$$

In Fig. 5.15, the parameters are $R = 0.07\lambda$, $\phi = 0.1\pi$, $\Omega = 200\gamma$. The position dependent Rabi frequencies are $\Omega(\mathbf{r}_1) = 61.8\gamma$ and $\Omega(\mathbf{r}_2) = 133.74\gamma$. The parallel dipole dipole coupling constants are $\Omega_{11} = \Omega_{33} = 11.17\gamma$ and $\Omega_{22} = -16.16\gamma$. The peak separation in the side band doublets is found to be 32.32γ. It is evident that this peak separation corresponds to $2|\Omega_{22}|$. We find the peaks in the second side-band doublet on right side of the spectrum occur at 118.765γ and 151.08γ. The numerical calculation using Ω_{22} gives the interatomic distance. The error in the calculation of interatomic distance using Eq. (5.2) is 0.015%. Using this $R_{calculated} = 0.07001\lambda$ we proceed to find the value of ϕ.

It is noted that these parameters are not favorable for the calculation of ϕ. We propose making use of even higher amplitudes of the driving field for better determination of ϕ so that the two side band doublets are well separated. In Fig. 5.16, we have increased Ω to 350γ. The peaks in the spectrum of resonance fluorescence occur at $0, \pm 91.68\gamma, \pm 123.95\gamma, \pm 218.59\gamma, \pm 250.86\gamma$. Considering the mean values of the peak separation in the inner side band doublets as $\Omega(\mathbf{r}_1)$ and that in the exterior side band doublets as $\Omega(\mathbf{r}_2)$, we use Eq. (5.6) to estimate ϕ. Thus we obtain 0.091π as the value of ϕ, which deviates from the true value by about 9%. Eq. (5.2) is used to determine the percentage error.

This deviation can be attributed to the imperfect determination of the Rabi frequencies as the mean value of the two peaks in the doublets.

Increasing ϕ from the value that has been used in Fig. 5.16, the position-dependent Rabi

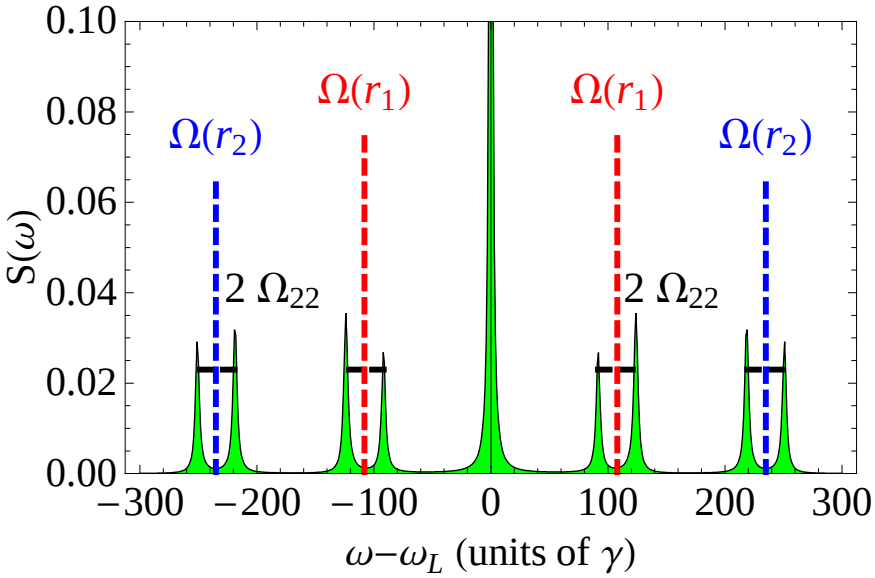

Figure 5.16: Incoherent spectrum of resonance fluorescence for two atoms in a geometry as shown in Fig. (5.14). The parameters are $R = 0.07\lambda$, $\theta = \pi/2$, $\phi = 0.1\pi$, and $\Omega = 350\gamma$.

frequencies change, until the sideband doublets corresponding to the two Rabi frequencies start to overlap, as the two position-dependent Rabi frequencies approach each other. In this case, it is difficult to estimate ϕ directly from the spectrum, since a clear identification of the different peaks is not obvious. One strategy is to increase the driving field intensity. Since the peak separation $|\Omega(\mathbf{r}_1)-\Omega(\mathbf{r}_2)|$ is proportional to Ω, this increase eventually leads to a splitting larger than the line widths of the involved peaks, such that an identification becomes possible. In any case, it can be concluded from overlapping peaks that ϕ is close to $\pi/2$ or $3\pi/2$, since then $\Omega(\mathbf{r}_1) \approx \Omega(\mathbf{r}_2)$.

In summary, the relative orientation of the two atoms with respect to the laser can be determined using stronger laser fields. This works well if the position dependent Rabi frequencies are different from each other, since then the spectral lines are well separated. This is the case for ϕ not close to $\pi/2$ or $3\pi/2$. Accordingly, if the corresponding spectral peaks overlap, it can be concluded that ϕ is close to $\pi/2$ or $3\pi/2$.

5.3.2 Unknown θ: Atoms on a Surface

In this section, we consider the case of two atoms on a surface, driven by a laser field propagating perpendicular to the surface, Fig. 5.17. Thus, ϕ is fixed to $\pi/2$, while θ is unknown. A setup of this type was realized, for example, in [18]. In this experiment, two fluorescent molecules were kept in a fixed geometry by putting them inside a thin organic crystal. From the measurement of a position-dependent Stark-shift map, the distance of the two particles was determined as 12nm. The measured data was then shown to be compatible with theoretical predictions from a system of two dipole-dipole interacting two-level systems. It can thus be concluded that this setup allowed to fix the

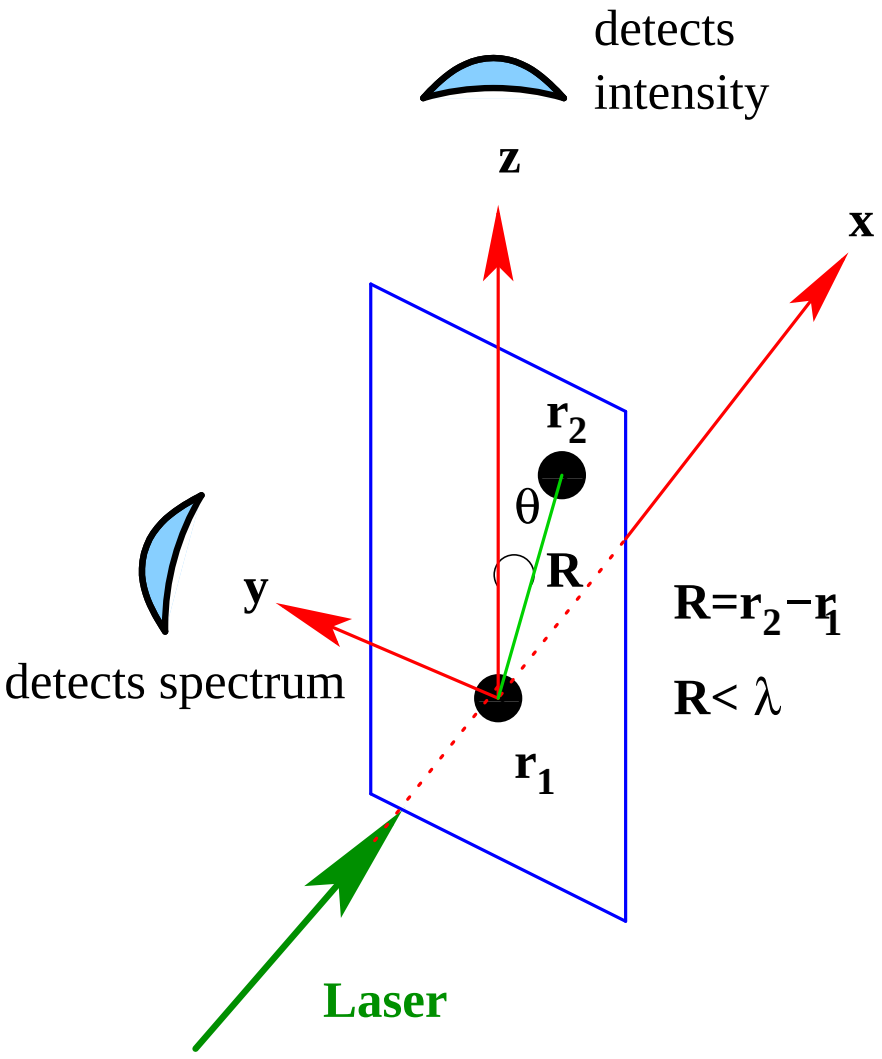

Figure 5.17: Example setup. $\phi = \pi/2$, atoms in the y-z plane

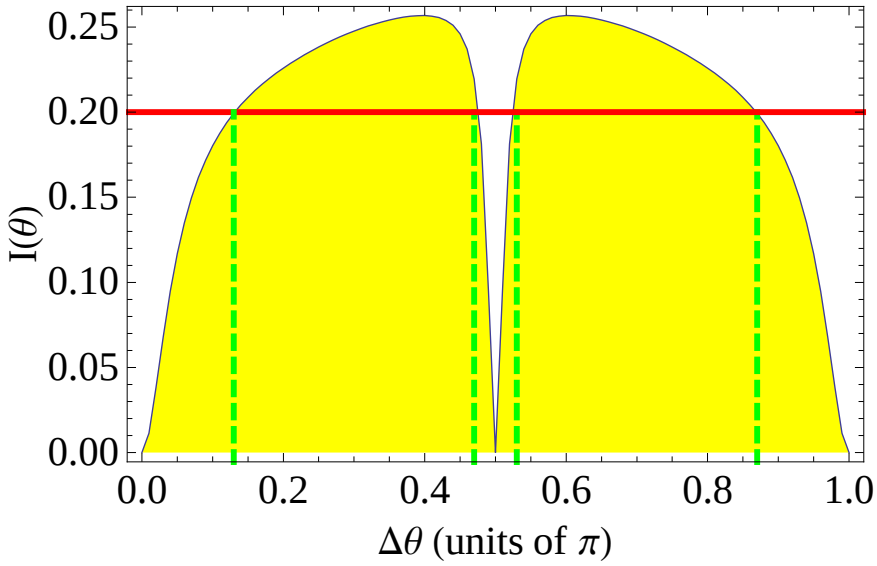

Figure 5.18: Fluorescence intensity emitted on the σ-transitions observed in z direction from two atoms on a surface. $\Delta\theta$ is the relative angle between laser polarization and interatomic distance vector. The green dashed lines indicate the four possible values of $\Delta\theta$ corresponding to a possible measured intensity indicated by the solid red line. The parameters are $R = 0.07\lambda$, $\phi = \pi/2$ and $\Omega = 200\gamma$.

position of the two quantum particles in space and time using the organic crystal host, essentially without perturbation of the optical properties. For atoms on a surface, the two Rabi frequencies experienced by the atoms are equal and independent of R and θ. Therefore, the standing wave driving fields can be replaced by running-wave driving fields without change in the results. This observation is of relevance if the surface of the host material does not allow for the application of standing wave fields. The standing wave driving would only provide more information in more general cases, such as atoms inside a host material at unknown depth, or with atoms which are not aligned parallel to the surface. Since no information can be gained via the position-dependent Rabi frequencies, in contrast to the previous Sec. 5.3.1, here, we determine the value of θ with the help of the resonance fluorescence intensity. In particular, we consider the σ-intensity emitted by the dipoles $\boldsymbol{d}_1$ and $\boldsymbol{d}_3$, measured by a detector placed in z direction since there is no σ-spectrum in y direction.

It turns out that the configuration is symmetric in the sense that a rotation of the laser polarization and the detectors around the x direction is equivalent to a corresponding rotation of the interatomic distance vector. Therefore, the measured resonance fluorescence intensity depends only on the relative angle $\Delta\theta$ between the laser polarization direction and the orientation of the two atoms θ on the surface. In Fig. 5.18, we show this resonance fluorescence intensity versus the relative angle $\Delta\theta$. A plot like this can either be recorded by rotating the sample in the y-z plane, or by rotating the polarization vector of the laser field around its propagation axis.

From Fig. 5.18, we find that the intensity is symmetric around $\Delta\theta = \pi/2$, and it is easy to see that one value of σ intensity corresponds to at most four values of $\Delta\theta$. These four values of $\Delta\theta$ can be roughly divided into the four ranges $0 \to \pi/4$, $\pi/4 \to \pi/2$, $\pi/2 \to 3\pi/4$ and $3\pi/4 \to \pi$, respectively. This can be understood by noting that the orthogonal coupling constants responsible for the σ intensity are the same for orientations θ, $\pi/2-\theta$, $\pi/2+\theta$ and $\pi-\theta$. At $\Delta\theta \in \{0, \pi/2, \pi\}$, the σ intensity is zero since the orthogonal dipole dipole coupling constants Ω_{32} and Ω_{21} vanish at these points, see Fig. 2.4(a). Thus there is no population in states $|1\rangle$ and $|3\rangle$, and the intensity of light emitted from these states is zero. The points of zero σ intensity $\Delta\theta \in \{0, \pi/2, \pi\}$ correspond to situations in which the polarization vector is parallel, perpendicular, or anti-parallel to $\boldsymbol{R}$, respectively. Since these values of $\Delta\theta$ with vanishing intensity can easily be identified, they allow to determine θ from the amount of sample or driving field polarization rotation required to reach these values. In particular, the symmetry point $\Delta\theta = \pi/2$ is well-suited for such a measurement.

5.4 Summary and Discussion

We have discussed methods to measure the relative distance and orientation of two nearby atoms in arbitrary geometry. Our methods are based on the driving of the two atoms with a standing wave field, and on detection of the resonance fluorescence intensity and spectrum in the far field. The distance and orientation information is encoded in the scattered light via the position-dependent Rabi frequencies and via the distance- and orientation-dependent dipole-dipole couplings. Since unlike in previous studies, we consider the case of arbitrary orientation, the atoms must be described using complete Zeeman manifolds in order to correctly model all relevant dipole-dipole couplings between parallel dipole moments as well as between orthogonal ones.

As preliminary work, we have analyzed the fluorescence spectra in particular known geometries, in order to identify dressed-state interpretations in the various limiting cases of interest. These in particular are the case of dominating laser-induced dynamics perturbed by the dipole-dipole interaction, and the case of dominating dipole-dipole coupling modified by the presence of a weaker laser field. Next, we have shown that the case of dominating dipole-dipole interaction enables one to measure the distance between two nearby particles independent of the relative orientation. The reason for this is that the eigenvalues of the total Hamiltonian describing the dynamics, and thus the position of the system dressed states, are independent of the orientation if the two atoms are undriven. We found that a weak driving field allows to probe these dressed states without perturbing the independence on the orientation. Finally, we discussed the measurement of the relative orientation. We presented two methods. The first is based on the position-dependent Rabi frequencies, which under certain conditions reveal the orientation of the two particles. The second method is based on the measurement of the resonance fluorescence intensity in a particular direction. This intensity is a measure for the population in the excited states not driven by the laser field, and therefore a signature for the magnitude of the dipole-dipole coupling between orthogonal dipole moments. We applied the two

methods to the two cases of atoms confined in a two-dimensional waveguide, and to atoms on a surface, in which either the polar or the azimuthal angle of the interatomic distance vector is known.

In principle, these methods to determine the orientation can also be applied for the determination of both polar and azimuthal angle. The most promising ansatz is to make use of the resonance fluorescence intensity in a particular direction as discussed in Sec. 5.3.2 together with a rotation of the sample or of the driving laser polarization in order to fix one of the two angles at a value which renders the spectrum simpler (e.g., 0, $\pi/2$ or π). Then, the methods described in Secs. 5.3.1 and 5.3.2 can be used to determine the other angle. The most straightforward implementation, however, strongly depends on the experimental possibilities to modify the setup. For example, in many cases, a rotation of the sample will be difficult.

Our results rely on a number of model assumptions. First, we have neglected possible residual motion of the two atoms. This is justified, for example, if the two atoms are fixed on a surface, but not in other setups such as tightly trapped atoms. Some effects of residual motion on the dipole-dipole coupling were studied, for example, in [22]. Residual motion could also lead to Doppler effects in the laser driving. Second, if the particle motion is constrained by a host material, interactions with the host could lead to modifications of the optical properties of the atoms. Finally, imperfections in the experimental implementation would lead to uncertainties in the measurements. Examples are light intensity fluctuations, misalignment of light polarizations, or the phase stability of the standing wave field.

For many applications, the generalization to more than two particles is desirable. It remains to be seen whether methods based on the dipole-dipole interaction can also be applied in such cases. One approach could be to combine methods presented here together with a selective addressing of individual atoms at least in one or two dimensions, for example, by position-dependent state transfer.

Chapter 6

Quantum Teleportation of a High Dimensional Entangled State

6.1 Introduction

Entanglement, which leads to nonlocal correlations between observable physical properties of the system, is one of the most counterintutive features in quantum mechanics. Assisted with entangled states, tasks that are impossible within the classical world can be accomplished. It has been realized for long that the striking non-classical nature of entanglement reveals fundamental issues in quantum mechanics, as witnessed by Einstein, Podolsky and Rosen [41], Bell in his famous Bell's theorem [42], and its subsequent experimental verifications [43, 44]. A more promising view of entanglement is shown up when it is considered an essential resource for many ingenious applications such as quantum teleportation [23,45] and quantum cryptography [24]. These applications rely on the ability to engineer and manipulate entangled states in a controlled manner. So far, the generation and manipulation of entangled states have been demonstrated with photon pairs produced in optical processes such as parametric down-conversion [45,46], with ions in an ion trap [47], and with atoms in cavity-QED experiments [48].

A new interest in quantum entanglement is triggered by the discovery that it allows us to transfer (teleport) an unknown quantum state from one particle to another distant particle without sending the particle itself. As the particle itself is not sent, this represents a method of secure transfer of information from the sender to the receiver (commonly called Alice and Bob). The idea of teleportation was first given by Bennett *et al.* [23], who proposed a scheme for the teleportation of an unknown quantum state from one observer to another through dual channels based on quantum entanglement and classical communication. It can be accomplished in three steps. First, both the parties, the sender (Alice) and the receiver (Bob) prepare a maximally entangled state, one particle of which is kept by either of them. Second, the sender disassembles the information of the quantum state of her particles into two parts, one of which is sent through a quantum channel run by the non-local correlations between the two entangled quantum entities and the other is sent through the classical channel. Finally, the receiver reconstructs the state utilizing

the information gained through the quantum and classical channels.

Owing to its vital importance, quantum teleportation has been intensively explored both on theoretical as well as experimental grounds with the investigations yet being hectically persuaded [49–53]. Many proposals for quantum teleportation in a variety of systems have been presented [54–66]. Recently Yang *et al.* [67] and Tao *et al.* [68] proposed deterministic schemes for the teleportation of unknown atomic entangled states. Their schemes do not need Bell state measurements and are insensitive to cavity decay. Furthermore, quantum teleportation has been experimentally verified in systems with continuous variables [69], photonics based techniques [45] as well as systems utilizing cavity QED tools [70].

However, in many potential applications of quantum computing such as factorizing a very large number [71] or searching an unordered database [72], one needs the system of many qubit states. For the teleportation of a single qubit state, a two-qubit maximally entangled state is needed. Now the question arises: What kind of entangled state is required if a two-particle entangled state is to be teleported? Lee [73], in his scheme for the teleportation of two-qubit entangled state, showed that entangled state of four-particle is a prerequisite, with Alice and Bob sharing two-particles each forming a quantum channel between them. Ikram *et al.* [25] showed that for the teleportation of a two-particle entangled state, the entangled state of four-particles is not necessary. Two entangled states of two-particles each can form the quantum channel for the teleportation of two-qubit entangled state.

Entangled states are of utmost importance in quantum computation and it will not be wrong to say that quantum computation relies only on quantum entanglement. The quantum computer is based on the superposition principle of quantum mechanics. A qubit can have the value of both 0 and 1 simultaneously if the quantum states are labelled by binary numbers. However, increase in the number of terms in the superposition allows one to do parallel processing on more numbers. A quantum register may have a superposition of many qubits in N-dimensions or more, and we know that this state cannot be copied to another quantum register [74]. The only way for the communication of such states is the quantum teleportation. Here we present a scheme for the teleportation of a bipartite entangled state with quantum correlations shaping over $(N+1)^2$ states of each system.

The chapter is organized as follows. In section 6.2, we present our model for the teleportation of a bipartite entangled state of $(N+1)^2$ dimensions, elaborating all the three steps of teleportation process. Then in the proceeding Secs. (6.3, 6.4 and 6.5) we give the implementation detail of each step of teleportation process of our proposed entangled state using the standard cavity QED techniques. We conclude our discussion in Sec. 6.6 emphasizing that our proposed scheme is experimentally realizable with the current experimental techniques.

6.2 Teleportation of a Bipartite Entangled State

We consider the teleportation of a two-particle entangled state of radiation field in two separate high-Q cavities A_1 and A_2 to another pair of high-Q cavities C_1 and C_2. The

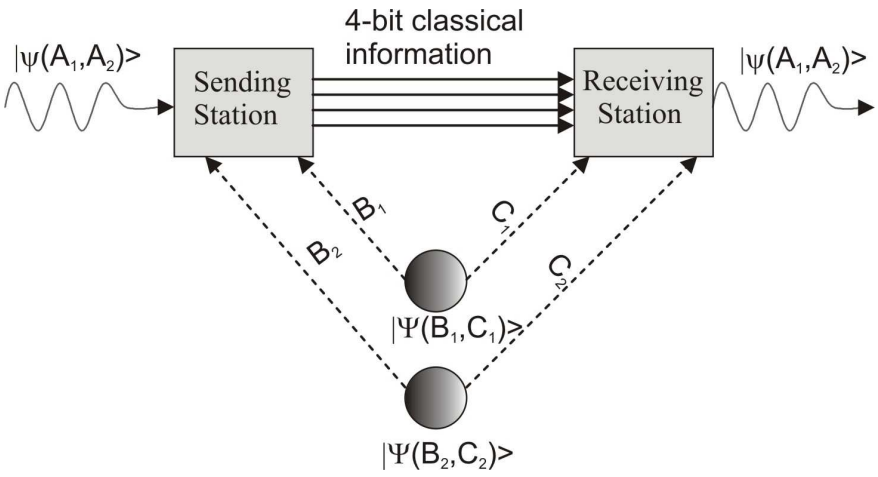

Figure 6.1: Quantum teleportation of a bipartite entangled state $|\Psi(A_1, A_2)\rangle = \sum_{n_1,n_2=0}^{N} C_{n_1,n_2} |n_1\rangle_{A_1} |n_2\rangle_{A_2}$. $|\Psi(B_1, C_1)\rangle$ and $|\Psi(B_2, C_2)\rangle$ are entangled states forming a quantum channel for the teleportation process.

entangled state of radiation field is assumed to be

$$|\Psi(A_1, A_2)\rangle = \sum_{n_1,n_2=0}^{N} C_{n_1,n_2} |n_1\rangle_{A_1} |n_2\rangle_{A_2} , \tag{6.1}$$

with $\sum_{n_1,n_2=0}^{N} |C_{n_1,n_2}|^2 = 1$. It is a bipartite entangled state which is a correlated superposition of $(N+1)^2$ states. The method we describe here is valid only if $N + 1 = 2^n$ (n being an integer). It is because of the measurement of the basis states and explained in Sec. 6.4. The teleportation of entangled state (6.1) can be done in three steps as shown in Fig. 6.1. In the first step of teleportation, Alice and Bob share a four-particle state of the form

$$|\Psi(B_1, B_2, C_1, C_2)\rangle = \frac{1}{N+1} \sum_{p,q=0}^{N} |p\rangle_{B_1} |q\rangle_{B_2} |N-p\rangle_{C_1} |N-q\rangle_{C_2} . \tag{6.2}$$

A careful look at Eq. (2) shows that it is not an entangled state of four particles but a product state of the form

$$|\Psi(B_1, B_2, C_1, C_2)\rangle = |\Psi(B_1, C_1)\rangle \otimes |\Psi(B_2, C_2)\rangle , \tag{6.3}$$

where

$$|\Psi(B_1,C_1)\rangle = \frac{1}{\sqrt{N+1}}\sum_{p=0}^{N}|p\rangle_{B_1}|N-p\rangle_{C_1}\,,$$
$$|\Psi(B_2,C_2)\rangle = \frac{1}{\sqrt{N+1}}\sum_{q=0}^{N}|q\rangle_{B_2}|N-q\rangle_{C_2}\,, \tag{6.4}$$

are the entangled states for fixed number of photons in two cavities B_i and C_i $(i=1,2)$. Thus for the teleportation of two-particles entangled state it is not necessary to have a four-particle entangled state but two entangled states of two-particles are enough for the teleportation procedure to take place. The cavities B_1 and B_2 are possessed by Alice while the cavities C_1 and C_2 are possessed by Bob, thus forming a quantum channel for the teleportation between two parties.

The combined six-particles state is written as

$$|\Psi(A_1,A_2,B_1,B_2,C_1,C_2)\rangle = \frac{1}{N+1}\sum_{n_1,n_2,p,q=0}^{N} C_{n_1,n_2}|n_1\rangle_{A_1}|n_2\rangle_{A_2}|p\rangle_{B_1}|q\rangle_{B_2}|N-p\rangle_{C_1}$$
$$\times|N-q\rangle_{C_2}\,. \tag{6.5}$$

The four particles A_1, A_2, B_1 and B_2, out of these six particles are kept by Alice. Here we define the $(N+1)^4$ basis states containing the particles kept by Alice as

$$|\Psi_{j,k,l,m}(A_1,A_2,B_1,B_2)\rangle = \frac{1}{N+1}\sum_{p,q=0}^{N} e^{\frac{2\iota\pi(jp+kq)}{N+1}}|p\rangle_{A_1}|q\rangle_{A_2}|(N-p-l)\bmod(N+1)\rangle_{B_1}$$
$$\times|(N-q-m)\bmod(N+1)\rangle_{B_2}\,, \tag{6.6}$$

where j and k are relative phases between A_1 and B_1, A_2 and B_2, respectively, while l and m refer to photon numbers in two high-Q cavities B_1 and B_2, respectively. The subscripts j,k,l and m vary from 0 to N, thus for $N=3$, we have 256 basis states. The combined field state in six cavities in terms of basis states can be written as

$$|\Psi(A_1,A_2,B_1,B_2,C_1,C_2)\rangle = \sum_{l,m,p,q=0}^{N} C_{p,q}e^{\frac{2\iota\pi(jp+kq)}{N+1}}|\Psi_{j,k,l,m}(A_1,A_2,B_1,B_2)\rangle$$
$$\times|(p+l)\bmod(N+1)\rangle_{C_1}|(q+m)\bmod(N+1)\rangle_{C_2}\,. \tag{6.7}$$

In the next step of teleportation, Alice makes measurements in the cavities A_1, A_2, B_1 and B_2 possessed by her. A detection of the four-particles basis state $|\Psi_{j,k,l,m}(A_1,A_2,B_1,B_2)\rangle$ projects the field state in the cavities C_1 and C_2 as

$$|\Psi(C_1,C_2)\rangle = \sum_{p,q=0}^{N} C_{p,q}e^{-\frac{2\iota\pi(jp+kq)}{N+1}}|(p+l)\bmod(N+1)\rangle_{C_1}|(q+m)\bmod(N+1)\rangle_{C_2}\,. \tag{6.8}$$

This state is possessed by Bob. Alice communicates the outcome of her measurement through some classical channel to Bob and then Bob makes necessary transformations to bring back the quantum state of the field in the cavities C_1 and C_2 to the quantum state (1). In the following sections we give the details of each step of teleportation using the cavity QED techniques .

6.3 Generation of the Entangled State

In order to generate the entangled field states in two cavities as in Eqs. (4), we use our earlier technique [26]. We consider a stream of N two-level atoms in their excited states undergo an interaction with two high-Q cavities B and C. The atoms are resonant with the field inside the cavities and interact through Jaynes-Cummings Hamiltonian. The field inside the two cavities is initially in vacuum state. The atoms interact with the field inside the cavities for pre-calculated interaction times for the entangled state to be generated. For the generation of N photons entangled state between two cavities, we need to know $2N$ parameters, the interaction time of each atom with two cavities, before carrying out the actual procedure.

A single two-level atom interacts with the quantized cavity field through the unitary operator [27]

$$\begin{aligned} U(\tau) = &\cos(g\tau\sqrt{a^\dagger a+1})\,|a\rangle\langle a| + \cos(g\tau\sqrt{a^\dagger a})\,|a\rangle\langle a| \\ &- \iota\frac{\sin(g\tau\sqrt{a^\dagger a+1})}{\sqrt{a^\dagger a+1}}a\,|a\rangle\langle b| - \iota a^\dagger\frac{\sin(g\tau\sqrt{a^\dagger a+1})}{\sqrt{a^\dagger a+1}}\,|b\rangle\langle a|\,, \end{aligned} \tag{6.9}$$

where g is the coupling constant, a and $a^\dagger$ are the field annihilation and creation operators, respectively. $|a\rangle$ and $|b\rangle$ are upper and lower states of the two-level atom and τ is the interaction time of the atom with the field. After interaction of the first atom with the fields in the two cavities B and C, the atom field-state can be determined by

$$\left|\Psi_\tau^{(1)}(B,C)\right\rangle = U(\tau_{1C})U(\tau_{1B})\left|\Psi_{\tau=0}^{(1)}(B,C)\right\rangle, \tag{6.10}$$

where τ_{1B} and τ_{1C} are interaction times of the first atom with the field inside the cavities B and C, respectively. If the initial field state in the two cavities is taken as vacuum then the state evolves as

$$\begin{aligned} \left|\Psi_\tau^{(1)}(B,C)\right\rangle = &\cos(g\tau_{1B})\cos(g\tau_{1C})\,|a,0_B,0_C\rangle - i\cos(g\tau_{1B})\sin(g\tau_{1C})\,|b,0_B,1_C\rangle - i\sin(g\tau_{1B}) \\ &\times|b,1_B,0_C\rangle\,. \end{aligned} \tag{6.11}$$

If we choose the interaction times $g\tau_{1B} = \pi/4$ and $g\tau_{1C} = \pi/2$, then the field inside the two cavities become one-photon Bell state

$$|\psi(B,C\rangle = \frac{1}{\sqrt{2}}\left(|0_B,1_C\rangle + |1_B,0_C\rangle\right), \tag{6.12}$$

with the unit probability of detecting the atom in ground state $|b\rangle$. This one photon entangled state serves as initial condition for the interaction of second atom with the field

inside the cavities. This procedure is continued till the final N^{th} atom in its excited state $|a\rangle$ is passed through the two cavities. After interaction with the N^{th} atom, the atom-field state can be determined by

$$\left|\Psi_{\tau}^{(N)}(B,C)\right\rangle = U(\tau_{NC})U(\tau_{NB})\left|\Psi_{\tau=0}^{(N)}(B,C)\right\rangle, \tag{6.13}$$

where τ_{NB} and τ_{NC} are interaction times of N^{th} atom with the cavities B and C, respectively. We use the condition that all the atoms must be detected in their ground states after interaction with the cavities for the entangled state (4) to be generated, otherwise we need to empty the cavities and repeat the procedure. When the N^{th} atom is detected in ground state $|b\rangle$, we have

$$\left|\Psi_{\tau}^{(N)}(B,C)\right\rangle = K_N \sum_{j=0}^{N} G_{j,N-j}^{(N)} \left|b, j_B, (N-j)_C\right\rangle, \tag{6.14}$$

where K_N is the normalization constant and $G_{j,N-j}^{(N)}$ is the probability amplitude of the state after the passage of the Nth atom through the two cavities having j photons in the cavity B, $N-j$ photons in the cavity C and the atom in the ground state $|b\rangle$. This is the required entangled state (4) with all $C_{j,N-j}^{(N)}$ same. For the calculation of interaction times of the atoms with the cavity fields, we use the condition that after detecting the atom in ground state, all the probability amplitudes should be same, which gives N equations. For further N equations, we choose N probability amplitudes of excited states equal to zero. Then we solve these $2N$ equations for $2N$ interaction parameters, keeping the probability of detecting all the atoms in ground state maximum. Therefore this scheme for the generation of entangled state is probabilistic. As an example, for the generation of entangled state of four photons in two cavities B and C as

$$|\Psi(B,C)\rangle = \frac{1}{\sqrt{5}}\left[|0_B, 4_C\rangle + |1_B, 3_C\rangle + |2_B, 2_C\rangle + |3_B, 1_C\rangle + |4_B, 0_C\rangle\right], \tag{6.15}$$

the interaction times $g\tau_{1B}$, $g\tau_{1C}$, $g\tau_{2B}$, $g\tau_{2C}$, $g\tau_{3B}$, $g\tau_{3C}$, $g\tau_{4B}$, $g\tau_{4C}$ are 5.6042, 1.5708, 3.0506, 1.1107, 3.9331, 0.6069, 1.9425, 0.7854, respectively, with 0.1956 probability of detection of atoms in ground state [26].

6.4 Measurement of the Basis States

For the measurement of basis states $|\Psi_{j,k,l,m}(A_1, A_2, B_1, B_2)\rangle$, we need to find out precisely the relative phases (j,k) and the photon numbers (l,m) *i.e.*, four bits of classical information, which Alice has to communicate to Bob through classical channel. The state of A_1, A_2, B_1, B_2 system can be determined in two sets of measurement, the first determining l and m via total number of photons in the selected cavities and then determining j and k via the relative phases between A_1, B_1 and A_2, B_2, respectively.

6.4.1 Measurement of Photon Numbers

There are number of ways for the determination of number of photons inside the cavities. We propose to use Ramsey interferometry. In this scheme we consider two-level atoms initially prepared in ground state $|b\rangle$ and which are off resonant with the radiation field inside the cavities. The cavities are placed between two classical microwave fields (Ramsey zones R_1 and R_2) driving the $|a\rangle \rightarrow |b\rangle$ transition. When the atom passes from first zone R_1 with a microwave field tuned at frequency ω_{ab}, it is prepared in a coherent superposition of states $(|a\rangle + |b\rangle)/\sqrt{2}$. This atom is then passed through the two selected cavities with the same interaction time θ in each cavity. During the passage through the cavities, a phase shift proportional to the photon number s in the two cavities is introduced as a phase of the state $|b\rangle$ [27]. The resulting state of the atom then becomes

$$\frac{1}{\sqrt{2}}\left[|a\rangle + e^{is\theta}\,|b\rangle\right]. \tag{6.16}$$

The atom is then passed through the second zone R_2 again resonant with ω_{ab}. The interaction time and the coupling parameters are chosen such that $|a\rangle \longrightarrow (|a\rangle + |b\rangle)/\sqrt{2}$ and $|b\rangle \longrightarrow (|a\rangle - |b\rangle)/\sqrt{2}$. The final atomic state is

$$e^{is\theta/2}\left[\cos(s\theta/2)\,|a\rangle - i\sin(s\theta/2)\,|b\rangle\right]. \tag{6.17}$$

The complete atom field state is entangled and is rather complicated. We have therefore not reproduced it here. It is however clear that a measurement of the atom in state $|a\rangle$ or $|b\rangle$ would reduce the fields inside the cavities to states with only appropriate number of total photons in the two cavities.

For the determination of l of the basis state $|\Psi_{j,k,l,m}(A_1, A_2, B_1, B_2)\rangle$, let us fix j, k and m as 0 and measure the photon number in the cavities A_1 and B_1 by the procedure mentioned above.

$$\begin{aligned}|\Psi_{0,0,l,0}(A_1, A_2, B_1, B_2)\rangle = \frac{1}{N+1}\sum_{p,q=0}^{N} |p\rangle_{A_1}\,|q\rangle_{A_2}\,|(N-p-l)\bmod(N+1)\rangle_{B_1} \\ \times\,|(N-q)\bmod(N+1)\rangle_{B_2}\,.\end{aligned} \tag{6.18}$$

For $N = 3$, the basis state $|\Psi_{0,0,l,0}(A_1, A_2, B_1, B_2)\rangle$ can be written as

$$\begin{aligned}|\Psi_{0,0,0,0}(A_1, A_2, B_1, B_2)\rangle = \frac{1}{4}[&|0,0,3,3\rangle + |0,1,3,2\rangle + |0,2,3,1\rangle + |0,3,3,0\rangle + |1,0,2,3\rangle \\ &+ |1,1,2,2\rangle + |1,2,2,1\rangle + |1,3,2,0\rangle + |2,0,1,3\rangle + |2,1,1,2\rangle \\ &+ |2,2,1,1\rangle + |2,3,1,0\rangle + |3,0,0,3\rangle + |3,1,0,2\rangle + |3,2,0,1\rangle \\ &+ |3,3,0,0\rangle],\end{aligned}$$

$$\begin{aligned}|\Psi_{0,0,1,0}(A_1, A_2, B_1, B_2)\rangle = \frac{1}{4}[&|0,0,2,3\rangle + |0,1,2,2\rangle + |0,2,2,1\rangle + |0,3,2,0\rangle + |1,0,1,3\rangle \\ &+ |1,1,1,2\rangle + |1,2,1,1\rangle + |1,3,1,0\rangle + |2,0,0,3\rangle + |2,1,0,2\rangle \\ &+ |2,2,0,1\rangle + |2,3,0,0\rangle + |3,0,3,3\rangle + |3,1,3,2\rangle + |3,2,3,1\rangle \\ &+ |3,3,3,0\rangle],\end{aligned}$$

$$|\Psi_{0,0,2,0}(A_1,A_2,B_1,B_2)\rangle = \frac{1}{4}[|0,0,1,3\rangle + |0,1,1,2\rangle + |0,2,1,1\rangle + |0,3,1,0\rangle + |1,0,0,3\rangle + |1,1,0,2\rangle + |1,2,0,1\rangle + |1,3,0,0\rangle + |2,0,3,3\rangle + |2,1,3,2\rangle + |2,2,3,1\rangle + |2,3,3,0\rangle + |3,0,2,3\rangle + |3,1,2,2\rangle + |3,2,2,1\rangle + |3,3,2,0\rangle],$$

$$|\Psi_{0,0,3,0}(A_1,A_2,B_1,B_2)\rangle = \frac{1}{4}[|0,0,0,3\rangle + |0,1,0,2\rangle + |0,2,0,1\rangle + |0,3,0,0\rangle + |1,0,3,3\rangle + |1,1,3,2\rangle + |1,2,3,1\rangle + |1,3,3,0\rangle + |2,0,2,3\rangle + |2,1,2,2\rangle + |2,2,2,1\rangle + |2,3,2,0\rangle + |3,0,1,3\rangle + |3,1,1,2\rangle + |3,2,1,1\rangle + |3,3,1,0\rangle].$$

We can clearly see that if we make measurement in the cavity A_1 and the cavity B_1 then $|\Psi_{0,0,0,0}(A_1,A_2,B_1,B_2)\rangle$ and $|\Psi_{0,0,2,0}(A_1,A_2,B_1,B_2)\rangle$ contain odd number of photons, while the states $|\Psi_{0,0,1,0}(A_1,A_2,B_1,B_2)\rangle$ and $|\Psi_{0,0,3,0}(A_1,A_2,B_1,B_2)\rangle$ contain even number of photons. The first atom is sent through the cavities A_1 and B_1 with $\theta = \pi$. It follows from Eq. (15) that if the atom is detected in $|a\rangle_1$, the number of photons s is even which implies that l is odd $(1,3)$ and the detection of atom in $|b\rangle_1$ corresponds to odd value of s and thus even value of l $(0,2)$. The subscript 1 represents the atomic level of the first atom. For the first atom detected in $|a\rangle_1$ *i.e.*, odd value of l, send second atom through the same cavities A_1 and B_1 with $\theta = \pi/2$. If the atom is detected in excited state $|a\rangle_2$ then $l = 3$, otherwise $l = 1$. If the first atom was detected in ground state $|b\rangle_1$ *i.e.*, even value of l, then add a photon in the cavity B_1 and send the second atom through the cavities A_1 and B_1 with $\theta = \pi/2$. Second atom found in excited state $|a\rangle_2$ means $l = 0, 4, ..., N-3$. If the second atom is found in ground state $|b\rangle_2$ then $l = 2, 6, ..., N-1$. If the second atom is found to be in excited state, send third atom with $\theta = \pi/4$. If the second atom is found in ground state, add two photons in the cavity B_1 before sending the third atom with $\theta = \pi/4$. If the third atom is found in excited state, send fourth atom with $\theta = \pi/8$. However, if third atom is found in ground state, add three photons in the cavity B_1 and then send the third atom through cavities A_1 and B_1 with $\theta = \pi/8$. This process is repeated until the N outcomes uniquely determine l. The detection of first two atoms in the sequence below determines the value of l as

$$\begin{aligned}
|a\rangle_1 |b\rangle_2 &\longrightarrow l = 1, 5, ..., N-2 \\
|a\rangle_1 |a\rangle_2 &\longrightarrow l = 3, 7, ..., N \\
|b\rangle_1 |b\rangle_2 &\longrightarrow l = 2, 6, ..., N-1 \\
|b\rangle_1 |a\rangle_2 &\longrightarrow l = 0, 4, ..., N-3
\end{aligned}$$

For $N = 3$, the passage of two atoms uniquely determines the value of l. For higher values of N, we have to send another atom through the cavities A_1 and B_1 according to the procedure mentioned earlier. The third atom uniquely determines the value of l ranging from 0 to 7. Thus the scheme is valid only for those values of N which satisfy the relation $N + 1 = 2^n$, where n is an integer and represent the number of atoms which we pass through the high-Q cavities in order to uniquely determine the value of l in the

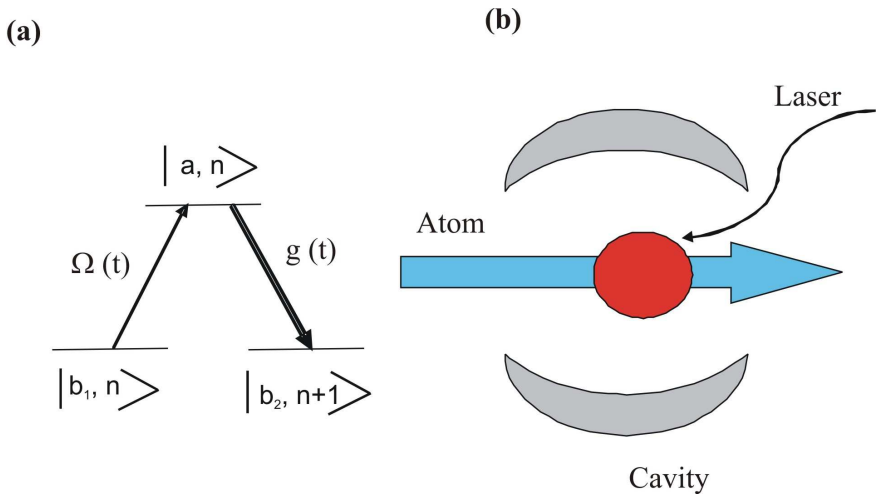

Figure 6.2: (a) A three level atom . (b) Proposed configuration for the adiabatic transfer of photons using three-level atoms. The propagation direction of the pump laser is perpendicular to the page.

basis states. The other value m can be found in a similar manner by passing the atoms through the cavities A_2 and B_2.

For the determination of l and m we have to add photons in the cavities B_1 and B_2 depending upon the detection of atom in ground states or excited states as mentioned above. There are many ways for the addition or removal of photons in the cavities. We propose the addition of photons employing the technique based on adiabatic passage [28]. Here we describe it briefly as it is very crucial for the determination of phase factors j and k.

Consider a three-level atom in Λ configuration as shown in Fig. 6.2. The lower levels $|b_1\rangle$ and $|b_2\rangle$ are coupled to the upper level $|a\rangle$ via a classical field of Rabi frequency $\Omega(t)$ and a cavity field with coupling strength $g(t)$, respectively. The interaction Hamiltonian is given by

$$H(t) = \hbar g(t)(|a\rangle\langle b_2| a + a^\dagger |b_2\rangle\langle a|) - \frac{\hbar\Omega(t)}{2}(|a\rangle\langle b_1| + |b_1\rangle\langle a|), \tag{6.19}$$

where a and $a^\dagger$ are the annihilation and creation operators of the cavity field. This Hamiltonian has an eigenstate that contains no contribution of the level $|a\rangle$ and is given by

$$|E_n\rangle = \frac{g(t)\sqrt{n+1}\,|b_1, n\rangle + \Omega(t)/2\,|b_2, n+1\rangle}{\sqrt{g(t)^2(n+1) + \Omega(t)^2/4}}. \tag{6.20}$$

As a function of time, $|E_n\rangle$ behaves asymptotically as

$$|E_n\rangle \to \begin{cases} |b_1, n\rangle & \text{for } \Omega(t)/g(t) \to 0 \\ |b_2, n+1\rangle & \text{for } g(t)/\Omega(t) \to 0 \end{cases}. \tag{6.21}$$

According to adiabatic theorem, if the Hamiltonian at time t_0 is in an eigenstate of $H(t_0)$ and its time evolution is slow, the system will evolve into the eigenstate $H(t_1)$, where

$t_1 > t_0$. Thus if the atom-cavity system is initially in state $|b_1\rangle$, for the pulse sequence in which $\Omega(t)$ is time delayed with respect to $g(t)$, the state with which the atom exits is $|b_2, n+1\rangle$. This produces a single photon shift in the cavity-field state. The reverse will remove a single photon from the field state. We can shift multi-photons in a similar way by considering virtual levels between $|b_2\rangle$ and $|a\rangle$.

6.4.2 Measurement of the Phases j and k

Next we determine the phase factors j and k in the basis state (6). The basis states after determination of l and m have the form

$$|\Psi_{j,k,l,m}(A_1, A_2, B_1, B_2)\rangle = \frac{1}{\sqrt{N+1}} \sum_{p=0}^{N} e^{\frac{2\iota\pi(jp+kq)}{N+1}} |p\rangle_{A_1} |q\rangle_{A_2} |(N-p-l) \bmod (N+1) + x\rangle_{B_1} \times |(N-q-m) \bmod (N+1) + y\rangle_{B_2}, \tag{6.22}$$

where x and y are the number of photons added during the measurement process in A_1, B_1 and A_2, B_2 systems, respectively. For the determination of j, which is relative phase between the radiation fields in the cavities A_1 and B_1, we have to evacuate the cavities A_2 and B_2. The relative phase may change while we carry out the process of evacuating the cavities. The evacuation can be done by the process of adiabatic passage mentioned earlier.

After evacuating the cavities A_2 and B_2 we consider the cavities A_1 and B_1 only. The index j designates their relative phase. We remove all the photons from the cavity B_1 using adiabatic passage so that the cavities A_1 and B_1 become decoupled. For this purpose we send $N+x$ three-level atoms in Λ configuration in level $|b_2\rangle$ interacting with field in the cavity B_1 only and a classical field via interaction Hamiltonian (17). The first x atoms remove x photons and so are found in $|b_1\rangle$. The remaining N atoms, after passage from the cavity B_1 undergo a mixing of levels by a classical field such that $|b_1\rangle \rightarrow (|b_1\rangle + |b_2\rangle)/\sqrt{2}$ and $|b_2\rangle \rightarrow (|b_1\rangle - |b_2\rangle)/\sqrt{2}$. Detection of the atom in $|b_1\rangle$ does not add any phase whereas detection of the atom in $|b_2\rangle$ would add a phase π for all those constituent states where the cavity B_1 has no photon. We consider only the cases when all the N atoms are detected in $|b_1\rangle$. In this case the cavity B_1 has no photons and is decoupled from the cavity A_1. The state of the cavity A_1 is

$$|\Psi_j(A_1)\rangle = \frac{1}{\sqrt{N+1}} \sum_{p=0}^{N} e^{\frac{2\pi\iota jp}{N+1}} |p\rangle_{A_1}. \tag{6.23}$$

Now we send $(N+1)/2$ three-level atoms in Λ configuration in $|b_2\rangle$ through the cavity A_1. The first atom removes $(N+1)/2$ photons via multi-photon transition and ends up in $|b_1\rangle$. Then we apply strong classical field which transforms the states $|b_1\rangle$ and $|b_2\rangle$ in such a way that $|b_1\rangle \rightarrow (|b_1\rangle - |b_2\rangle)/\sqrt{2}$ and $|b_2\rangle \rightarrow (|b_1\rangle + |b_2\rangle)/\sqrt{2}$. The atom is then detected in $|b_1\rangle$ or $|b_2\rangle$. If the atom is detected in $|b_1\rangle$, then $j = 0, 2, ..., N-1$, whereas,

if it is detected in $|b_2\rangle$, then $j = 1, 3, ..., N$. In both cases, the field inside the cavity becomes

$$|\Psi_j(A_1)\rangle = \sqrt{\frac{2}{N+1}} \sum_{p=0}^{(N+1)/2-1} e^{\frac{2\pi\iota jp}{N+1}} |p\rangle_{A_1} . \tag{6.24}$$

The second atom removes $(N+1)/4$ photons from the cavity A_1, followed by the strong classical field which transforms the states $|b_1\rangle$ and $|b_2\rangle$ into $(|b_1\rangle + ie^{\iota\varphi}|b_2\rangle)/\sqrt{2}$ and $(\iota e^{-\iota\varphi}|b_1\rangle + |b_2\rangle)/\sqrt{2}$, respectively. We choose $\varphi = \pi/2$ or π depending upon whether the first atom was detected in $|b_1\rangle$ or $|b_2\rangle$, respectively. The detection of the atoms in the sequence below determines the value of phase factor j as

$$\begin{aligned}
|b_1\rangle_1 |b_1\rangle_2 &\longrightarrow j = 0, 4, ..., N-3 \\
|b_1\rangle_1 |b_2\rangle_2 &\longrightarrow j = 2, 6, ..., N-1 \\
|b_2\rangle_1 |b_1\rangle_2 &\longrightarrow j = 1, 5, ..., N-2 \\
|b_2\rangle_1 |b_2\rangle_2 &\longrightarrow j = 3, 7, ..., N
\end{aligned}$$

For $N = 3$, the passage of two atoms completely determines the phase j. However for larger N, the resulting state will be

$$|\Psi_j(A_1)\rangle = \frac{2}{\sqrt{N+1}} \sum_{p=0}^{(N+1)/4-1} e^{2\pi\iota jp/(N+1)} |p\rangle_{A_1} . \tag{6.25}$$

The third atom removes $(N+1)/8$ photons. Then comes the strong classical field and follows the detection process. If the sequences of measurements are $|b_1\rangle|b_1\rangle, |b_1\rangle|b_2\rangle, |b_2\rangle|b_1\rangle$ or $|b_2\rangle|b_2\rangle$, we choose $\varphi = \pi/2, \pi, \frac{3\pi}{4}$ or $\frac{5\pi}{4}$, respectively. After the passage of third atom, the sequence of measurements gives the value of phase j as

$$\begin{aligned}
|b_1\rangle_1 |b_1\rangle_2 |b_1\rangle_3 &\longrightarrow j = 0, 8, ..., N-7 \\
|b_1\rangle_1 |b_1\rangle_2 |b_2\rangle_3 &\longrightarrow j = 4, 12, ..., N-3 \\
|b_1\rangle_1 |b_2\rangle_2 |b_1\rangle_3 &\longrightarrow j = 2, 10, ..., N-5 \\
|b_1\rangle_1 |b_2\rangle_2 |b_2\rangle_3 &\longrightarrow j = 6, 14, ..., N-1 \\
|b_2\rangle_1 |b_1\rangle_2 |b_1\rangle_3 &\longrightarrow j = 1, 9, ..., N-6 \\
|b_2\rangle_1 |b_1\rangle_2 |b_2\rangle_3 &\longrightarrow j = 5, 13, ..., N-2 \\
|b_2\rangle_1 |b_2\rangle_2 |b_1\rangle_3 &\longrightarrow j = 3, 11, ..., N-4 \\
|b_2\rangle_1 |b_2\rangle_2 |b_2\rangle_3 &\longrightarrow j = 7, 15, ..., N
\end{aligned}$$

Thus for $N = 7$, the passage of three atoms and their detection in different atomic states completely determine the phase factor j.

For larger value of N we continue the process. The subsequent atoms remove $(N+1)/16$, $(N+1)/32, ..., 1$ photons from the cavity A_1 having an adequate number of photons, then atomic levels are mixed by a strong classical field with appropriate choice of φ and follows it the detection process. The N outcomes uniquely determine the phase factor j. The other phase factor k can also be determined in the same way treating cavities A_2 and B_2 divorced from the cavities A_1 and B_1, *i.e.*, after evacuating the cavities A_1 and B_1.

6.5 Transformation

A determination of the entangled state of the field inside the high-Q cavities A_1, A_2, B_1 and B_2, say, in state $|\Psi_{j,k,l,m}(A_1, A_2, B_1, B_2)\rangle$, projects the state of the field in the cavities C_1 and C_2 into the state $|\Psi(C_1, C_2)\rangle$ as given by Eq. (8). In the final step of teleportation, Bob transforms this state into the original state (1). It is quite vivid that the above state differs from (1) in terms of phase factor $e^{2\iota\pi(jp+kq)/(N+1)}$ and the displacement of photon numbers. Thus the transformation of the state $|\Psi(C_1, C_2)\rangle$ into the state given by Eq. (1) involves two steps. One is the removal of phases $\exp(i\pi j)$ and $\exp(i\pi k)$ and other is an appropriate transformation of photon numbers l and m.

6.5.1 Transformation of Phases

For the transformation of phases $\exp(i\pi j)$ and $\exp(i\pi k)$, let us consider the situation when $l = m = 0$, then

$$|\Psi(C_1, C_2)\rangle = \sum_{p,q=0}^{N} C_{p,q} e^{-\frac{2\iota\pi(jp+kq)}{N+1}} |p\rangle_{C_1} |q\rangle_{C_2} . \tag{6.26}$$

The state in the cavities C_1 and C_2 is the same as the state in the cavities A_1 and B_2 (Eq. (1)) except the phase factor $e^{-2\iota\pi(jp+kq)/(N+1)}$. We employ Ramsey interferometry to remove these phase factors. We pass a non-resonant atom in its superposition state $(|a_1\rangle + |b_1\rangle)/\sqrt{2}$ through the cavity C_1 such that $|b_1\rangle$ of the atom picks up a phase $e^{2\pi\iota jp/(N+1)}$, where p is the number of photons present in the cavity C_1. This reduces the state function to

$$|\Psi(C_1, C_2)\rangle |Atom\rangle_1 = \frac{1}{\sqrt{2}} \sum_{p,q=0}^{N} C_{p,q} \left(e^{-\frac{2\iota\pi(jp+kq)}{N+1}} |p\rangle_{C_1} |q\rangle_{C_2} |a_1\rangle + e^{-\frac{2\iota\pi kq}{N+1}} |p\rangle_{C_1} |q\rangle_{C_2} |b_1\rangle \right) . \tag{6.27}$$

If the first atom is detected in excited state $|a_1\rangle$, we repeat the process until it is detected in the ground state. When the atom is detected in the ground state $|b_1\rangle$, we pass another non-resonant atom in its superposition state $(|a_2\rangle + |b_2\rangle)/\sqrt{2}$ through the cavity C_2 such that $|b_2\rangle$ of the atom picks up a phase $e^{2\pi\iota jq/(N+1)}$ where q is the number of photons present in the cavity C_2. Then the above state becomes

$$|\Psi(C_1, C_2)\rangle |Atom\rangle_2 = \frac{1}{\sqrt{2}} \sum_{p,q=0}^{N} C_{p,q} \left(e^{-\frac{2\iota\pi kq}{N+1}} |p\rangle_{C_1} |q\rangle_{C_2} |a_2\rangle + |p\rangle_{C_1} |q\rangle_{C_2} |b_2\rangle \right) . \tag{6.28}$$

If the second atom is detected in ground state $|b_2\rangle$ then the state is recovered, otherwise we repeat the process until the atom is detected in ground state.

6.5.2 Transformation of Photon Numbers

The procedure of this phase transformation becomes complicated if l and m are non-zero. In this case we have to transform the photon numbers in the cavities C_1 and C_2 such that

the number of photons in two cavities corresponds to subscripts p and q of the probability amplitude $C_{p,q}$ of the quantum state (24). For this purpose we first add $N+1-l$ photons in C_1 and $N+1-m$ photons in C_2, using the method of adiabatic passage as discussed earlier. This will transform the state (8) into

$$|\Psi(C_1,C_2)\rangle = \sum_{p,q=0}^{N} C_{p,q} e^{-\frac{2\iota\pi(jp+kq)}{N+1}} |(p+l) \bmod (N+1) + N + 1 - l\rangle_{C_1} \\ |(q+m) \bmod (N+1) + N + 1 - m\rangle_{C_2} . \tag{6.29}$$

Then we remove $N+1$ photons from each of the cavities C_1 and C_2 via multi-photon absorption process mentioned in the adiabatic passage scheme. This process removes $N+1$ photons from the $|N+1+l\rangle_{C_1}$ with $p<l$, and $N+1$ photons from the $|N+1+m\rangle_{C_2}$ with $q<m$. First we remove $N+1$ photons from C_1, which results in the entanglement of the full atom-field state

$$|\Psi(C_1,C_2)\rangle \otimes |Atom\rangle_1 = \frac{1}{\sqrt{2}} \sum_{q=0}^{N} \left[\sum_{p=0}^{l-1} e^{-\frac{2\iota\pi jp}{N+1}} C_{p,q} |p\rangle_{C_1} |b_2\rangle + \sum_{p=l}^{N} e^{-\frac{2\iota\pi jp}{N+1}} C_{p,q} |p\rangle_{C_1} |b_1\rangle \right] \\ \times e^{-\frac{2\iota\pi kq}{N+1}} |(q+m) \bmod (N+1) + N + 1 - m\rangle_{C_2} . \tag{6.30}$$

Atomic levels of the atom exiting C_1 are mixed by a classical field such that $|b_1\rangle \rightarrow (|b_1\rangle - |b_2\rangle)/\sqrt{2}$ and $|b_2\rangle \rightarrow (|b_1\rangle + |b_2\rangle)/\sqrt{2}$. If the atom is detected in $|b_1\rangle$, we get

$$|\Psi(C_1,C_2)\rangle = \sum_{p,q=0}^{N} C_{p,q} e^{-\frac{2\iota\pi(jp+kq)}{N+1}} |p\rangle_{C_1} |(q+m) \bmod (N+1) + N + 1 - m\rangle_{C_2} . \tag{6.31}$$

If the atom is detected in $|b_2\rangle$, a negative sign appears in phase with the terms having less than $N+1$ photons in the cavity C_1 since the absorption process does nothing to such states. Then we repeat the same process with the cavity C_2. Removal of the $N+1$ photons from C_2 and detection of second atom in $|b_1\rangle$ transform the above state to (24), however if the atom is detected in $|b_2\rangle$, a negative sign appears in phase with the terms having less than $N+1$ photons in the cavity C_2. Correction of these phase factors brings the state in the form (24). Then we remove the phase factors by the method discussed earlier for the transformation of phases.

6.6 Conclusions

We have presented a scheme for the quantum teleportation of an entangled field state of the form (6.1) from a pair of high-Q cavities to another pair of high-Q cavities. All the three steps of teleportation process *i.e.*, generation of entangled state for fixed number of photons in two high-Q cavities, measurement of basis state and finally the transformations are carried out using standard cavity QED techniques including the Ramsey interferometry and adiabatic passage. The scheme demands controlled interaction times between

atoms and cavities, no spontaneous decay of atoms and no cavity losses during the whole teleportation process.

The interaction times of the atoms with the cavity fields can easily be controlled through Stark field adjustment to the atomic levels of the two-level atoms *i.e.*, by applying timed sequences of pulsed electric fields on the atoms while they interact with the cavity fields. [48, 56, 75]. The atoms can be made resonant or off-resonant so that the interaction of the atoms with the cavity fields can be made resonant or dispersive for a pre-calculated time. For the suppression of spontaneous decay, we propose to use Rubidium atoms with adjacent circular Rydberg states of principal quantum numbers 50 and 51 (frequency 51.099 GHz). These atoms have long radiative life times ($\simeq 30\ ms$) and very strong coupling to radiation [76]. High-Q cavities is another requirement in order to complete the teleportation before the field decoherence. For the teleportation of entangled state with $N = 3$, the total number of interactions of the atoms with the fields in all the processes is around 40. The interaction times of the atoms with the fields vary from 1 μs to 6 μs. On the average if we take 3 μs per interaction and include all spacing and other times, the total time for the teleportation to be completed is less than 250 μs, whereas the superconducting cavities with quality factors $10^8 - 10^{10}$ corresponding to photon life time in the range $1 - 200\ ms$ have been reported [70, 77]. It ensures that the whole teleportation process can be completed before any decoherence occurs due to atomic decay or cavity loss. The above parameters show that the proposed teleportation scheme is experimentally realizable with the current experimental techniques.

Chapter 7

Summary and Outlook

In the project related to high-precision measurements, we have presented the techniques for the measurement of interatomic distance as well as the relative orientation of two nearby four-level atoms in arbitrary geometry. We make use of the dipole-dipole interaction between the two atoms and observe its effects on the optical properties of the system through the inelastic components of resonance fluorescence spectrum and intensity.

The generally complicated spectra of resonance fluorescence simplify considerably when studied under certain limiting cases, *e.g.*, when the distance separating the atoms is very large or when the atoms are very closed to each other. This is because in the former situation the dipole-dipole interaction is negligible so the main interaction is that between the atoms and the laser and the latter scenario corresponds to a strong dipole-dipole interaction in which the laser acts as a small perturbation.

The system is studied first for a simple, fixed, known orientation in which the atoms are placed in a line with respect to the incident laser. The intuitive understanding of the positions of the differnet peaks in the resonance fluorescence spectra is developed by the analysis of the eigen values of the interaction picture Hamiltonia. The pictorial dressed state descriptions have been illustrated for this purpose. Afterwards, the analysis has been extended for a completely unknown orientation. The interatomic distance can be measured without any prior knowledge of the orientation of the two atoms via the strong dipole-dipole interaction at small interatomic distances. The orientation of the system can be determined by putting the system inside a planar wave guide and by observing the resonance fluorescence intensity while the atoms are confined to a surface and the laser field propagates perpendicular to the surface.

For practical purposes, it may be required to generalize the discussion to many particle systems. It remains to be seen whether methods based on the dipole-dipole interaction can also be applied in such cases. One approach could be to combine methods presented here together with a selective addressing of individual atoms at least in one or two dimensions, for example, by position-dependent state transfer.

In the project based on quantum teleportation of a high dimensional entangled state, a scheme for the quantum teleportation of an entangled field state from a pair of high-Q cavities to another pair of high-Q cavities has been presented. The process is divided

into three major steps. First is the preparation of the entangled state which is done by assuming a resonant interaction with high-Q cavities whose initial state is assumed to be a vacuum state. Second step involves the measurement of the basis states and in the third step, transformation process is carried out by the receiver such that he recovers the original state sent by the sender. All the three steps of teleportation process *i.e.*, are carried out using standard cavity QED techniques including the Ramsey interferometry and adiabatic passage. The scheme demands controlled interaction times between atoms and cavities, no spontaneous decay of atoms and no cavity losses during the whole teleportation process.

Stark field adjustment to the atomic levels of the two-level atoms can help control the atom-field interaction time *i.e.*, by applying timed sequences of pulsed electric fields on the atoms while they interact with the cavity fields. The atoms can be made resonant or off-resonant so that the interaction of the atoms with the cavity fields can be made resonant or dispersive for a pre-calculated time. The unwanted decay due to spontaneaous emission can be handled by using Rydberg atoms. These atoms have long radiative life times and very strong coupling to radiation. To make the field decohernce time large, cavities with a high quality factor are needed so that no losses due to the cavity obstacle the teleportation process. Thus we show that the proposed teleportation scheme is experimentally realizable with the current experimental techniques.

Bibliography

[1] E. Abbe, Arch. Mikrosk. Anat **9**, 413 (1873); L. Rayleigh, Phil. Mag. **8**, 261 (1879).

[2] E. H. Synge, Phil. Mag. **6**, 356 (1928); R. C. Dunn, Chem. Rev. **99**, 2891 (1999).

[3] S. W. Hell, Nat. Biotechnol. **21**, 1347 (2003).

[4] E. Betzig, Opt. Lett. **20**, 237 (1995).

[5] M. O. Scully and K. Drühl, Phys. Rev. A **25**, 2208 (1982); U. W. Rathe and M. O. Scully, Lett. Math. Phys. **34**, 297 (1995);

M. D'Angelo, M. V. Chekhova, and Y. Shih, Phys. Rev. Lett. **87**, 013602 (2001).

[6] A. N. Boto, P. Kok, D. S. Abrams, S. L. Braunstein, C. P. Williams, and J. P. Dowling, Phys. Rev. Lett. **85**, 2733 (2000).

[7] W. Denk, J. H. Strickler and W. W. Webb, Science **248**, 73 (1990).

[8] P. R. Hemmer, A. Muthukrishnan, M. O. Scully, and M. S. Zubairy, Phys. Rev. Lett. **96**, 163603 (2006).

[9] D. D. Yavuz and N. A. Proite, Phys. Rev. A **76**, 041802(R) (2007); M. Kiffner, J. Evers, and M. S. Zubairy, Phys. Rev. Lett. **100**, 073602 (2008); A. V. Gorshkov, L. Jiang, M. Greiner, P. Zoller, and M. D. Lukin, Phys. Rev. Lett. **100**, 093005 (2008).

[10] G. S. Agarwal, *Quantum Statistical Theories of Spontaneous Emission and their Relation to Other Approaches*, edited by G. Höhler (Springer, Berlin, 1974).

[11] Z. Ficek and S. Swain, *Quantum Interference and Coherence: Theory and Experiments* (Springer, Berlin, 2005).

[12] G. V. Varada and G. S. Agarwal, Phys. Rev. A **45**, 6721 (1992).

[13] J. Evers, M. Kiffner, M. Macovei, and C. H. Keitel, Phys. Rev. A **73**, 023804 (2006).

[14] D. F. V. James, Phys. Rev. A **45**, 6721 (1992).

[15] J.-T. Chang, J. Evers, M. O. Scully, and M. S. Zubairy, Phys. Rev. A **73**, 031803(R) (2006); J.-T. Chang, J. Evers, and M. S. Zubairy, Phys. Rev. A **74**, 043820 (2006).

[16] M. Macovei, J. Evers, G.-x. Li, and C. H. Keitel, Phys. Rev. Lett. **98**, 043602 (2007).

[17] Z. Ficek, Phys. Rev. A **44**, 7759 (1991).

[18] C. Hettich, C. Schmitt, J. Zitzmann, S. Kühn, I. Gerhardt, and V. Sandoghdar, Science **298**, 385 (2002).

[19] G. S. Agarwal and A. K. Patnaik, Phys. Rev. A **63**, 043805 (2001).

[20] M. Kiffner, J. Evers, and C. H. Keitel, Phys. Rev. A **76**, 013807 (2007).

[21] M. Kiffner, J. Evers, and C. H. Keitel, Phys. Rev. A **75**, 032313 (2007).

[22] S. I. Schmid and J. Evers, Phys. Rev. A **77**, 013822 (2008).

[23] C. H. Bennett, G. Brassard, C. Crepeau, R, Joza, A. Peres, and W. K. Wootters, Phys. Rev. Lett. **70**, 1895 (1993).

[24] A. K. Ekert, Phys. Rev. Lett. **67**, 661 (1991).

[25] M. Ikram, S. Y. Zhu, and M. S. Zubairy, Phys. Rev. A, **62** 022307 (2000).

[26] M. Ikram, S. Y. Zhu and M. S. Zubairy, Opt. Commun. **184**, 417 (2000).

[27] M. O. Scully and M. S. Zubairy, *Quantum Optics*,(Cambridge University Press, Cambridge, 1997).

[28] A. S. Parkins, P. Marte, P. Zoller, and H. J. Kimble, Phys. Rev. Lett. **71**, 3095 (1993); A. S. Parkins, P. Marte, P. Zoller, O. Carnal, and H. J. Kimble, Phys. Rev. A **51**, 1578 (1995); J. R. Kuklinski, U, Gaubatz, F. T. Hio, and K. Bergmann, Phys. Rev. A, **40**, 6741 (1989).

[29] M. Kiffner, PhD thesis, *Coherence effects in vacuum-induced processes*, University of Heidelberg (2007).

[30] J. J. Sakurai, *Modern Quantum Mechanics* (Addison-Wesley, Reading, MA, 1994).

[31] R. R. Puri, *Mathematical Method of Quantum Optics*, Springer, Berlin (2001).

[32] B. R. Mollow, J. Phys. A **8**, L130 (1975).

[33] M. Lax, Phys. Rev. **129** 2342 (1963).

[34] H. Carmichael, *An Open System Approach To Quantum Optics*, Springer, (1993).

[35] B. R. Mollow, Phys. Rev. **188**, 1969 (1969).

[36] H. Gauck, M. Hartl, D. Schneble, H. Schnitzler, T. Pfau, and J. Mlynek, Phys. Rev. Lett. **81**, 5298 (1998).

[37] B. Rohwedder, Phys. Rev. A **63**, 053604 (2001).

[38] M. Montagna, M. Ferrari, F. Rossi, F. Tonelli, and C. Tosello, Phys. Rev. B **58**, 547(R) (1998).

[39] R. Wüest, D. Erni, P. Strasser, F. Robin, H. Jäckel, B. Buchler, A. F. Koenderink, V. Sandoghdar, and R. Harbers, Appl. Phys. Lett. **87**, 261110 (2005).

[40] F. Benabid, J. C. Knight, G. Antonopoulos, and P. St. J. Russell, Science **298**, 399 (2002).

[41] A. Einstein, B. Podolsky, and N. Rosen, Phys. Rev. **47**, 777 (1935).

[42] J. S. Bell, Physics (Long Island City, N. Y.) **1**, 195 (1964).

[43] S. J. Freedman and J. F. Clauser, Phys. Rev. Lett. **28**, 938 (1972) ; J. F. Clauser and A. Shimony, Rep. Prog. Phys. **41**, 1881 (1978).

[44] A. Aspect, P. Graingier, and G. Roger, Phys. Rev. Lett. **47**, 460 (1981); A. Aspect, P. Graingier, and G. Roger, Phys. Rev. Lett. **49**, 91 (1982); A. Aspect, J. Dalibard, and G. Roger, Phys. Rev. Lett. **49**, 1804 (1982).

[45] D. Bouwemeester, J. W. Pan, K. Mattle, M. Eibl, H. Weinfurter, and A. Zeilinger, Nature (London) **390**, 575 (1997); D. Boschi, S. Branca, F. D. De Martini, L. Hardy, and S. Popescue, Phys. Rev. Lett. **80**, 1121 (1998).

[46] P. J. Kwiat, K. Mattle, H. Weinfurter, A. Zeilinger, A. V. Sergienko, and Y. Shih, Phys. Rev. Lett. **75**, 4337 (1995).

[47] C. Monroe, D. M. Meekhof, B. E. King, and D. J. Wineland, Science **272**, 1131 (1996).

[48] E. Hagley, X. Maitre, G. Nogues, C. Wunderlich, M. Brune, J. M. Raimond, and S. Haroche, Phys. Rev. Lett. **79**, 1 (1997).

[49] A. Grudka and J. Modlawska, Phys. Rev. A **77**, 014301 (2008).

[50] S. M. Cohen, Phys. Rev. A **77**, 012304 (2008).

[51] L. C. Venuti, S. M. Giampaolo, F. Illuminati, and P. Zandari, Phys. Rev. A **76**, 052328 (2007).

[52] H. Wei, Z. J. Deng, X. L. Zhang, and M. Feng, Phys. Rev. A **76**, 054304 (2007).

[53] S. K. Ozdemir, K. Bartkiewicz, Y. X. Liu, and A. Miranowicz, Phys. Rev. A **76**, 042325 (2007).

[54] Y. H. Kim, S. P. Kulik, and Y. Shih, Phys. Rev. Lett. **86**, 1370 (2001).

[55] A. Fursawa, J. L. Sorenson, S. L. Braunstein, C. A. Fuchs, H. J. Kimble, and E. S. Polzik, Science **282**, 706 (1998).

[56] L. Davidovich, N. Zagury, M. Brune, J. M. Raimond, and S. Haroshe, Phys. Rev. A **50**, R895 (1994).

[57] J. I. Cirac and A. S. Parkins, Phys. Rev. A **50**, R4441(1994).

[58] S. B. Zheng and G. C. Guo, Phys. Lett. A **232**, 171 (1997).

[59] S. B. Zheng, Opt. Commun. **167**, 111 (1999).

[60] S. Bose, P. L. Knight, M. B. Plenio, and V. Vedral, Phys. Rev. Lett. **83**, 5158 (1999).

[61] S. Bandyopadhyay, Phys. Rev. A **62**, 012308 (2000).

[62] S. B. Zheng, Chin. Phys. **14**, 1825 (2005).

[63] H. C. Yuan and K. G. Qi, Chin. Phys. **14**, 0898 (2005).

[64] M. S. Zubairy, Phys. Rev. A **58,** 4368 (1998).

[65] Y. B. Zhan, Chin. Phys. **13**, 1801 (2005).

[66] H. W. Lee and J. Kim, Phys. Rev. A **63**, 012305 (2000).

[67] M. Yang and Z. L. Cao, arXiv: quant-ph/041195v1 (2004).

[68] W. Tao, Y. Liu and N. Zhi-Xiang, Chin. Phys. **15**, 11 (2006).

[69] W. P. Bowen, N. Treps, B. C. Buchler, R. Schnabel, T. C. Ralph, H-A. Bachor, T. Symul, and P. K. Lam, Phys. Rev. A **67**, 032302 (2003).

[70] J. M. Raimond, M. Brune, and S. Haroche, Rev. Mod. Phys. **73**, 565 (2001).

[71] P. Shor, SIAM, J. Comput, **26**, 1484 (1997).

[72] L. K. Grover, Phys. Rev. Lett. **79**, 325 (1997); L. K. Grover, Phys. Rev. Lett. **79**, 4709 (1997).

[73] H. W. Lee, Phys. Rev. A **64**, 014302 (2001).

[74] W. K. Wootters and W. H. Zurek, Nature, **299**, 802 (1982).

[75] A. Rauschenbeutel, P. Bertet, S. Osnaghi, G. Nogues, M. Brune, J. M. Raimond, and S. Harosche, Phys. Rev. A **64**, 050301 (2001).

[76] M. Brune, F. Schmidt-Kaley, A. Malli, J. Dreyer, E. Hagley, J. M. Raimond, and S. Haroche, Phys. Rev. Lett. **76**, 1800 (1996); M. Brune, E. Hagley, J. Dreyer, X. Maitre, C. Wonderlich, J. M. Raimond, and S. Haroche, Phys. Rev. Lett. **77**, 4887 (1996).

[77] M. Weidinger, B. T. H. Varcoe, R. Heerlein, and H. Walther, Phys. Rev. Lett. **82**, 3795 (1999).

Acknowledgment

I humbly thank Almighty Allah, the most Merciful and the most Beneficent, who gave me health, thoughts and co-operative people to enable me achieve this goal.

The deepest regards, no doubt, go to none other than Dr. Jörg Evers for his continuous guidance throughout this work. I am deeply indebted to him for his guidance and support. He mentored and supported me with passion. His advice and patience are highly appreciated.

Special regards go to Peter Brunner, who is an ever-ready person and do not let our time go wasted as far as computational facilities are concerned. Along with him the secretaries first Vera Beyer and after her Sibel Babacan were pretty helpful when I needed them.

I am grateful to my former and present office-mates specially Erik Lötstedt, Huayu Hu, Benedikt Wundt, Bastian Jungnitsch, Luling Jin, Felix Mackenroth, Sarah Müller, Tim O. Müller and many more for establishing such a nice atmosphere of our room having some chit chats on different topics.

Also, I would like to acknowledge Atif Shahbaz, who has been very helpful as far as my social life is concerned.

Special thanks to Higher Education Commission (HEC), Pakistan, the International Max Planck Research School for Quantum Dynamics in Physics, Chemistry and Biology, Heidelberg, Germany, and by Deutscher Akademischer Austauschdienst (DAAD) for the financial support and Max-Planck-Institute for Nuclear Physics for providing me workspace.

I would like to say thanks to my parents and siblings.

Last but not the least, I am very grateful to my husband, Gulfam Saleem who stood by me through thick and thin and my cute baby, Ahmed.